Experimental Study of Film Cooling and Heat Transfer on a Gas Turbine Vane with Shaped Holes

Tarek Elnady

A Thesis

in

The Department

of

Mechanical and Industrial Engineering

Presented in Partial Fulfillment of the Requirements
for the Degree of Doctor of Philosophy (Mechanical Engineering) at
Concordia University
Montreal, Quebec, Canada

August 2010

Your file Votre référence
ISBN: 978-0-494-71104-0
Our file Notre référence
ISBN: 978-0-494-71104-0

Abstract

Experimental Study of Film Cooling and Heat Transfer on a Gas Turbine Vane with Shaped Holes

Tarek Elnady, Ph.D.

Concordia University, 2010

Improving the film cooling technique provides more cooling capacity to withstand the harsh thermal environment in the next generation of gas turbines. A two-dimensional cascade has been designed and constructed in a subsonic wind tunnel in order to investigate the heat transfer of shaped holes over a gas turbine stator. An in-situ calibration technique has been developed to obtain the film cooling performance without disturbing the aerodynamic flow around the vane surface. Subsequently, the cooling performance of two types of shaped holes is measured at different positions over the entire surface. Firstly, a louver scheme was investigated on the convex surface of the suction side and on the concave surface of the pressure side. In addition, a proposed smooth expansion was investigated over the highly curved surface of the leading edge. The location of the hole has a high impact on the cooling performance due to the difference in curvature. The investigated blowing ratios slightly affect the cooling performance of the presented schemes due to the considerable reduction in the jet momentum that impedes the jet lift-off at exit. The shaped holes provide a higher net heat flux reduction compared with the similar cylindrical holes and other shaped holes in the literature. The contribution of this study will help to enhance the cooling performance in the next generation of gas turbines.

Acknowledgements

Praise be to GOD for giving me the patient and ability to complete my thesis.

This work would never have been completed without the help of a number of people who, in one way or another, made their contributions during this journey. First of all, I would like to give my deepest appreciation and gratitude to Prof. Hassan, my supervisor and mentor who has been my source of guidance and support in every step of my program and research style. You are not only my mentor but also my elder brother in my life in Canada. Without your contribution, I would not have been where I am and what I am. My appreciation is also to Dr. Kadem for his guidance and support in my degree program. I am also grateful for the support from Pratt and Whitney Canada (PWC). A deep thanks to the Egyptian defence Ministry for supporting my life in Canada. Secondly, I would like to thank my research colleagues in the research group at Concordia University. Special thanks to Dr. W. Saleh for assisting me in the experimental work and Dr. S. Kim and M. Rahman in the numerical designs. The graduated colleagues include C. Zhang, T. Ahmed, and M. Ghorab, the present members D. Bowden, O. Hassan, Y. Fan, C. Elayoubi, K. Cook, L. Ling, and H. Li, and the undergraduate students M. quan, A. Chaudhry, H. Assi, and H. Damlaj. Finally, I would like to thank my parents for their moral support in this endeavour. My wife Mai deserves a heartfelt thank for being by my side through all the ups and downs for the past eight years. Thanks also go to my elder daughter Mariam for her understanding of my working during some of the weekends when we should be together.

Table of Contents

List of Figures

List of Tables

Nomenclature

C	true chord, (m)
C_p	specific heat capacity at constant pressure, (J/(kg·K))
C_v	specific heat capacity at constant volume, (J/(kg·K))
C_x	axial chord, (m)
d	hole diameter, (m)
h	heat transfer coefficient with film cooling, (W/(m^{2}K))
h_o	heat transfer coefficient without film cooling, (W/(m^{2}K))
I	momentum flux ratio, $I = [(\rho v^2)_j/(\rho v^2)_m]$
k	thermal conductivity, (W/m·K)
l	hole length, (m)
L	actual chord, (m)
P	pressure, (kPa)
p	pitch, lateral distance between two holes, (m)
q	heat load, (W)
s	surface distance, (m)
T	temperature, (K)

T_i initial temperature of the surface, (K)

t time, (second)

v velocity, (m/s)

w thickness of the investigated surface (m)

Greek Symbols

α thermal diffusivity, (m^2/s)

β compound angle, (°)

γ specific heat ratio, $\gamma = C_p/C_v$

ε least square error

ϕ overall cooling effectiveness, $\phi = \dfrac{(T_m - T_w)}{(T_m - T_j)}$

η film cooling effectiveness, $\eta = \dfrac{(T_f - T_m)}{(T_c - T_m)}$

λ inclination angle, (°)

θ dimensionless wall temperature, $\theta = \dfrac{(T_m - T_j)}{(T_m - T_w)}$

ρ density, (kg/m^3)

τ color change time, (second)

Subscripts

c	coolant
elec	electric
f	film
h	heater
j	jet
loss	losses
m	main flow
o	total
p	pressure side
s	suction side
w	wall (surface)

Acronyms

BL	Boundary layer
Br	Blowing Ratio, $[(\rho v)_j/(\rho v)_m]$
DR	Density Ratio (ρ_j/ρ_m)
HTC	Heat Transfer Coefficient

IR Infrared

LBFS Laid-back fan shaped hole

NACA National Advisory Committee for Aeronautics

NHFR Net Heat Flux Reduction

P.R. Pressure Ratio (P_j/P_m)

PS Pressure Side

PIV Particle Image Velocimetry

PSP Pressure Sensitive Paint

RGB Red, Green, and Blue

ROI Region Of Interest

SS Suction Side

TLC Thermochromic Liquid Crystal

TSP Temperature Sensitive Paint

Chapter 1 – Introduction

Gas turbines are the power source for planes, power generation units, and many other applications. With an elevated importance on environmental sustainability and the depletion of fossil fuel resources around the world, it has become increasingly necessary to improve the efficiency and hence increase the power/weight ratio for the next generation of gas turbines. The inlet rotor temperature of the current gas turbines is typically near 1900 K, which is beyond the thermal strength of the material, and it is subjected to further increase in the next generation of the gas turbines. Therefore, innovative cooling techniques are essential in order to withstand this harsh thermal environment. The impingement cooling on the inner surfaces, the internal passage cooling, and the film cooling are the cooling techniques that have been used to increase the cooling capacity of the gas turbine airfoil, as shown in Figure 1.1. Heat transfer designers are concerned with the distribution of the heat transfer over the airfoil surface, shown in Figure 1.2, in order to optimize the cooling requirements for the airfoil. Film cooling is a technique whereby a stream of compressed air is injected onto the surface of gas turbine airfoil. As a result, a thin buffer layer of cool air insulates the airfoil surface from the harsh effects of the hot combustion gases. The buffer layer is maintained by a continuous stream of coolant which flows from the internal airfoil passages through a series of well-designed slots and onto the blade surface. Film cooling is used at both the pressure side and the suction side of the airfoil. Moreover, it is also used on the leading and trailing edges, blade tip, and the airfoil platform. Many factors play a role in the film cooling performance and they can be divided into three main groups:

1. Geometrical factors, such as the shape of the cooling hole exit, hole spacing and alignment, surface angle, compound angle, entrance length, and multiple row configurations.
2. Coolant and main stream ratios such as blowing, density, temperature, pressure, and momentum ratios. The blowing ratio $[(\rho v)_j/(\rho v)_m]$ is considered to be the main dimensionless number that describes the film cooling characteristics, where j and m are the jet and mainstream, respectively. Blowing ratios up to 0.7 are classified as low blowing ratio, 0.8 to 1.5 is moderate, while blowing ratios greater than 1.5 are considered high blowing ratios.
3. Flow characteristics, such as Reynolds number, main stream turbulence, and unsteady wakes.

Two parameters are considered to measure the performance of the film cooling holes, the cooling effectiveness and the heat transfer coefficient. Effectiveness is the measure of how the jet affects the surface temperature compared with the main stream temperature. While the heat transfer coefficient indicates the amount of heat transferred from the main flow to the surface.

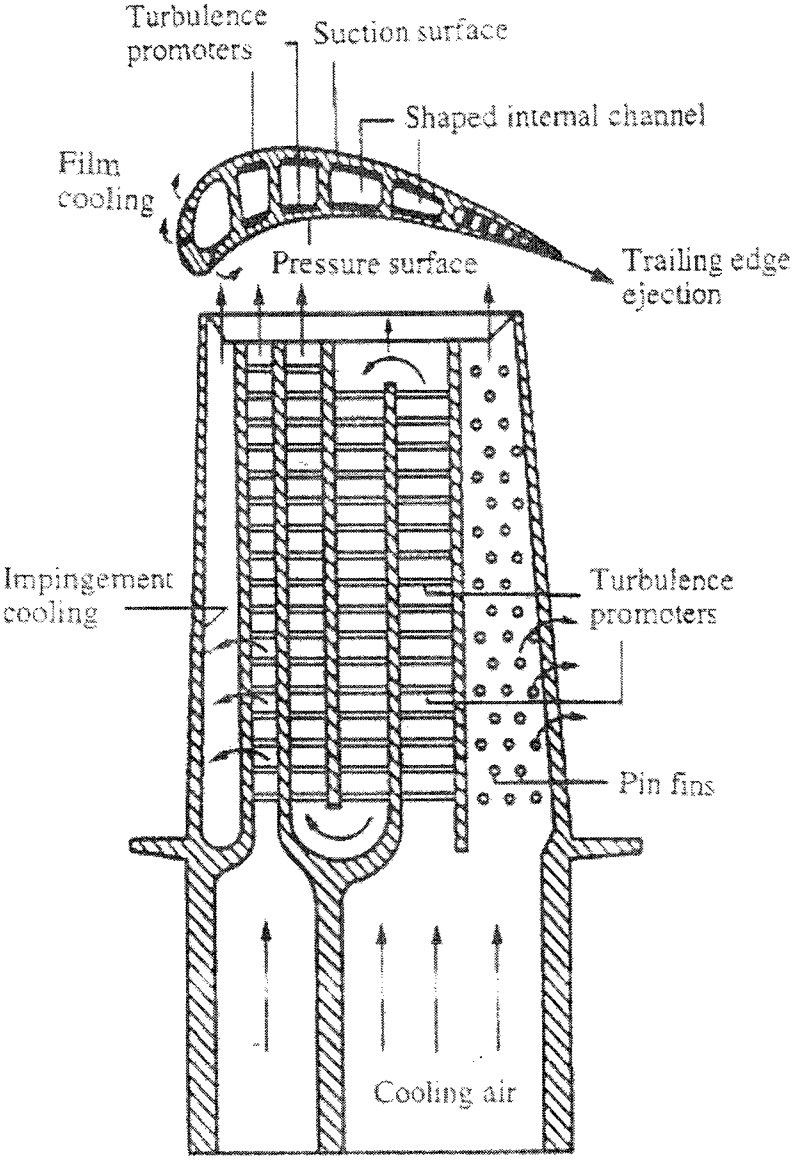

Figure 1-1 Cooling techniques used for gas turbine airfoil

(Han et al.1984)

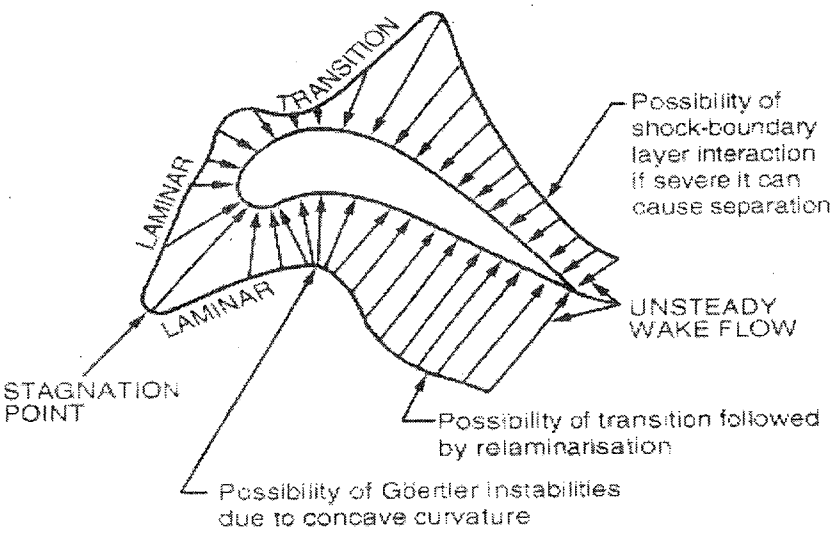

Figure 1-2 Variation of heat transfer rate around a turbine airfoil

(Daniels and Schultz, 1982)

1.1 Motivation

Many investigations have been conducted to optimize the film cooling geometry, aiming to maximizing the cooling effectiveness and minimizing the heat transfer coefficient. Those studies concluded the benefits of shaping the hole exit to improve the film cooling performance by decreasing the jet momentum in order to eliminate the jet lift-off. Due to the high demand of increasing the gas turbine cooling capacity, different hole shapes have been proposed to maximize the cooling capacity of the injected coolant, some of these shapes are shown in Figure 1.3. In addition, the lateral spreading of the exit trailing edge was increased in order to distribute the coolant and the thermal stresses to approach a slot-like performance.

Immarigeon and Hassan (2006) proposed the louver scheme, with the support of Pratt and Whitney Canada, to increase the airfoil cooling capacity. Zhang and Hassan (2008a) investigated numerically the geometrical parameters to optimize the film cooling performance and they presented a superior cooling effectiveness for the louver scheme. Continuing with numerical investigations, Zhang and Hassan (2008b) investigated the performance of the proposed scheme under a variety of conditions. Numerical simulations predicted that the louver scheme has better performance compared with different shaped holes in the literature, and an experimental investigation over a flat plate supported this finding, Ghorab (2009). However, measuring the performance over a real airfoil is highly required to evaluate the cooling performance of the proposed schemes with the curved surfaces.

In addition, the leading edge is characterized by the highest heat transfer rate over the entire surface of the airfoil and this region needs be provided with the proper cooling

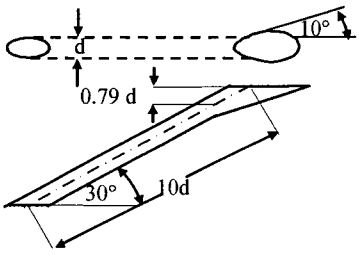

a) Laid back

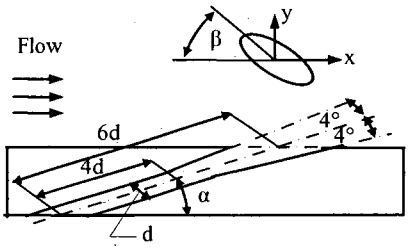

b) Conical exit

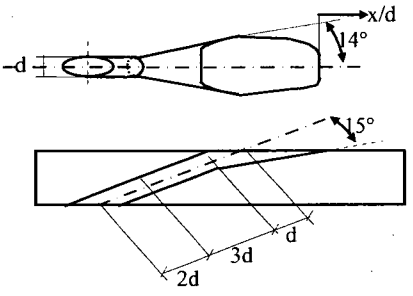

c) Laidback fan-shaped

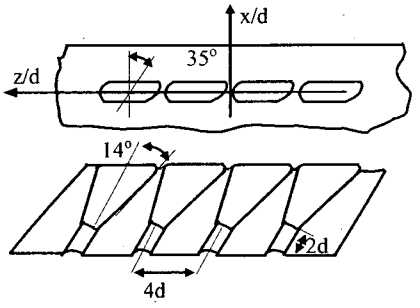

d) Shaped compound hole

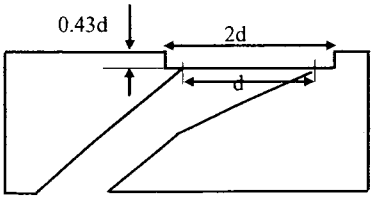

e) Shaped with trench

Figure 1-3 Different film hole schemes

capacity. A smooth expansion at the standard cylindrical hole is proposed to be used at the leading edge, just at the stagnant point of the gas turbine stator. The hole exit is designed such that the streamlines of coolant flow are expanded smoothly in all directions around the exit, distributing the coolant uniformly to provide more coverage.

1.2 Objectives and organization of the thesis

Based on the previous investigations, the louver scheme was examined numerically on an airfoil and experimentally on a flat plate. However, it was not examined experimentally over the curved surface of the airfoil. The principle objective of the present study is to investigate experimentally the cooling performance of unconventional cooling schemes on a gas turbine vane. The objectives of this study are:

- Design, re-construct, and commission a fully automated heat transfer test facility to investigate the heat transfer and aerodynamic characteristics of cooling schemes on gas turbine blades and vanes.
- Determine the heat transfer performance of the advanced louver film-cooling schemes on a vane in order to meet the cooling needs of the next generation of gas turbines.
- Investigate the film cooling performance of a new shape at the leading edge of a gas turbine stator.

The thesis consists of six chapters. This chapter introduces the film cooling technique and presents the motivations and objective of the present study. Chapter Two reviews previous studies that investigated the influence of the design and operating parameters on film cooling performance. The literature includes the studies that investigated the film cooling over a flat plate, curved surfaces on the pressure and suction sides of airfoil, and

the highly curved surface of the leading edge. The experimental test facility, the methodology, and the uncertainty analysis have been mentioned in detail in Chapter Three. The cooling performance of the louver scheme over the suction side and the pressure side is presented in Chapter Four. The performance of the louver has been investigated on different positions over a gas turbine vane in addition to the interactions between different staggered rows. The cooling effectiveness and the heat transfer coefficient have been presented in both the detailed local distribution and the lateral-average forms. Chapter Five presents a smooth expansion at the exit of the standard cylindrical hole that has been proposed to improve the cooling capacity at the leading edge. Two expansion levels in addition to two inclination angles have been examined and their cooling performances have been presented. The conclusion of the current investigation is presented in Chapter Six in addition to the recommendation for future works.

Chapter 2 – Literature Review

Several studies have been conducted to investigate the influence of different factors that have been mentioned in the previous chapter, on the film cooling performance. Most of the published studies presented the film cooling effectiveness only while actual engine airfoils are subjected to an additional heat load due to the heat transfer from the mainstream to the airfoil surface. In addition to those studies which focused on the cooling effectiveness, some of the studies that presented the enhancement in the heat transfer coefficient (HTC) along with the adiabatic cooling effectiveness are mentioned in the coming sections. Those studies were conducted over either a flat plate or over curved surfaces of vane and blade. Some studies focused on the cooling performance over the leading edge.

2.1 Film cooling over a flat plate

The cooling performance over a film-holed flat plate has been investigated in order to overcome some of the challenges associated with a true airfoil curved surface. The results of those investigations are considered as the primary key to understand the complexity of the interaction between the two streams, in addition to simplify the problem of solving three temperatures interaction flow. Some studies have been performed to evaluate the impact of the mainstream flow conditions. Others have been performed to investigate the effect of the geometrical aspects on the film cooling performance. Other studies have been conducted to measure the cooling performance using shaped holes.

2.1.1 Effect of flow conditions

Flow conditions have a great impact on film cooling performance. The properties ratios between the mainstream and the jet flow control the interaction between both streams. The pressure ratio is represented by the blowing ratio and the temperature ratio is represented by the density ratio to account for the huge difference between the realistic engine condition and the testing conditions. The blowing ratio is the main dimensionless parameter used to describe film cooling characteristics, and it is therefore explored in most of the studies.

The mainstream characteristics play an important role in the film cooling performance. Lebedev et al. (1995) studied the effect of turbulence intensity of the mainstream on the cooling effectiveness of a coolant injected from an annular slot in a tubular duct. They found that at low and moderate blowing ratios, the effectiveness decreased severely with the main stream turbulence, while higher blowing ratios provided more stability to the cooling effectiveness. The strong effect of turbulence was attributed to the lack of the velocity gradient inside the boundary layer and to the enhancement of the mixing process. While at higher blowing ratios, the energy of the turbulent flow was less than the average kinetic energy of the coolant injection, so the boundary layer was more stable with respect to external disturbances. The jet lift-off pushed the coolant away from the surface, hence the effect of the mixing process decreased. Al-Hamadi et al. (1998) studied the effect of turbulence intensity on the cooling performance of double rows injection. They reported that the heat transfer coefficient increased with turbulence level, while the cooling effectiveness decreased with more uniform coverage over the

protected surface. It was found that the compound angle provided better coverage than that obtained by the axial angle hole.

Investigating main-jet interaction ratios, Ekkad et al. (1997) used both air and CO_2 as coolants to investigate the effect of the density ratio on the cooling performance of three different orientation angles: axial, radial and compound. For axial injection, the higher density coolant provided higher effectiveness with a maximum performance at moderate blowing ratios. The compound angle provided more coverage and effectiveness than the axial injection at all blowing ratios, with the best performance also at moderate ratios. The lower density injection, however, performed better with the compound angle. They also found that the high-density injection reduced the heat transfer coefficient better than the low-density coolant, especially at higher momentum ratios.

Using the Thermochromatic Liquid Crystal (TLC) transient technique, Mayhew et al. (2003) investigated the effect of turbulence intensity on the cooling performance of cylindrical hole. They developed an in-situ calibration method to eliminate the variations in the hue values due to the light source intensity, illumination angle, and the camera viewing angle, where the hue value is the combination of the main color components (red, green, and blue). They implemented the median filtering to reduce the random uncertainty in temperature measurements. This uncertainty results from noise in the camera/frame grabber system in addition to any random noise in the spatial resolution of the captured image. They reported a decrease in the cooling effectiveness at low blowing ratios due to the increased mixing with the main flow. At high blowing ratios, the jet is lifted-off and the higher turbulence level increased the coolant mixing with the

mainstream. However, this mixing entrained some of the penetrated coolant back to the surface causing a slight increase in the effectiveness.

2.1.2 Effect of geometrical aspects

Jubran and Maiteh (1999) focused on two geometrical parameters, the compound angle of the hole exit, and the relative position between two successive rows. They found that the staggered rows provided better coverage over the protected area, with higher heat transfer coefficients than that of the inline arrangement. The compound angles at the hole exit showed better performance as the jet was more laterally spread when compared to the simple angle exit.

Using the steady TLC technique in two companion studies, Yuen and Martinez (2003a&b) experimentally investigated the effect of various streamwise angles on the film cooling performance and the heat transfer characteristics for a single row of cylindrical holes. They expanded their investigation by studying the interaction between two rows with various streamwise angles, Yuen and Martinez (2005a&b). The low inclination angle demonstrated better performance, as the jet momentum did not severely interfere with the mainstream flow and remained close to the wall. The low angle yielded higher heat transfer as the jet flow stayed closer to the wall. Steeper angles directed the jet to penetrate the main stream, causing high mixing with the main flow while reducing its cooling effectiveness. Jet penetration in the main flow reduced the surface interaction, thereby decreasing the heat transfer, particularly at moderate and high blowing ratios. The higher blowing ratios, for all inclined angles, allowed the jet to penetrate the main stream causing the cooling effectiveness to decrease and the heat transfer to increase. An increase in the blowing ratio caused the peak point of cooling effectiveness to travel

further downstream of the hole exit. The maximum increase in the heat transfer tended to occur near to the hole edge rather than the centerline, where the shear with the main stream was maximized. The steepest inclination angle of 90 degrees was not preferred for use in film cooling due to its high heat transfer and low effectiveness. However, it can be used in certain regions, such as near the leading edge where the incoming flow may force the jet close to the wall. The staggered rows gave better coverage and increased the effectiveness uniformity compared to the inline rows on the other side they increased the heat transfer at all blowing ratios. On the basis of providing the same coolant mass flow, they reported lower HTC for the double row injection compared with single row. The in-line arrangement showed lower averaged heat transfer than the staggered one; however the staggered arrangement provided a wider lateral coverage with more uniform distribution of the heat load over the surface.

Gritsch et al. (2005), using the infrared steady technique, investigated different geometrical parameters with a single fan shaped hole. They found that increasing the hole spacing to hole diameter ratio (p/d) significantly decreased the effectiveness, which matches with previous results. The decreasing of hole length to hole diameter ratio (l/d) and the hole coverage ratio (width of hole) insignificantly decreased the lateral-averaged effectiveness. Increasing the area expansion ratio (exit to inlet area) insignificantly decreased the lateral-averaged effectiveness at moderate and high blowing ratio. However, at a low blowing ratio, this finding was reversed due to less penetration from the weak jet momentum. It should be mentioned that these insignificant changes were within their experimental uncertainty. The most interesting finding in their work was the effect of the compound angle of the shaped hole. Increasing the compound angle in the

cylindrical holes increases the effectiveness but consequently the heat transfer coefficient decreases. In their study they reported a decrease in the effectiveness by increasing the compound angle, especially at high blowing ratios. They attributed this finding to the increase of the flow interaction on the windward side. They changed the symmetrical shaping by decreasing the windward side angle and keeping the leeward side angle as it was, and they reported a significant increase in the effectiveness.

2.1.3 Effect of hole shape

Using thermocouples in a steady state technique, Sen et al. (1996) compared the film cooling performance for 60 degree compound angled with axially oriented holes for both cylindrical and shaped exits. They found that the compound holes had higher cooling effectiveness and improved lateral distribution, while the shaped hole demonstrated better results. The shaped holes provided the best performance at all momentum flux ratios due to the decrease of jet momentum at the hole exit. Gritsch et al. (1998) compared experimentally the performance of three different cooling holes. The hole geometries included a laid-back fan shaped hole (LBFS), a fan shaped hole, and the standard cylindrical hole. Their findings emphasized the improved performance of the shaped holes, particularly for the LBFS geometry. The double modification on the hole geometry decreased the jet momentum and increased the lateral coverage.

Gritsch et al. (2000) measured the temperature distribution downstream of a single hole using an infrared camera. They reported a decrease in the heat transfer coefficient (HTC) using two different shaped holes compared with the cylindrical one, with a quantitative increase in all cases as the blowing ratio increases. Bell et al. (2000) used thermocouples to investigate the cooling performance of the same exit shapes in

addition to the effect of a 45° compound angle. They made similar observations and reported an additional increase in the HTC with the compound angle.

Using the naphthalene sublimation method, Cho et al. (2001) investigated the cooling performance of three hole shapes; laid-back hole, cylindrical hole with conical end, and standard cylindrical. Three different blowing ratios were investigated with three lateral injection angles; axial, radial, and compound at 45°. The radial injection provided the lowest peak effectiveness with the widest and the most uniform cooling distribution over the protected area. The hole with a conical end improved the effectiveness compared to the shaped and cylindrical holes due to the decrease in the jet momentum and the well attached coolant to the surface. In addition, the conical hole provided the lowest heat transfer to the surface due to the decrease in the jet velocity that yielded to less diffusion of the coolant into the boundary layer. The low blowing ratio had an insignificant effect either on the effectiveness or on the heat transfer coefficient because of the suppressed jet that was fully attached to the surface. Increasing the blowing ratio caused a severe jet lift-off and lower effectiveness on the cylindrical exit with axial injection. The shaping of the hole exit decreased the effect of the blowing ratio causing an increase in the effectiveness due to the increase in the delivered coolant amount. The net heat flux reduction (NHFR), the ratio between the heat transferred to the surface with film cooling to that without film cooling, reflected the decrease in the surface protection with the high blowing ratio due to the increase in the heat transfer rate and the corresponding jet lift-off.

Using the TLC transient technique, Yu et al. (2002) compared the cooling performance for cylindrical, fan-shaped (laterally diffused) and LBFS axially oriented film cooling holes. The film cooling effectiveness and lateral coolant coverage were

significantly increased immediately downstream of the shaped holes and mainly at higher blowing ratios. The reduction of the mean velocity of the coolant jet at the hole exit caused lower jet momentum enabling the main stream momentum to force the coolant to flow closer to the surface. The shaped holes demonstrated lower heat transfer than the cylindrical holes due to reduced shear mixing of the injection jet with the mainstream. The LBFS holes provided higher values of spanwise averaged effectiveness and lower values of spanwise averaged heat transfer coefficients than the laterally-expanded holes. However, the former has a tendency to allow hot mainstream ingestion into the windward portion of the hole exit. The cylindrical and fan-shaped holes provided similar results due to the similarity in the interaction flow features, which were supported by flow visualization. In their study they discussed two competing mechanisms that affect the heat transfer around the film cooling holes. Indeed, the injection of coolant delivers more mass flow to the boundary layer and it has also a momentum component in the normal direction to the wall. The first mechanism, the boundary layer thickness, is increased by adding flow mass. Thickening the boundary layer provides more heat convection resistance between the mainstream and the protected surface yielding to a decrease in the HTC. The second, the normal momentum, increases the interaction between the injection and the mainstream. Therefore, the flow shear induced by the interaction enhances, yielding an increase in the HTC. By observing the flow visualization, the cylindrical hole provided the greatest boundary layer thickness as well as flow shear. The LBFS hole presented the opposite extreme while the laid-back hole was mid-level between both geometries. The ultimate combination of both factors resulted in the LBFS exit providing lower heat transfer compared with the cylindrical exit with a heat transfer slightly lower

than that of the lateral shape. Using the infrared transient technique, Gritsch et al. (2003) investigated the same hole geometries at higher Mach numbers up to 0.6. They ended up with the same findings and reported a decrease in the cooling effectiveness with an increase in the Mach number.

Huiren et al. (2004) investigated the effect of two hole shapes in addition to the standard cylindrical exit on the heat transfer using a stainless-steel foil and heater technique. They reported an increase in the film cooling HTC with further increase at higher turbulence intensity. Increasing the blowing ratio led to an increase in the HTC. This was because of the jet blockage effect that allowed narrower passage for the mainstream causing higher velocity, hence higher HTC. Another reason was the increase in the coolant amount that allowed a merge between adjacent jets, causing higher disturbance.

Using air and CO_2 as coolants, Guangchao et al. (2008) studied the effect of the density ratio on the cooling performance of three different hole geometries: cylindrical, fan shaped, and fan shaped in both the inlet and the exit of the cooling hole. For all investigated geometries, the higher density coolant provided the highest effectiveness accompanied by a slight increase in the heat transfer. The total heat load is then decreased, supporting the findings of Ekkad et al. (1997). The fan shaped hole yielded the highest effectiveness compared to both other shapes at all mass flux ratios. The heat transfer of the fan shaped hole was also the lowest yielding to the lowest heat load especially at near downstream of the hole exit.

2.2 Film cooling over an actual airfoil

The previous section described the studies that were conducted on a flat plate; however the flow physics on highly curved surfaces, such as an actual turbine airfoil, differs from the one on a flat surface. Therefore, several research studies have been conducted to investigate and quantify the film cooling performance over actual curved surface of the turbine airfoils. Similar to the investigations over the flat plate, some studies have been performed to investigate the mainstream flow conditions, some investigated the change of the geometrical aspects and the airfoil curved surface effects, and others were performed to measure the cooling performance of the shaped hole.

2.2.1 Effect of flow conditions

The vane (stator) endures high thermal stresses, as it is the first part subject to the hot stream after the combustion chamber. Nirmalan and Hylton (1990) experimentally investigated the film cooling performance over the turbine nozzle guide vane. Pressure measurements were also done for all cases: with and without film cooling, and with and without leading edge shower. The suction side in all cases affected the pressure distribution, while the pressure side had only minor effects on the pressure distribution, far downstream along the mid span. This type of pressure distribution allowed for a steady heat transfer coefficient on the pressure side with varying Mach numbers, while the heat transfer increased with the Mach number on the suction side. Two main mechanisms, thermal dilution and turbulence augmentation, characterized the heat transfer coefficient at the vane surface. The injection process itself caused an increase in the turbulence level by disturbing the main boundary layer, causing an increase in the heat transfer coefficient. Injection of warmer gas caused the thermal dilution to decrease

with reductions in the heat transfer coefficient and the thermal effectiveness. The dilution level increased the dependency of the film cooling performance on the interaction between the two flows blowing strength, Mach number, and exit Reynolds number.

Ames (1998) investigated the influence of the turbulent intensity over a gas turbine stator using a four-vane cascade. He found that increasing the turbulence intensity caused a decrease in the adiabatic cooling effectiveness. The local values of turbulence had a high level, such that it had a significant effect on the pressure side and showerhead region. On the suction side, the local values of the turbulence had a low level so its effect was less pronounced. The high local values of the turbulence along with the favorable pressure gradient on the pressure surface caused a rapid decrease in the effectiveness. Staggered rows caused a moderate increase in the effectiveness over that estimated from superposition of individual rows.

Drost and Bolcs (1999) investigated the film cooling performance over a gas turbine stator using the TLC technique. They found that the injection into the laminar boundary layer (BL) provided higher effectiveness if compared with injection into the turbulent BL. In agreement with Ames (1998), they founded that the turbulence had a weak influence on the suction side. The lower density injection yielded lower effectiveness on both suction and pressure sides. They also reported that the double injection improved the cooling effectiveness over the effectiveness expected by superposition of individual rows. They reported an increase in the heat transfer coefficient with the increase of both the blowing ratio and the number of rows used on the suction side. On the pressure side, they used only compound angle holes, which gave a higher HTC compared with the axial orientation hole on the suction side. They

examined the influence of the turbulence intensity on the performance of both sides and they reported an increase in the heat transfer on the suction side while a decrease on the pressure side by increasing the turbulence intensity. They also observed that the heat transfer enhancement increased on the suction side and decreased on the pressure side at a lower density ratio.

Ethridge et al. (2001) investigated the performance of cylindrical holes at two different density ratios and two different turbulent intensities over the suction side of a gas turbine stator. They reported a decrease in the effectiveness as the density ratio decreased at moderate and high blowing ratios, with a reverse trend at low blowing ratios. They observed a decrease in the effectiveness by increasing the turbulent intensity at higher blowing ratios, while there was no effect at low blowing ratios. The fact that the jet remained attached to the surface at low blowing ratio yields to the stability of cooling performance at high turbulent intensities. The turbulent intensity showed decay in this effect by increasing the momentum flux ratio over 0.9 in other studies, such as Drost and Bolcs (1997), which was not observed in the investigation of Ethridge et al. They attributed this to the highly curved surface of their vane, which prevented high turbulent eddies from getting back to the surface after the lift-off.

Similar to the flat plate investigations, Ethridge et al. (2001) experimentally investigated the effect of the density ratio and main stream turbulence on the cooling performance of cylindrical holes along the vane suction side. They found that at low blowing ratios, there is an effectiveness peak just downstream of the hole followed by a rapid decay. For moderate blowing ratios, the peak was moved downstream by a distance equivalent to double the hole diameter, due to local jet lift-off, however the momentum of

the main stream was strong enough to rapidly reattach the coolant to the surface. For higher blowing ratios, the jet momentum was large enough to penetrate the main stream, such that the effectiveness just downstream of the hole was less than that of the moderate blowing ratio. Far downstream, the jet reattached to the surface, causing a better recovery of effectiveness than that of the moderate blowing ratio. The higher density ratios provided better effectiveness, as the coolant tended to remain attached to the surface at all blowing ratios, supporting results obtained by Ekkad et al. (1997). The turbulence intensity decreased the effectiveness due to the dispersion effect of turbulent flow on the coolant. However, they found that there was a decrease in the effectiveness at higher blowing ratios, which contradicts previous studies conducted on the flat plate, such as that by Lebedev et al. (1995). The turbulence dispersion forced some of the detached coolant back onto the flat plate surface, while the coolant lifted much further from the vane surface, so turbulence eddies could not force the coolant back onto the surface.

2.2.2 Effect of geometrical aspects and surface curvature

Comparing the cooling performance on different surfaces, Schwarz and Goldstein (1989) investigated experimentally the film cooling performance on a concave surface that simulates the pressure side. Soon after, Schwarz et al. (1991) performed a similar experiment on a convex surface and combined both observations to conclude the factors that mainly affect the flow on curved surfaces. They found that the curved surfaces of the airfoil caused a difference in performance between the concave surfaces and the convex surfaces. The concave surfaces causing instability in the flow yielded a reduction in the effectiveness. In addition, the cross-stream pressure gradient changed from the concave surface to the convex surface, causing additional jet lift-off over the concave surfaces.

Drost and Bolcs (1997) measured the temperature distribution downstream a row of circular holes on a flat plate using the TLC transient technique. They observed an increase in the normalized HTC by increasing the blowing ratio. They implemented the same technique on a five-airfoil cascade to investigate the film cooling performance on both pressure side and suction side. They reported an increase in the normalized HTC for both sides with a significant increase on the suction side. In the same test facility, Reiss et al. (1998) discussed in details the experimental procedure and the calibration method used. They also compared the results obtained from the transient method with that obtained from the adiabatic wall method (steady method) and they found a consistency between both findings.

Colban et al. (2006) investigated the effect of the boundary layer transition location, surface curvature, acceleration, and hole spacing on the film cooling performance at different blowing ratios. The heat transfer peaked in the stagnation region, followed by a decrease on the pressure side, to a distance lower than 25% of the vane chord, where the heat transfer became constant. On the suction side, the heat transfer decreased until the boundary layer transitioned from laminar to turbulent. This transition caused a sudden increase in the heat transfer, exceeding the peak value at the stagnant region, followed by a decrease caused by the boundary layer development. The boundary layer transition position differs along the suction side of the vane according to the location of the film-cooling injection. Jet lift-off increased with the blowing ratio on both sides of the vane surface, reducing the cooling effectiveness. The convex shape on the pressure side, however, allowed the jet to reattach to the surface. The presence of the upstream showerhead increased the turbulent diffusion of the jet to the vane surface,

causing an increase in the effectiveness. However, the increase in the showerhead blowing changed the direction of the jet, and reduced its lateral spreading.

To enhance the film cooling performance, Zhang and Moon (2007) investigated the effect of hole location on the cooling performance of the blade on the pressure side. Three rows of cylindrical holes were examined individually in addition to the combination of two rows and the full coverage as well. The velocity changes along the mid-span of the blade yield changes in the blowing ratios along each row for the same mass flow ratio. Because of these changes, the jet lift-off tends to attach more to the blade surface as the row position approaches the trailing edge, yielding a higher effectiveness value and longer coverage. The combination of two rows increases the effectiveness coverage just downstream of the second row. The accumulation of both injections further downstream increases the effectiveness and the uniformity of the coverage. The full coverage gives better cooling for the blade. This coverage is higher than the one expected from the superposition method for the individual rows. The higher performance was attributed to the high turbulence intensity and high curvature of the pressure side, allowing the combined injection to overcome the disturbances.

With the same facility as Ethridge et al. (2001), Waye and Bogard (2007) investigated the performance of axial and compound cylindrical holes at different turbulent intensities, density ratios, and hole spacing. They found that effectiveness doubled by decreasing the hole spacing to half. Using PSP, Zhang and Moon (2007) investigated the effect of shaped hole location on the cooling effectiveness over a blade pressure side in a linear cascade. They found that the effectiveness dropped quickly downstream of the injection point. They noticed an increase in the effectiveness of the

downstream single row compared with the upstream rows. They also reported an increase in the effectiveness downstream of the second row in the double injection compared with the single injection.

Mhetras et al. (2007) studied the variation of the flow parameters on the cooling performance of the full coverage blade. They found that the pressure side is sensitive to changes in blowing ratio, while the suction side is nearly unaffected. The cooling traces, however, are longer on the suction side. The pressure gradient in the cooling cavity affects the uniformity of the cooling on the pressure side. As the coolant is injected from the hub side, a region of stagnant pressure is formed in the cooling cavity near the tip side. Over the blade surface, the pressure distribution is nearly the same along the span of the blade, resulting in a larger pressure difference across the hole ends near the tip, and an increase in the resultant blowing ratio. The formation of a vortex near the tip region affects the distribution of the cooling effect and pushes the cooling effect away from the tip region. Finally, they found that increasing the Mach number does not significantly affect the cooling coverage at the same blowing ratio.

Chappell et al. (2008) studied the effect of the hole orientation on cooling performance using cylindrical and fan-shaped holes on the gill-region of the vane suction side. The cylindrical axial holes provided lower effectiveness and less coverage, while the shaping of such axially oriented holes, or reorienting the cylindrical holes, improved the effectiveness while increasing the costs. The best solution was found to be tilting the hole orientation to be radial, which improved the effectiveness with lower manufacturing costs. They reported an increase in the HTC of the shaped hole compared with the axial cylindrical hole but lower than that of radial and compound angles.

2.2.3 Effect of hole shape

Teng et al. (2001) studied the effect of hole shapes on the heat transfer distribution over the blade surface. They found that the cylindrical shape has the highest heat transfer just downstream of the injection point compared to the other shapes. The shaped holes decrease the momentum of the jet so it tends to stay attached to the surface. The mixing between both streams decreases, hence the heat transfer decreases. The jet attached to the surface induces earlier boundary layer transition from the laminar to turbulent region, causing a higher heat transfer further downstream of the shaped hole. As the blowing ratio increases, the jet penetrates further through the main stream, and the mixing between both flows increases, resulting in an increase in heat transfer. They reported better heat transfer enhancement of the two shaped holes compared with the cylindrical exit. The increase of the blowing ratio increases the heat transfer enhancement especially far downstream the injection location.

Investigating the hole exit shape on the vane film cooling performance, Dittmar et al. (2003) studied the cooling performance of different cooling hole configurations. They investigated the performance of double rows of cylindrical holes, double rows of discrete slots, a single row of axial fan-shaped holes, and a single row of compound angle fan-shaped holes, using a large scale suction side of turbine guide vanes. They found that at low blowing ratios the effectiveness of all configurations had close values along the streamwise direction. By increasing the blowing ratio, the fan-shaped holes provided better effectiveness than the cylindrical or slot holes. The fan-shaped exit hole decreased the jet momentum, while the other shapes caused jet lift-off. Jet penetration increased dramatically with an increase in blowing ratio, and caused a decrease in the effectiveness

just downstream of the cylindrical and slot holes. The main stream momentum forced the jet to reattach to the vane surface, causing an increase in the effectiveness. Further downstream, the mixing between both flows increased, yielding the normal decrease in effectiveness. The shaped holes improved the cooling effectiveness, with an increase in heat transfer due to the flow separation in the expanded part at the exit, which increased the turbulence kinetic energy. The increase in turbulence, transported to the boundary layer downstream of the injection hole, increased the heat transfer coefficient. They reported an increase in the HTC just downstream of the hole while the double row injection caused a reduction on the heat transfer enhancement compared with the single row. The cylindrical geometry caused a wake region right behind the injection, yielding a complex vortex generation. This vortex caused the transportation of the hot mainstream to the vane surface. The use of slot geometry reduced this effect causing a decrease in the heat transfer. NHFR showed that the moderate blowing ratios yielded the highest cooling effect just downstream of the exit for all hole shapes. The higher blowing ratios provided the best thermal protection at mid-location and further downstream.

Using the PSP technique, Gao et al. (2008) measured the cooling effectiveness of axial fan-shaped laid-back hole along both sides of a turbine blade. They found an increase in the cooling effectiveness on the suction side compared with that on the pressure side with a noticeable reduction on both due to the presence of upstream wakes. Soon after, they measured the effectiveness of the compound angle shaped hole (2009). In both works, the effect of the upstream wakes was investigated at four different phase locations along the pitch-wise direction to simulate the relative locations of the stator with the moving blade. The laid back forward expansion helped the coolant to stay close

to the surface, and the lateral expansion reduced the coolant momentum, such that the mainstream-jet interaction was decreased. The results showed that the upstream wakes affected the performance at the midspan, while the tip leakage and end wall vortices affected the performance at the near hub and near tip regions. The shaped holes produced better coolant coverage on both sides of the blade except for those regions affected by the secondary vortices on the suction side, which swept the coolant to the midspan region. The tip leakage flow from the pressure side goes towards the suction side directed the coolant towards the tip on the pressure side. The convex surface of the suction side produced a favourable pressure gradient and flow acceleration that helped the coolant to stay close to the surface. On the other side, the concave surface of the pressure side caused flow separation, resulting lower film coverage compared with that of the suction side. The moderate blowing ratios showed better effectiveness on both sides near downstream of the shaped hole. Further downstream, higher blowing ratios provided wider coverage. The compound angle gave better performance than the axially oriented hole as the main stream redirects the flow to the stream wise direction providing better coverage, especially at higher blowing ratios. Variations in the blowing ratio showed a steady increase in effectiveness on both sides for the given wake phase locations. The presence of the stationary upstream wake resulted in lower film cooling effectiveness on both sides as the mixing between the coolant and mainstream was enhanced by the wakes. The effectiveness was lower as the wakes were more attached to the blade surface, and the effectiveness increased as the wakes were far from the surface.

2.3 Film cooling using non-conventional shapes

The above studies presented the benefits of shaping the hole exit in improving the film cooling performance and increasing the cooling capacity of an airfoil surface. Due to the high demand of increasing the gas turbine cooling capacity, different hole shapes had been proposed and their cooling performance were presented. Besides the standard cylindrical cooling hole and the well-known shaped injection hole, some research was conducted to present new hole shapes to improve the cooling performance and to reduce the cooling air flow. The complex exit shapes may lead to manufacturing constraints and high machining cost, however progress in the machining processes encourages such trend.

Immarigeon and Hassan (2006) proposed the louver scheme, with the support of Pratt and Whitney Canada, to increase the cooling effectiveness downstream of the injection point by shaping the hole exit. They investigated numerically the geometrical parameters to optimize the film cooling performance and they presented a superior cooling effectiveness for the louver scheme. Zhang and Hassan (2006a&b) investigated the performance of the proposed scheme under a variety of conditions. They investigated the performance of the new scheme with different multi-row arrangements, two inline rows, two staggered rows, and three staggered rows. The two staggered rows provided more lateral coverage, hence more uniform thermal stresses in addition to the heat transfer improvement. The three row arrangement provided a slight increase in the effectiveness compared with two rows. Therefore, they recommended two rows with smaller pitch rather than three rows even though there is a significant improvement in the heat transfer. Moreover, the coolant passes through a bend before being delivered to the

shaped exit, decreasing the jet momentum and hence minimizing the jet lift-off. Another advantage of the louver is the impingement of the coolant on the blade surface inside the bend, which also enables further cooling upstream the injection point.

Another scheme was introduced by Okita and Nishiura (2007). They numerically and experimentally investigated an arrowhead shape as a new geometry for film cooling holes, and compared its performance with that of the fan shaped holes on both sides of a turbine blade. The new shape showed an increasing performance with the blowing ratio on the suction side, however the fan-shaped hole shows a peak effectiveness at moderate blowing ratio (Br = 1.2) with less performance than that of arrowhead shape after this peak. This performance was attributed to lower penetration of the jet in the arrowhead shape, which decreased the mixing between both streams. Both shapes demonstrated better effectiveness on the pressure side than on the suction side, as the higher pressure of the main stream forced the jet to remain attached to the surface. The new shape, however, had a slightly better performance. The position of film holes also affected this performance. The main stream was continuously accelerated after the injection point on the pressure side. It started to accelerate upstream of the injection point to a peak velocity followed by deceleration downstream of the injection on the suction side. The numerical investigation showed that the jet was well attached to the surface with better lateral diffusion in the case of new shape compared with the fan-shaped hole. The interaction between the arrowhead jet and the main flow generated a counter rotating vortex pair structure in the jet that opposed the rotation of the vortex pair generated in the main flow, enhancing the performance of the coolant.

Guangchao et al. (2008) used thermocouples to investigate the cooling performance of a 3-in-1 hole with shaping at the inlet section as well as at the exit section. They compared its performance with the cylindrical and fan shaped hole and they concluded that the best reduction in the HTC was achieved by using the fan shaped hole with an increase in the HTC as the momentum flux increased.

Using a transient infrared technique, Lu et al. (2009a&b) investigated the cooling performance of cylindrical holes with different crater depths with a numerical study to clarify the jet-mainstream interaction. They compared three different crater arrangements that may be formed when blades are coated with a thermal barrier coating, with a baseline cylindrical hole, a trenched hole, and a shaped hole. The cratered holes achieved good film cooling effectiveness enhancement, especially at low blowing ratios, compared to standard cylindrical holes. They reported an increase in the HTC by using the cratered holes compared with the fan shaped holes but still lower than that of the cylindrical holes. The numerical prediction showed that a weaker jet vortex was formed compared to that formed with a standard cylindrical hole.

Developing the numerical investigation over the curved surface of a symmetrical airfoil, Zhang and Hassan (2009) investigated the louver scheme effectiveness under transonic and supersonic conditions. The convex surface of the airfoil along with the flow acceleration created a favourable pressure gradient. This gradient forced the jet to stay close to the surface causing better performance on the convex surface compared with the flat plate. They presented an increase in the effectiveness due to an increase in the blowing ratio, along with a severe reduction in effectiveness due to the shock wave formation. Ghorab (2009) experimentally measured the film cooling performance of the

louver scheme over a flat plate compared with different cooling schemes. The centerline and lateral average HTC of the louver scheme provided lower values compared with the circular hole and similar values compared with the shaped hole. In addition, the blowing ratio had an insignificant effect on the HTC. These studies were performed on a flat plate to examine the performance of the new shapes, and their performance has not yet been examined on the curved surface of an airfoil.

2.4 Leading edge film cooling

The leading edge is extremely exposed to the hottest flow temperature resulting in the highest heat transfer coefficient over the entire airfoil. Despite protecting the leading edge from the hot gases, film cooling disturbs the boundary layer and affects the aerodynamics and heat transfer over the entire airfoil. Moreover, the stagnation film cooling includes additional aspects of a highly accelerated flow with a thin boundary layer, accompanied with injection at angles almost opposite to the cross flow. Due to these tremendous challenges, it is important to evaluate the benefits of film cooling and its effect on the heat transfer criteria at the leading edge. Therefore, many studies have been conducted to investigate the cooling performance at this critical region either on an airfoil cascade or on simulated surfaces.

2.4.1 Half cylinder model

Simulating the leading edge as a half cylinder, Mehendale and Han (1992) experimentally studied the effect of hole geometry and turbulence intensity on the leading edge film cooling performance. They found that without injection, the heat transfer reduced with the distance downstream of the stagnation line until the point of separation due to the growing of the boundary layer. The heat transfer slightly increases downstream

of the separation due to flow reattachment. With injection, there was a heat transfer peak just downstream of the hole, due to the interaction between both flows followed by a decrease in heat transfer due to the increase of the boundary layer thickness. Increasing the blowing ratio increased the interaction between both streams downstream of the hole trailing edge, hence increasing the heat transfer. Farther downstream, the effect of the blowing ratio was less distinguishable. The moderate blowing ratio gave the best lateral cooling performance as it was neither weak enough to be diluted in the mainstream nor strong enough to deeply penetrate through the mainstream. The heat transfer was found to decrease with increasing hole spacing as was the effectiveness, because of less flow interaction and less coverage. As the mainstream turbulence increased, the flow fluctuations penetrated more through the boundary layer hence the heat transfer increased. However, the effect of the turbulence reduced with the increase of the blowing ratio due to the severe jet lift-off that leads the coolant away from the surface. In addition to the heat transfer increase, the effectiveness decreased with the mainstream turbulence as the dilution of coolant in the main flow increased. Using the same model, Ou and Han (1992) obtained the same findings for slot holes.

Salcudean et al. (1994) experimentally investigated the effect of coolant density through single and double row injections on the film cooling effectiveness over a half cylindrical model. They found that the position of the holes in the stream wise direction affected the effectiveness as each position had its own pressure gradient, local velocity, boundary layer thickness, and local static pressure acting on the hole. The effectiveness of air as a coolant is better than that of the CO_2 near downstream of the injection for all blowing ratios, with a peak value at moderate ratios. This peak value changed with the

variation of hole position. The effectiveness of both coolants decreased farther downstream, with better performance for CO_2 injection at higher blowing ratios. Due to the difference in local static pressure for each row of holes, the coolant flow rate on the front row severely dropped at lower blowing ratios, especially at higher density ratios. The two rows in line rather than the staggered holes improved the effectiveness for moderate and higher blowing ratios. However, this arrangement is not favorable from an internal cooling point of view rather than the structure integrity.

Hoffs et al. (1997) measured the cooling performance of the showerhead with three-row and four-row configurations over a cylindrical model using the TLC technique. They reported a decrease in the cooling effectiveness with the blowing ratio accompanied with an increase in the heat transfer coefficient. They found a strong decrease in the effectiveness with the positive incident angle at low blowing ratio. This investigation is the expansion of the study of Karni and Goldstein (1990). They varied the injection location relative to the stagnation line using one row injection. They reported a significant change in the mass transfer distribution with the change of the injection location.

Reiss and Bolcs (2000) measured the cooling performance of three different cooling hole shapes on the showerhead region at two different Mach numbers. They reported a decrease in the effectiveness by increasing the Mach number due to the thinner boundary layer associated with the high velocity mainstream. The jet then has more of a tendency to penetrate through the thinner boundary layer with different penetration degrees for each exit shape. With a more expanded exit, the jet penetration is reduced and the effect of Mach number becomes insignificant.

2.4.2 Highly curved model

All the aforementioned studies were done on the model of a cylinder in a cross flow. This model simulates the leading edge region with certain approximation downstream of the hole due to the difference of curvature between the cylindrical model and the airfoil profile. Modeling the leading edge as an elliptic surface, York and Leylek (2002a,b,&c) numerically investigate the cooling performance of standard cylindrical hole and diffused shaped hole at the stagnation line. They found that the higher blowing ratios, limited by Br = 2, provided higher effectiveness with better lateral coverage when injected from the stagnation line for the cylindrical hole. Contrarily, the higher blowing ratios had lower effectiveness if injected from the downstream rows, because of the lower local static pressure that allowed the jet lift-off. In both locations there was a heat transfer augmentation increase with the blowing ratio due to the corresponding increase in the flow interaction, particularly for the confronting flows. They also reported an increase in the effectiveness with the diffused exit, however it was accompanied by an increase in the flow ingestion downstream of the hole exit.

Investigating the hole exit shape, Weigand et al. (2006) experimentally studied the cooling performance of different showerhead cooling geometries (cylindrical, fan-shaped, and conical), on a blunt body using TLC technique. The heat transfer without film cooling showed a peak at the stagnation point, and decreased as the boundary layer thickness increased, until the point of separation then a sharp increase due to reattachment of the flow, similar to the findings of Mehendale and Han (1992). They found that the hole presence, in the case of no injection, provoked a transition in the boundary layer, leading to a strong enhancement in heat transfer just behind the hole.

Especially for shaped holes, this increase changed with the change in the hole geometry. The conical shape showed the best effectiveness over a wide range of blowing ratios with moderate heat transfer compared to other geometries. The fan-shaped gave the best lateral coverage with the highest heat transfer, especially at higher blowing ratios. The cylindrical shape gave the lowest lateral coverage at higher blowing ratios.

Using the PSP technique with a linear cascade, Zhang and Moon (2006) measured the cooling performance of the showerhead with different geometrical aspects with the same coolant amount. They found that reducing the injection compound angle or increasing the hole diameter improved the cooling effectiveness.

Lu et al. (2007) studied the effect of the hole angle and shape on the cooling performance of turbine blade showerhead film cooling using a blunt body model. They found that the peak effectiveness just downstream of the hole decreased with an increase in the traverse angle of the cooling hole, with better performance far downstream. At low blowing ratios, however, the effectiveness increased with increasing traverse angle. Higher blowing ratios resulted in lower enhancement of heat transfer, as the jet lift-off caused less mixing between both streams, and hence less turbulence. The effect of the blowing ratio variation was small compared to the effect of the injection itself. The shaping of the hole helped to reduce the jet lift-off and decreased the lateral momentum, improving the effectiveness. The heat transfer was also enhanced with the shaping of the hole, however this enhancement was not significant compared to the gained effectiveness, resulted in a lower heat flux reduction ratio.

Using the PSP technique and a blunt body model, Gao and Han (2009) also studied the effect of the hole angle and shaping on the cooling performance of seven-row and three-row showerhead cooling. In the stagnation regions for all geometries, the mainstream momentum was small, so the coolant ejected along the radial direction without deflection provided the poorest effectiveness. For the next rows, the mainstream momentum increased causing a noticeable deflection in the cooling jet along the streamwise direction, improving the coverage and effectiveness. This deflection decreased with increasing blowing ratio. The effectiveness of the compound angle was less than the radial injection due to the smaller relative angle between both flows. As the relative angle was reduced, the jet deflection reduced as did the spreading of the coolant, especially at higher blowing ratios. The radial shaped holes provided the best effectiveness among all the tested geometries as the expansion shape reduced the momentum of the jet and the radial injection provided more coolant spreading. The lower showerhead density provided similar behavior as the heavy one with lower effectiveness at the same amount of coolant flow because of more coolant accumulation from row to row at higher showerhead density.

Islami et al. (2010) numerically investigated seven different film cooling holes at the leading edge with two rows, one on the pressure side and the other on the suction side. They found the coolant trace on the suction side was much longer with lower effectiveness than that on the pressure side. The sidewall boundary layer of the hole passage arose a pair of kidney vortices that pushed the coolant upward and pulled the hot gases towards the surface yielding to jet lift-off. The convex surface produced a favourable pressure gradient that allowed the coolant to reattach close to the surface far

downstream yielded to a long trace. On the pressure side, the pressure difference between the far-field cross-flow and the lowered pressure in the wake downstream the trailing edge of the hole yielded a strong reverse flow just downstream of the hole. This reverse flow acted as a cross-flow, causing an anti-kidney vortices pair. This anti-vortex pair located underneath the jet near to the surface and tended to suppress the jet vertical velocity at the centerline and near downstream the hole edge, therefore further jet lift-off was prevented on the pressure side. The concave surface of the pressure side caused a flow separation due to the adverse pressure gradient, yielding to a shorter trace. Shaping the hole exit generally increased the cooling effectiveness with different mechanisms according to the shape geometry. The cylindrical hole with the trench increased the strength of the vortices with tendency to laterally spreads rather than vertically penetrates especially on the suction side. Diffusing the hole exit reduced the jet velocity in addition to reducing the strength of the formed vortices yielding overall enhancement on the effectiveness on both the pressure and the suction sides. The conical hole caused a spread in both stream and spanwise direction, yielding an effectiveness enhancement on both sides.

2.5 Summary

Many studies have been performed to investigate the film cooling and to explain this complex flow interaction. The studies over the flat plate explain the effect of the mainstream flow characteristics and its ratio with respect to the similar characteristics of the jet on the film cooling performance. (e.g. Lebedev et al., 1995, Bons et al., 1996, Ekkad et al., 1997, Al-Hamadi et al., 1998, and, Bell et al., 1999, Hale et al., 2000, Jung and Lee, 2000, Mayhew et al., 2003, Coulthard et al., 2006, and Aga et al., 2008). Some

other studies investigated the effect of the geometrical aspects or the effect of hole shape on the cooling performance (e.g. Sen et al., 1996, Jubran and Maiteh, 1999, Bell et al., 2000, Cho et al., 2001, Yu et al., 2002, Huiren et al, 2004, Yuen and Martinez, 2003 and 2005, Gritsch et al., 1998, 2000, 2003, and 2005).

The previous studies helped to understand the physics of the film cooling and revealed some of its interaction complexity. However, other studies were performed on curved surfaces (e.g. Schwarz and Goldstien, 1989, Schwarz et al., 1991, and Lutum et al., 2001) or on airfoil cascades to investigate and quantify the film cooling performance over actual curved surface of the turbine airfoils (e.g. Nirmalan and Hylton, 1990, Ames, 1998, Reiss et al., 1998, Drost and Bolcs, 1997 and 1999, Ethridge et al., 2001, Colban et al., 2006, Waye and Bogard, 2007, Zhang and Moon, 2007, Mhetras et al., 2007, and Chappell et al., 2008). Some of those studies were focused on the shaping of the hole exit to improve the film cooling performance (e.g. Teng et al., 2001, Dittmar et al., 2003 and 2004, and Gao et al., 2008 and 2009). Some other studies proposed a non conventional exit shapes and measured their performance over a flat plate (e.g. Guangchao et al., 2008, and Lu et al., 2009) or over an airfoil in cascade (e.g. Okita and Nishiura, 2007)

The objectives of these investigations were to increase the film cooling performance and reduce the effect of jet lift-off. The jet lift-off, particularly at high blowing ratios, is one of the main criteria that affect the film cooling of gas turbine airfoils, yielding significant reduction in its cooling performance. The literature review reveals some points regarding film cooling development and can be summarized as follows. The hole geometry is a significant factor in film cooling performance. The shaped holes have the best overall performance, particularly at high blowing rates, when compared to standard

circular holes. Compound angle injection, whether for shaped or circular holes, leads to an increase in the spanwise averaged effectiveness compared to that obtained with axially oriented holes. However, compound jets generally produce higher heat transfer coefficient on the surface than do axial jets. This trend is amplified as the blowing ratio increases. Small hole spacing results in better coverage of the wall, and thus higher effectiveness values than larger ones. However, overly small spacing decreases the strength of the airfoil and increases the machining cost. The turbulence intensity affects the cooling performance at lower blowing ratios, and slightly affects the performance at high blowing ratios. The investigation of the film cooling over flat plate shows acceptable results to evaluate the cooling performance; however the investigation over an actual airfoil shape provides more precise results which is closer to the real engine conditions.

Previous studies presented the benefits of shaping the hole exit to improve the film cooling performance and increase the cooling capacity over the flat plate. Therefore, Immarigeon and Hassan (2006) proposed the louver scheme to increase the cooling capacity of the shaped exit in addition to make use of the upstream impingement in the internal cooling. Zhang and Hassan, 2006, 2008, and 2009, improved numerically the geometry of the louver scheme and measured its performance under different and flow geometrical conditions. Those studies predicted a superior performance of the louver scheme under different operating conditions. Ghorab (2009) measured experimentally the performance of the louver scheme over a flat plate showing superior performance compared with other hole shapes.

The leading edge is extremely exposed to the hottest flow temperature with the higher heat transfer coefficient. Many studies investigated the cooling performance at this

critical region on the airfoil. Some of those studies were performed on a half cylinder in a cross flow (e.g. Mehendale and Han, 1992, Ou and Han, 1992, Salcudean et al., 1994, Hoffs et al., 1997, and Reiss and Bolcs, 2000). These studies simulated the leading edge flow with certain approximation, therefore some other studies were conducted on more complicated curved surfaces (e.g. York and Leylek, 2002, Weigand et al., 2006, and Lu et al., 2007) on a blunt body or on an airfoil cascade (e.g. Zhang and Moon, 2006, Gao and Han, 2009, and Islami et al., 2010). The cooling of the leading edge provides a challenge as the mainstream is mainly stagnant in this region. Previous studies found that the coolant has a severe jet lift-off causing poor effectiveness accompanied by higher heat transfer.

Film cooling has been developed within the last four decades and many studies have investigated the factors that affect its performance. The jet lift-off, particularly at the high blowing ratio, is the greatest problem that causes a loss of the coolant capacity with further increase in the heat transfer coefficient. Shaping the hole exit provides a proper reduction on the jet momentum with wider spreading over the protected surfaces. The louver scheme has been proposed to combine the film cooling downstream of the hole exit and the impingement on the inner surfaces in order to cool the region upstream from the hole exit. In this study, the performance of the louver scheme has been measured over the actual surface of a gas turbine vane. In addition, a smooth expansion has been proposed at the leading edge to increase the cooling capacity at this critical region on the gas turbine airfoil.

Chapter 3 - Experimental Methodology

A subsonic wind tunnel was established in Concordia University to investigate the film cooling performance in industrial gas turbines. The tunnel is constructed in such a way that it can be used with a flat plate investigation or with different actual airfoils profiles. This chapter presents the experimental test facility, the methodology, and the uncertainty analysis.

3.1 Test facility and instrumentation

The test facility consists of three main systems: mechanical, electronic, and thermography measuring systems. Figure 3.1 presents a schematic diagram of the test facility with its subcomponents. The mechanical system consists of main and secondary flow loops. The air is supplied to both loops by a compressed air tank at a regulated pressure of 7 atm. Because of the tank volume limitation, there is not enough air to warm up the main flow to the desired temperature. Therefore, the secondary air is heated while the main stream is kept at the supply temperature; this approach has been used by Jung and Lee (2000). Each loop includes a pressure controller to maintain a steady operating pressure at the desired pressure ratio and gate and needle control valves to adjust the required flow rate. A Rosemount Multi-Variable Mass Flow Meter (3095MV) is used to measure the mainstream flow rate, pressure, and temperature, while a rotameter (FL-1502A) is used to measure the secondary flow rate. To ensure a fully developed flow at the test section, the main flow passes through a divergent-convergent nozzle then through a duct of 1.5 meter length with the same cross sectional area as the test section. The divergent-convergent nozzles and the main duct are made from cast acrylic sheets, 1.2 cm thick, with 91% light transmittance. A honeycomb mesh, 5 cm long with a cell size of

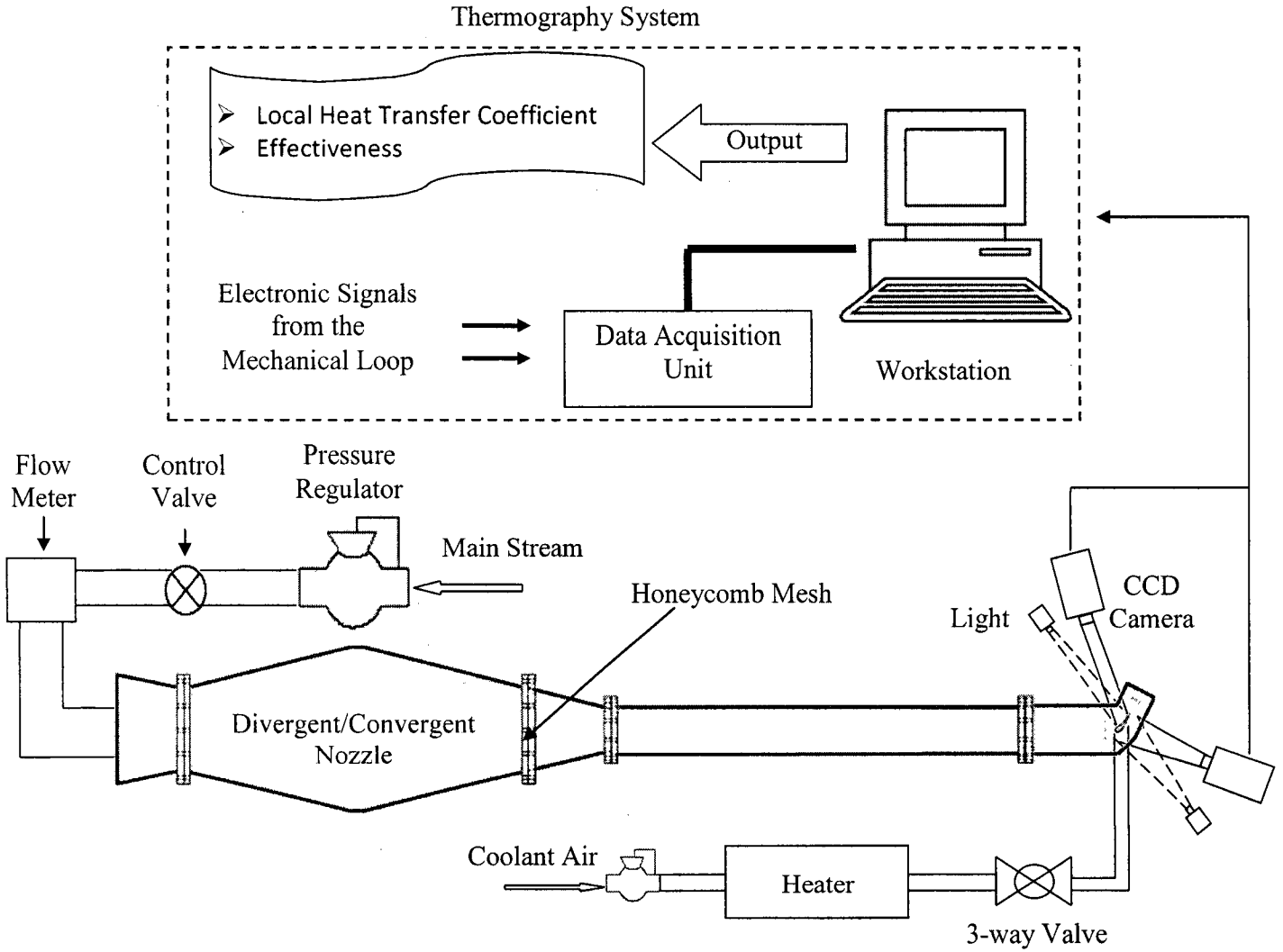

Figure 3-1 Schematic of the two dimensional cascade test facility

0.6 cm, is installed at the exit of the convergent nozzle to create a uniform velocity distribution upstream of the test section. The turbulence intensity has been measured using the Particle image Velocimetry technique (PIV) at five axial chord upstream the vane leading edge, ant it was 8.5%.

An electrical variable power air heater with a maximum capacity of 1200 Watts is used to heat the secondary flow before it is delivered to the test section. A fast acting three-way solenoid valve routes the flow through a bypass during the heating process. When steady state temperature is achieved, a Labview program triggers the solenoid valve allowing the secondary flow to pass to the test section through a plenum. The plenum is made from cast acrylic and it is assembled at the bottom of the base part of the test section. It was designed with external dimensions of 7×2×2cm and a cubic internal cavity of 1.5 cm length to reduce the heat loss through its wall. A thermocouple and a pressure sensor are inserted to record the static temperature and pressure of the jet before being delivered to the vane.

A pressure transducer (0 - 5.2 bar) is installed in the main duct to measure the pressure of the main flow. The output signal from the pressure transducer and the multi-variable mass flow transmitter has a digital display and an analog signal of 4-20 mA. Additionally, pressure gauges (Omega PGH-45L-100) were also placed in each loop in order to monitor the pressure. Different T-type thermocouples are distributed over both loops to monitor the temperature change at different points; the main flow upstream of the vane, and the secondary flow just before the injection point. The output signals from the instruments are connected to a M series NI data acquisition system (DAQ) and then monitored using Labview software. An in-house Labview code was developed in order to

monitor and save a variety of signals from pressure, flow and temperature instruments, as well as to control the secondary flow solenoid valve. The logical connections between the data acquisition system, the pressure scanner, and the imaging system with the workstation are illustrated schematically in Figure 3.2. The available input signals and data outputs are also presented in the figure. The DAQ system consists of a SCXI-1000 signal conditioning unit, with appropriate modules, NI PCI - 6281 18-bit (analog input resolution), M series DAQ with an output rate of 2.8 MS/s and a SCXI - 1160 16-channel SPDT relay model. The instrument output signals are mA and mV, as well as connect and disconnect signals. These signals are transferred to a DAQ card (PCI 6281) through a signal conditioner.

3.2 Test section and imaging techniques

The stator vane, shown in Figure 3.3, is proposed with the support of Pratt and Whitney Canada (PWC), to investigate its cooling performance with different cooling schemes. The test section consists of two main parts, the vane and the casing, whose external walls have a profile similar to the previous vane. This configuration provides flow passages, streamline curvature, and physical dimensions similar to those of a scaled vane used in an industrial power generation gas turbine. The test section passed through three stages during its design process: firstly, choosing the main dimensions of the casing cascade, then, manufacturing the vane and the first model of the casing using stereo lithography rapid prototyping technique, finally manufacturing the current casing using Plexiglas.

In the first stage, the vane profile and pitch angle at mid span are proposed by PWC, while the pitch and span designed according to the test facility capability to match

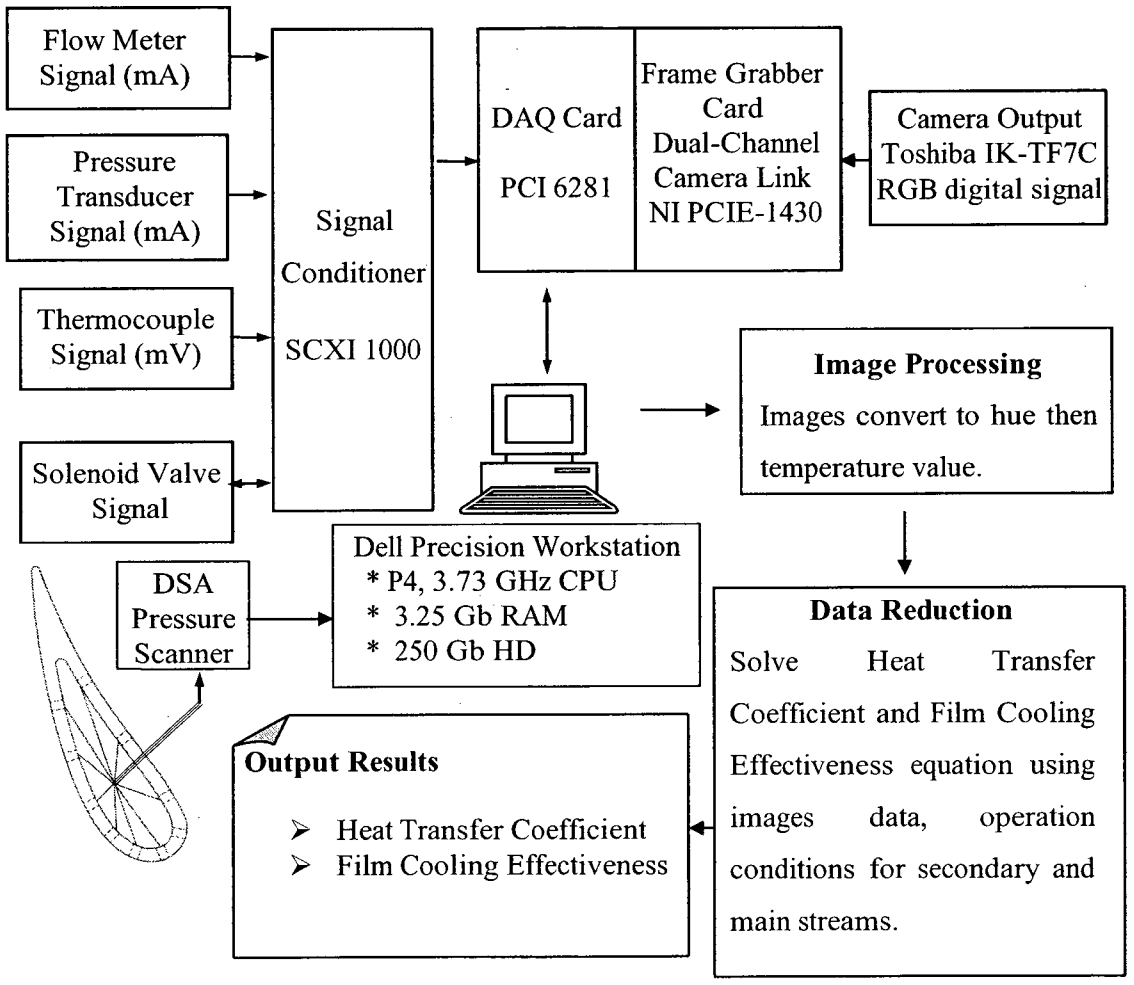

Figure 3-2 Schematic of the data processing system

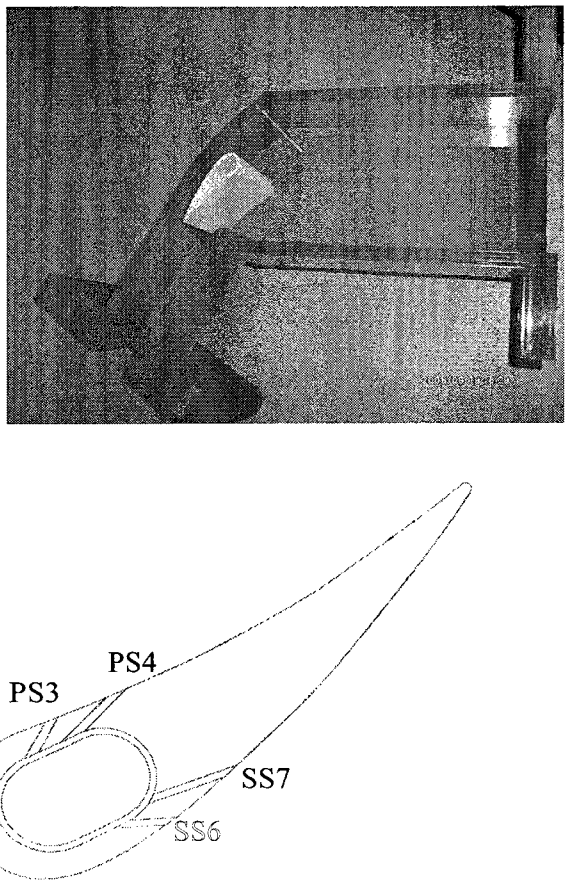

Figure 3-3 a) Vane test section b) vane with cooling holes

Reynolds and Mach number of the real engine condition. The span has to be wide enough to avoid end wall effects on the cooling phenomenon. This wideness is constrained by the maximum allowed cross section area that provides the proper flow conditions upstream of the vane. Different scaled vanes (chord and pitch) were assumed in conjunction with different spans and they were investigated numerically to optimize the relative dimensions with respect to the inlet and exit flow conditions. The trailing edge tailboards were contoured to ensure similar streamlined flow downstream of the vane.

After establishing the relative dimensions of the cascade, the manufacturing process was started by finding the proper material that can be used to form the cascade with the required visibility to allow the camera access to the region of investigation. The oncoming options were the manufacturing using either glass or any machine able material that provide the exact shape profile and insert a glass window ahead of the region of investigation. The first option is fraught of risk while in the second option the flow may be disturbed by the interaction between glass and cascade material. The technique of stereo lithography was proposed to allow the choosing of visible material that can be constructed in the required cascade with the exact profile shaping. A pressure tap is located one chord upstream the vane to scan the static inlet pressure of the main flow. The vane is located three chords downstream the fixation point between the test section and the upstream tube.

The selected material shows a good approach to the test section machining however the vision access was not sufficient due to the bluish shadow of the material and some noisy lines that appeared inside the material due to the method of manufacturing. The clarity of this material has been gained by a special polishing substance that covers

both the internal and external surface of the cascade. After several running the air flow affected the internal polish leading to a farther decay in the vision access. In addition to the manufacturing as a one piece that limits the physical access to the cascade and limits the ease of exchanging the test vanes, the need of remanufacturing the cascade has arisen. The casing was manufactured from Plexiglas to get full vision and physical access to the interest area.

The measurements are finally conducted in a two-dimensional cascade, providing flow passages similar to those of the scaled vane used in industrial power generation gas turbine. The inlet cross section of the cascade is 9.5 cm by 5.1 cm with an additional 30 cm entrance length upstream of the vane leading edge. All sides of the cascade were machined out of 1.2 cm thick acrylic sheets for optical access. The two side walls were glued to the base while the top plate is designed to be removable in order to ease the handling of the working vanes. In this design the upstream length is increased to be a five chords length and a thermocouple is inserted ahead of the casing entrance to record the main flow temperature. To assure the pressure reading in the main flow three pressure taps are located at one chord upstream the vane in addition to other three pressure taps are located at one chord downstream the vane. The cascade inlet and exit velocities are set to be 34 m/s and 85 m/s corresponding to Mach numbers 0.1 and 0.23, respectively. The exit Reynolds number based on the axial chord is 140,000 and the vane pressure ratio (p_{oi}/p_a) is 1.12.

A digital 3CCD IK-TF7C Toshiba camera was used to capture the Thermochromic Liquid Crystal (TLC) images over the downstream surface area of the film holes at a rate of 5 fps. The acquired simultaneous images are transferred to the

computing workstation through a NI PCIE-1340 dual frame grabber which can work with two different camera link configurations using the Labview program. The image quality depends on the adjustment of the lens and the light distribution and intensity. The light intensity was adjusted with a variable light source. A color calibration target is used as an objective to adjust the resolution. The captured, Red-Green-Blue (RGB) images are saved in Tagged Image File Format (TIFF) with a size of 1024 x 768 pixels. An in-house image processing code was created using MATLAB software to convert the RGB images to hue values. A calibration process has been developed to convert the obtained hue value to the surface temperature and it is described in detail in the next section. The test section was made from acrylic to allow for optical measurements; however the curved side walls have some corrugations that affect the clarity of the vision. After a few preliminary tests, the camera and the light are positioned slightly facing the straight side wall upstream of the vane. This leads to blocking around 40% of the target area of the pressure surface, see Figure 3.1. An image for the test section details and the thermography system component is presented in Figure 3.4.

3.3 Test vanes and hole configuration

The measurements have been conducted on a scaled vane with the relative geometrical dimensions that simulate the first stator of an industrial power generation gas turbine. The true and axial chord, vane span and pitch are 6.01 cm, 3.04 cm, 5.1 cm, and 5.38 cm respectively. Figure 3.3b shows the profile of the vane and the location of the cooling holes on both suction and pressure sides. The geometrical dimensions of the vane are tabulated in Table 3.1. Two rows of holes, of diameter d_s, are distributed on the suction side with a spanwise spacing of $7.5d_s$. The first row (SS6) consists of seven holes

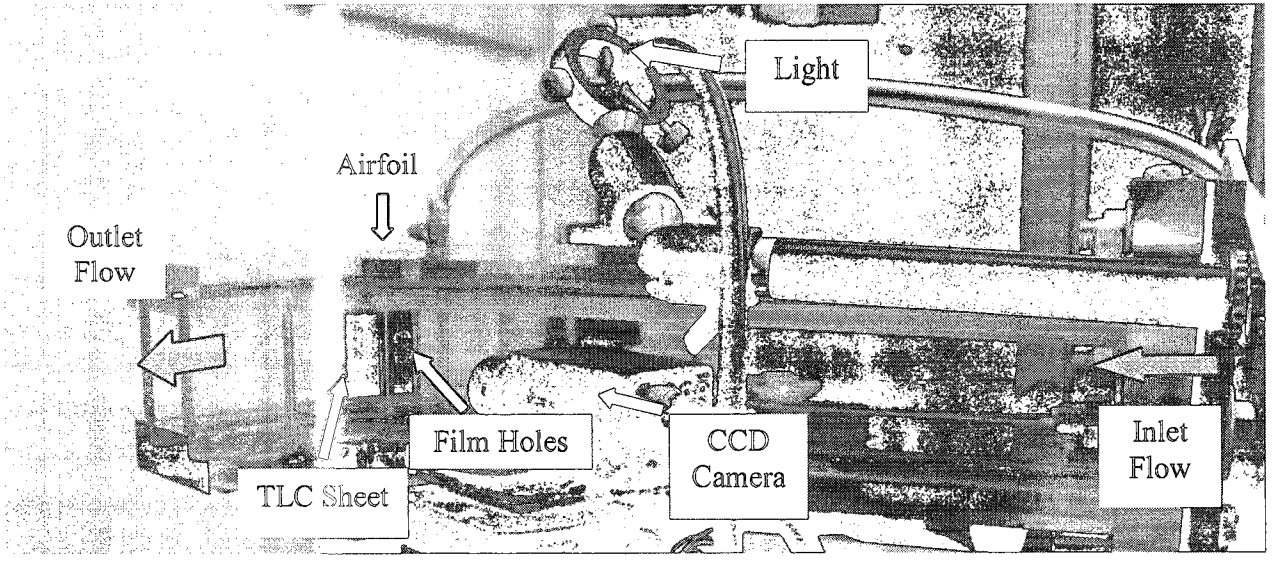

Figure 3-4 Image of the vane cascade

and is located at 57% of the axial chord. The second row (SS7) consists of six holes and is located at 67% of the axial chord. Both rows are in a stagger arrangement with axial spacing distance of $10d_s$. Two rows of holes, of diameter d_p, are also distributed on the pressure side with a spanwise spacing of $4.5d_p$ The first row (PS3) consists of eight holes and is located at 14% of the axial chord. The second row (PS4) consists of seven holes and is located at 28% of the axial chord. Both rows are in a stagger arrangement with axial spacing distance of $10d_s$. The geometrical details are tabulated in Table 3.2.

For each side, the first upstream row of holes only is employed, the second row of hole only is employed, or two rows of holes are employed, while the third row on the pressure side is employed alone. Three different hole configurations are used on each row, standard cylindrical, shaped hole, and louver. A different vane is used for each hole arrangement (first row, second row, both rows, third row) and for each hole configuration (cylindrical, shaped, louver). Thus a total of 12 vanes are employed. Each vane is manufactured with a groove, 0.254 mm equal to the TLC sheet thickness, downstream the cooling hole to embed the TLC sheet without disturbing the boundary layer development on the vane surface. The vanes were made using stereo lithography (SLA) and they are placed in a special recess in the middle of the cascade in both the base and top parts.

The vane was constructed from a new material, watershed, using the stereo lithography rapid prototyping technique. The accuracy of this technique is about 0.5% of the linear dimensions, according to the manufacturers. The used material has similar thermal properties as that of Plexiglas, however, its thermal properties, conductivity and diffusivity, are not tabulated. The thermal diffusivity was measured using NETZSCH Nano flash LFA 447 , which is a computerized thermal diffusivity measurement system

Table 3.1 Vane geometrical dimensions

Parameter	Value
True Chord, C	6.01
Axial Chord, C_x	3.04
Pitch, p	5.38
Span	5.40
Flow turning angle	59.61

Table 3.2 Cooling hole arrangement

	SS6	**SS7**	**PS3**	**PS4**
Location (% of axial chord)	57	67	14	28
Inclination angle	36	24	40	22
No. of holes	7	6	8	7
Spacing	7.5d	7.5d	4.5d	4.5d

based on flash method. Different samples of 12.7×12.7×1mm are manufactured to measure the thermal diffusivity using the device equipped in Concordia University. The thermal conductivity was calculated by measuring the heat capacity for a sample with a specified weight, 10 mg, using Ta DSC Q10. The thermal conductivity was found to be 0.211328 W/m.K, and the thermal diffusivity was $0.127e^{-6}$ m^2/s.

3.4 Pressure measurement

The pressure measurement is the first step in evaluating the cooling performance of an airfoil. Based on the measured pressure distribution along the vane surface the flow properties at each tap location can be calculated using isentropic gas laws. Figure 3.5 shows a special vane specially manufactured to measure the pressure distribution using high precision pressure scanner. The pressure distribution around the vane is recorded using a DSA3217/16PX-10psid Scanivalve pressure transducer. The pressure taps on the vane surface are connected to the pressure scanner channels using URTH-063 urethane flexible tubing with 1/16" inside diameter. The differential pressure between the reference point and the measured points is recorded using DSA Link 3.03 software. Fourteen pressure taps are drilled along the mid span, seven taps on the pressure side, six on the suction side, and a pressure tap on the leading edge just at the stagnation point. A tap located on the suction side of the vane close to the leading edge has a mean pressure value between all other tap readings, so it is selected to be the reference point. The readings of all pressure taps are referred to this reference tap reading, and a tap on the pressure scanner is subjected to the atmospheric pressure to get the absolute value for each point. The air stream flow rate is adjusted using the control valves and recorded using the orifice flow meter. After adjusting the flow rate, all valves are opened except

the solenoid valves. LabVIEW software is used to trigger the solenoid valves of the air stream as well as the pressure scanner after 3 seconds of the flow initiation to avoid the unsteadiness of the flow around the vane.

During each blow down test, the total pressure and Reynolds number at the test section inlet are maintained in a continuous and steady fashion for up to 20 seconds long time intervals. The pressure at each point is recorded at a rate of 20 Hz and averaged through the running time period. The inlet pressure to the test section is measured one axial chord length upstream of the vane leading edge and it ranges from 14.88 to 21 psi. This static pressure covers a range of 1.01 to 1.43 pressure ratio across the vane, which is the ratio between the inlet total pressure upstream the vane (P_{oi}) to the static pressure downstream the vane (P_a). These pressure ratios correspond to inlet Mach numbers of 0.07 to 0.24 and Reynolds numbers, based on the axial chord, from 0.48E5 to 2.4E5. Figure 3.6 shows the static pressure distribution along the vane midspan, normalized to the total inlet pressure, at different pressure ratios (P_o/P). Three pressure ratios were selected to be presented, 1.12 which is the pressure ratio selected to be investigated through the current study, and the extreme pressure ratios 1.01 and 1.43. At low pressure ratio, there is no change in the static pressure around the vane due to the low employed speed that yields no pressure gradient. At the moderate pressure ratio, there is a noticeable reduction on the static pressure over the suction side achieving the minimum value at the throat. At the higher pressure ratio, the pressure on the suction side achieves the lowest static pressure with tendency to shift the minimum point later downstream. The pressure distribution over the vane suction side is highly affected by the pressure

ratio, while the pressure ratio changes slightly affects the pressure distribution over the vane pressure side.

The total pressure is constant along the main flow streamlines and it can be calculated using the isentropic equations for compressible flow. The total pressure can be calculated from Mach number and the measured static pressure one chord upstream the vane leading edge using equation 3.1.

$$\frac{p_o}{p} = (1 + \frac{\gamma - 1}{2} M^2)^{\frac{\gamma}{\gamma - 1}} \tag{3.1}$$

Hence, Mach number distribution along the vane mid span can be calculated from the total pressure and the measured pressure using the same equation. Figure 3.7 shows the isentropic Mach number distribution along the vane suction and pressure sides at different pressures ratios. On the pressure side at all pressure ratios insignificant changes are occurred on the Mach number distribution. On the suction side, Mach number is subsonic for pressure ratios less than 1.3 with adverse pressure gradient at x/C_x greater than 0.5. For low pressure ratio there is no significant changes on the Mach number. At higher pressure ratios the flow is developed to be transonic with a possibility of a weak shock wave formation at x/C_x nearly equal to 0.65 and it moves toward the trailing edge as the pressure ratio increases. The pressure expansion yields to a drop in the local temperature along the vane surface. Same as pressure, the total temperature is constant along the main flow streamlines and it can be calculated using the isentropic equations for compressible flow, total temperature can be calculated from Mach number and the measured temperature five chords upstream the vane leading edge using equation 3.2.

$$\frac{T_o}{T} = (1 + \frac{\gamma - 1}{2} M^2) \tag{3.2}$$

Figure 3.8 shows the temperature distribution along the vane midspan calculated from equation 3.2 using the total temperature and the calculated Mach number.

The curvature surface of both pressure and suction sides of the vane needs to be correlated to get more precise measurements. A uniform rectangle grid of 5 mm spacing is drawn on the vane surface to account for this effect as shown in Figure 3.9b. This vane is assembled on the cascade as the actual case and an image is captured using the same camera setting. The x-distances between grid lines are measured as a number of pixels at different locations along the vane surface and correlated to the actual linear distance. This correlation shows lower number of pixels on the curved surface early downstream, $C_x <$ 50 %, compared with that later downstream, $C_x >$ 50 %. It means the measured distances, early upstream, using the image is shorter than the actual distance and a correlation should be applied to accurately predict the real distance. The z-distances are also checked and it presents uniform linear measurements along the vane span.

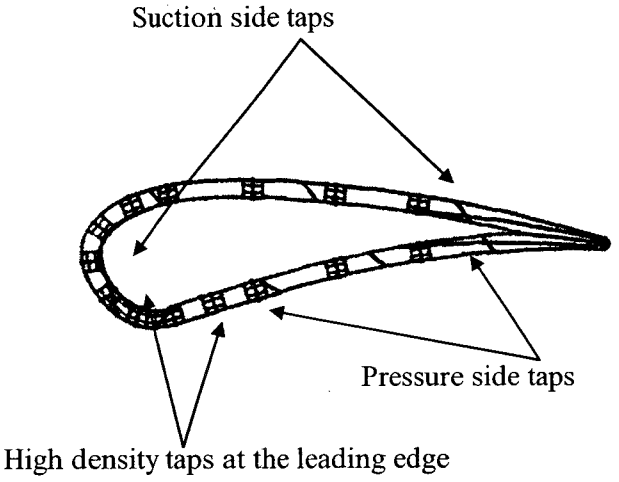

Figure 3-5 Pressure measurement vane

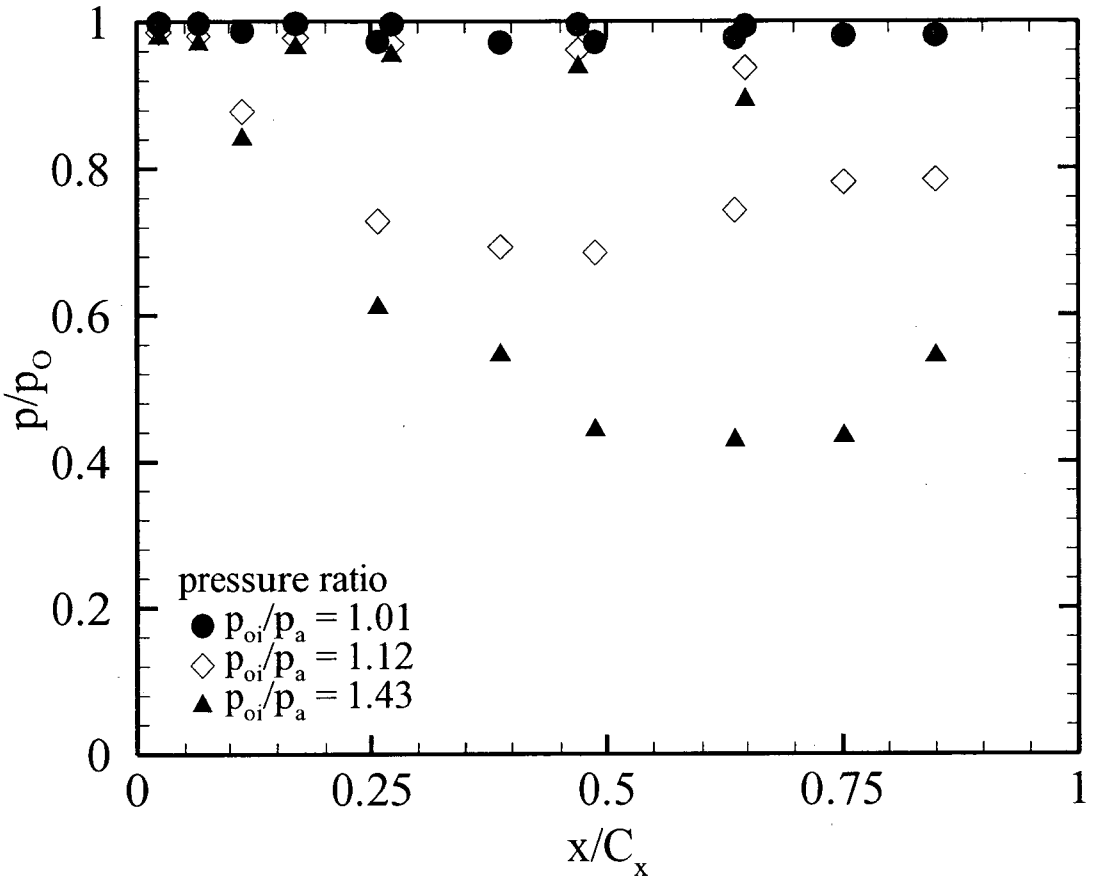

Figure 3-6 Mid-span pressure measurement along the vane

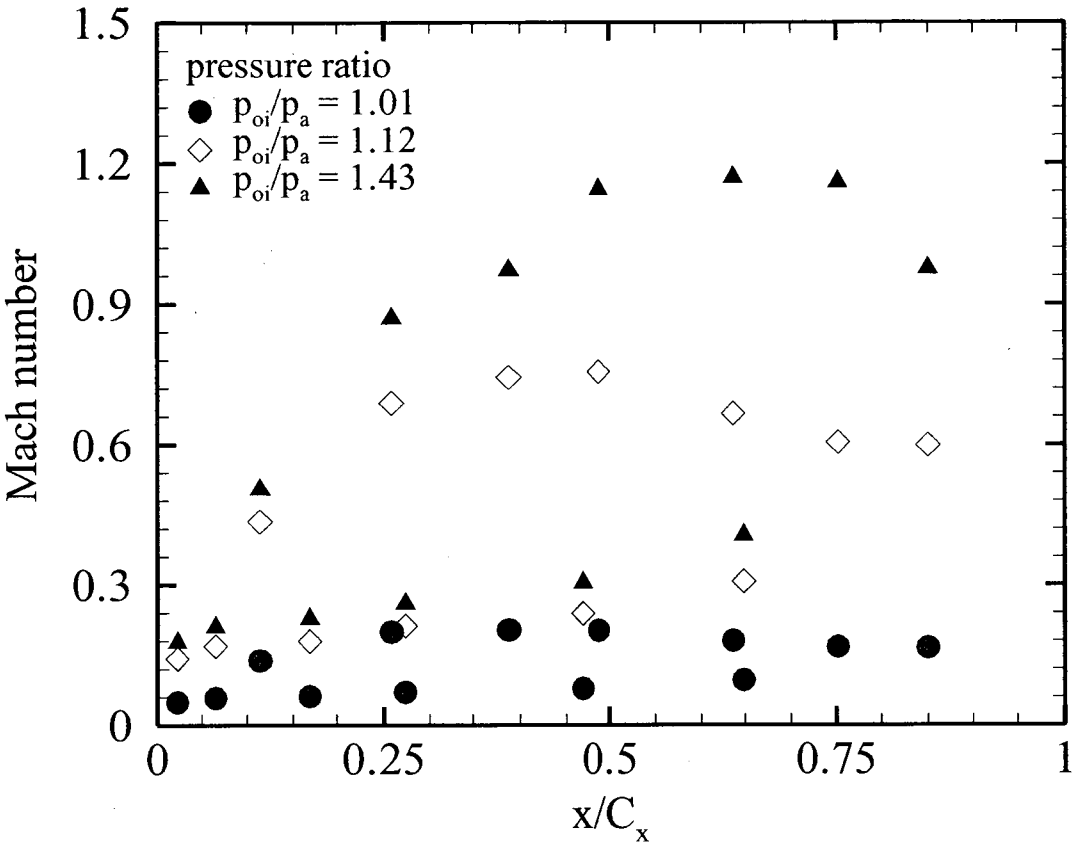

Figure 3-7 Mid-span Mach number distribution

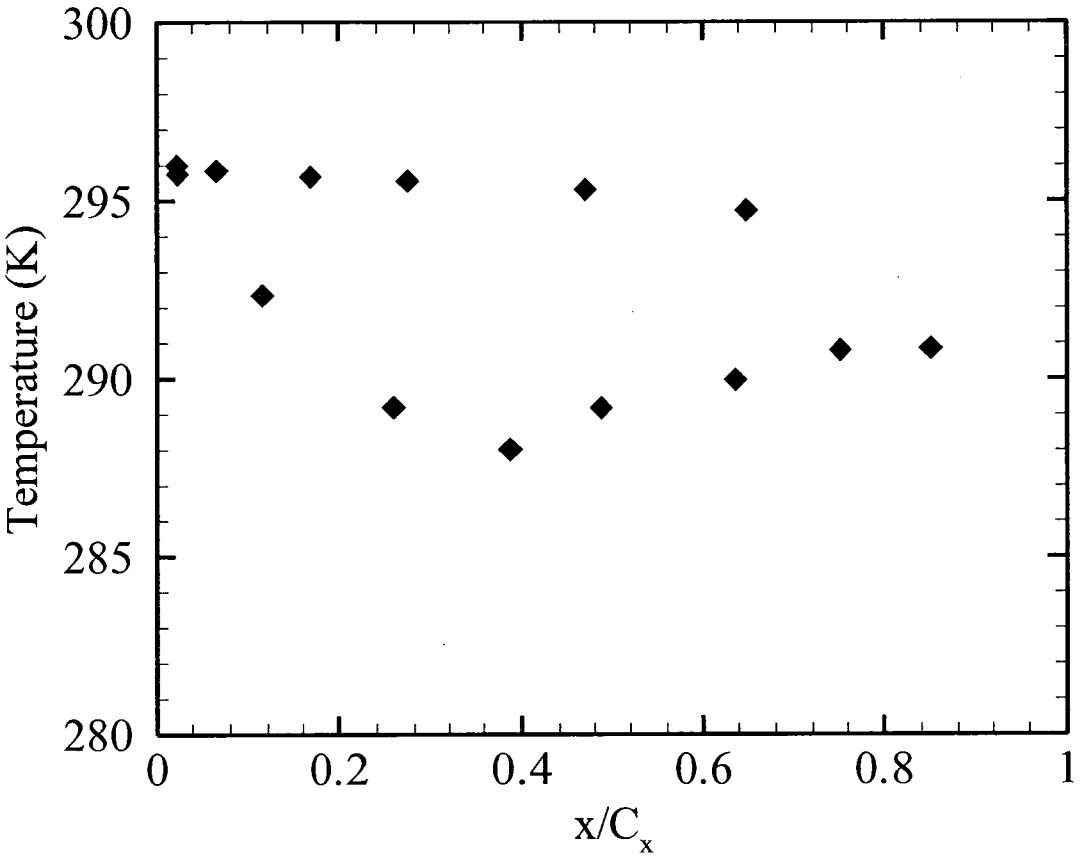

Figure 3-8 Mid-span temperature distribution

a)

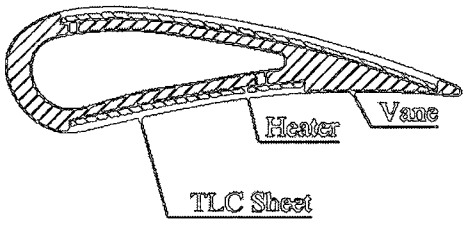

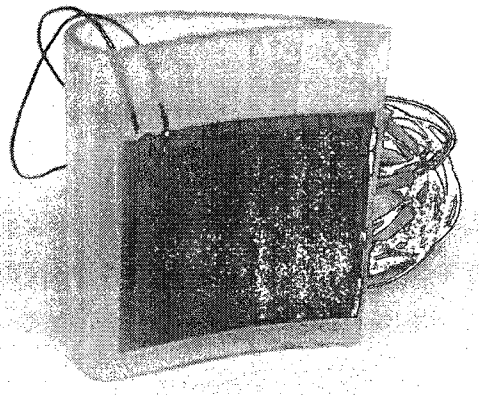

b)

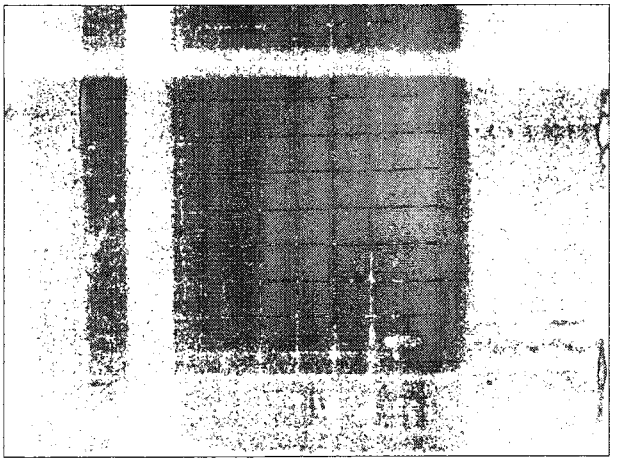

Figure 3-9 a) Calibration vane b) grid on vane surface

3.5 TLC calibration

Three main techniques were used to obtain the cooling performance of the film holes (steady state experiment, transient experiment with a single test, or transient experiment with multi tests). For the transient experiment with a single test, a narrow band TLC sheet with a range of 20°C to 25°C is used to map the temperature distribution along the target area on the vane surface. A new calibration process has been developed to overcome the difficulties that are encountered when using the TLC sheets on such curved surfaces. A special vane is designed for performing the in-situ TLC calibration process without disturbing the boundary layer development on the vane surface. The calibration vane is manufactured similarly to the test vane but without the film cooling holes; Figure 3.9 presents the details of the calibration vane. This vane has a special groove of 5cm×5cm×0.36mm to contain both the heater and the TLC sheet. The heater (Omega, KH608/205P), with a maximum power output of 0.78W/cm^2, is used to apply a uniform heat flux to the TLC sheet in the calibration process to achieve the same lighting and camera settings for both calibration and experimental running processes. The heater is fed through a DC regulator (BK PRECISION 1623A) to ensure infinitesimal power steps followed by steady state duration.

The calibration vane is placed in the same place as the testing vane and is illuminated using a high intensity light. A flexible fibre optic guide is used to get a uniform incident light distribution on the target area. The CCD camera, with 1024×768 pixel resolution, is placed perpendicularly to the midpoint of the target area. A set of images, with different TLC color plays, is captured at different power inputs. Two T-Type thermocouples are fixed on the vane in order to record the surface temperature at

two different positions. The duration between two successive images is long enough to ensure a steady state temperature of the surface, typically a 0.25°C difference for two successive steps. This set of images is processed through a developed MATLAB code to get the equivalent hue value and relate it to the corresponding recorded temperature. To ensure the precision of the calibration process, the area of interest is meshed through the code into a smaller Region Of Interest (ROI). Each ROI is a rectangle of 1 pixel in width with a spatial resolution of 0.1 mm/pixel. In this way, each ROI in the calibration process has its own light intensity and camera viewing angle, with a similar setting for the experiments.

3.6 Data reduction

This investigation has been conducted with the transient liquid crystal technique. The technique requires a uniform initial temperature of the vane surface, which is rapidly exposed to the mainstream flow for a limited time. The test duration is chosen short enough to ensure that the penetration of the heating pulse into the surface is small compared to the vane thickness. Using this assumption, the heat conduction can be considered to be transient and one dimensional into a semi infinite solid. An analytical model of the transient surface temperature is then used to obtain the film cooling performance in terms of cooling effectiveness and HTC.

The assumption of one-dimensional transient heat conduction through a semi-infinite solid is used to determine the local heat transfer coefficient (h) and cooling effectiveness (η). The unsteady heat conduction equation for one dimensional heat conduction into a semi-infinite solid is given as:

$$\rho C_p \frac{\partial T}{\partial t} = \frac{\partial}{\partial x}\left(k \frac{\partial T}{\partial x}\right) \tag{3.3}$$

with the initial and boundary conditions

$$\left.\begin{array}{lll} @ & t=0, & T=T_i, \\ @ & x=0 & h\left(T_w - T_f\right) = -k\dfrac{\partial T}{\partial x} \\ @ & x=\infty & T=T_i \end{array}\right\} \tag{3.4}$$

This approach is valid for relatively short measuring time which depends on the wall thickness of the investigated surface and its thermal properties using Equation (3.5), as it was given by Reiss et al. (1998).

$$t = \frac{w^2}{16\alpha} \tag{3.5}$$

The solution of Equation (3.3) using the boundary conditions (3.4) gives the system temperature as a function of the heat transfer coefficient and the thermal properties of the vane material as follows

$$\frac{T_w - T_i}{T_f - T_i} = 1 - \exp\left(\frac{h^2 \alpha t}{k^2}\right) erfc\left(\frac{h\sqrt{\alpha t}}{k}\right) \tag{3.6}$$

Where the wall temperature, T_w, is obtained from the TLC contours and the initial temperature, T_i, of the surface as well as the mainstream temperature, T_m, will be measured by using a thermocouple. α and k are the thermal diffusivity and the thermal conductivity of the vane material, t is the duration of the transient test. This relation is valid to obtain the convective HTC for normal convection problems. However, in the case of three temperatures, as in film cooling, there is a need to define T_f as a combination of two different streams with two different temperatures. The film

temperature, T_f, can be calculated as a function of coolant temperature, T_c, mean temperature, and film cooling effectiveness as follows

$$\eta = \frac{(T_f - T_m)}{(T_c - T_m)}$$

this can be reduced to $T_f = \eta T_c + T_m(1-\eta)$

Equations (3.6) & (3.7) have three unknowns, h, η, and T_f. A third equation is needed in order to find a unique solution. Based on the fact that the flow dynamics, rather than the thermal conditions, are the dominant factors that control the turbulent convection, Vedula and Metzegar (1991) introduced a solution. Equations (3.8) and (3.9) can be obtained by performing two different transient tests, using two different injection temperatures, under the same flow conditions.

$$\frac{T_w - T_{i1}}{T_{f1} - T_{i1}} = 1 - \exp\left(\frac{h^2 \alpha t_1}{k^2}\right) erfc\left(\frac{h\sqrt{\alpha t_1}}{k}\right) \qquad (3.8)$$

$$\frac{T_w - T_{i2}}{T_{f2} - T_{i2}} = 1 - \exp\left(\frac{h^2 \alpha t_2}{k^2}\right) erfc\left(\frac{h\sqrt{\alpha t_2}}{k}\right) \qquad (3.9)$$

Where t_1 is the time on the first test required to attain a certain wall temperature, T_w, and t_2 is the time on the second test required to attain the same wall temperature. Equations (3.7), (3.8) and (3.9) are solved together to get the film cooling performance (h & η).

In the actual experiment, conduction heat transfer causes a temperature change in either the mainstream or the coolant during the transient test. The true step change in both flows is not possible and hence the reference temperature, T_f varies with time. This effect

can be accounted for by modifying Equations (3.8) & (3.9) by applying Duhamel's superposition theorem and including the true temperature change into Equation (3.7). Ekkad et al. (1997) used this technique to investigate the film cooling performance with a compound angle. Ai et al. (2001) investigated the optimum two sets of the injection temperature that yielded the most stable solution for both (h & η) and reduced the data reduction error.

Due to the higher uncertainty in performing two separate tests with the same flow conditions, Ekkad et al. (2004) presented the film cooling performance using a single transient test with an infrared camera. The same methodology is employed in this study with some modifications adapted to the test facility and the measurement method. Equations (3.6) & (3.7) are solved together to eliminate the film temperature, T_f, and both equations are then reduced to one equation in two variables, h and η.

$$T_w - T_i = \left[1 - \exp\left(\frac{h^2 \alpha t}{k^2}\right) erfc\left(\frac{h\sqrt{\alpha t}}{k}\right)\right] * \left[\eta\left(T_j - T_m\right) + T_m - T_i\right] \qquad (3.10)$$

In Equation (3.10), T_w, T_j and T_m are changing with time during the transient test. The variation of these parameters can significantly alter the solution to the differential equation. However, due to the experimental limitations, noticeable changes have been observed in their values during the running times. Many modifications and technical investigations have been performed to minimize the variation in these values. The change in the jet temperature is the major source of error in this measurement. Decreasing the plenum volume and increasing the tubing insulation provided a significant reduction in the heat loss; however this could not eliminate the heat loss completely. Another source

of error is the conduction effect on the surface in the region around the hole exit. The heat is transferred from the plenum to the area under investigation through a thin wall. An additional material was added to the plenum to increase the wall thickness in order to minimize the heat conduction. Moreover, the mainstream temperature shows a slight decrease during each test of approximately 0.5°C.

The single transient test of 60 seconds at a rate of 5 Hz for a total of 300 images (N) is considered in this study to solve Equation (3.10). The color contours in each image are converted, using a MATLAB code and the calibration data, to the corresponding temperature contours as in the calibration process. The two unknown variables, h and η, are calculated using a non-linear least square regression method for each ROI over the target surface. The regression analysis technique reduces experimental error by considering the infinitesimal changes in each parameter during the fitting process. The surface temperatures of each ROI over the target surface are measured using TLC at each time step (τ) during transient measurements as,

$$T_{w(ROI)}(h,\eta)\Big|_{t=\tau} = T_{TLC}\Big|_{t=\tau} \qquad (3.11)$$

According to the initial condition, the surface temperature is uniform and it equals to 21°C ± 0.5°C according to the investigated case. This temperature yields to a red or black reddish color of the TLC material, which is not easily recognized by the matlab code. During the transient test, the coolant trace appears downstream the hole exit and starts to propagate farther downstream covering those reddish regions by a well-defined colors. Through the 300 captured images, each ROI has n images those have non-defined colors. The number of non-defined images (n) changes according to the position of the ROI with

respect to the hole exit. A subroutine investigates the history of each ROI individually and eliminates the first n images that have non-defined colors, hence non-defined temperature. As a result, N-n points are applied in Equation (3.10) to calculate the two parameters (h and η) using non-linear least square regression method. The optimum solution is achieved by minimizing the least square error (ε) for each ROI downstream of the film cooling surface as follows:

$$\varepsilon(h,\eta)=\frac{1}{2}\sum_{i=n}^{N}\left(\mathrm{T_{w(ROI)}}\,(\mathrm{h}\,,\,\eta)\Big|_{t=\tau}-T_{TLC}\Big|_{t=\tau}\right)^2 \qquad (3.12)$$

The number of unused images (n) had an effect on the final solution of h and η. The "n" is dependent on the time response of the secondary flow over the downstream TLC surface. Each ROI, over the surface, had a different value of n, based on the flow conditions. For each ROI, a logical loop is applied to determine the proper number of images (n) that can be selected to provide the minimum least square error (ε) in Equation (3.12). The best fit is achieved when the summation of squared residuals had a minimum value.

3.7 Experimental uncertainty

An error analysis is investigated to determine the accuracy in measuring the heat transfer parameters studied and the film cooling effectiveness. There are three types of errors; conservative error, relative uncertainty error for measuring quantities, and an average uncertainty error of the results. The error analysis is calculated using the same methodology of Kline and McClintock, 1953 and by Moffat, 1988. The accuracy for various measurement signals is presented in Table 3.3. The accuracy for the pressure

Table 3.3 Accuracy of the instrumentation

Sensor	Accuracy
3095Mv multi-variable mass flow transmitter	Measuring differential pressure and static pressure, and temperature with 1% (for right length before and after the orifice)
Type-T thermocouple	Greater of 0.5°C or 0.4% of the reading
Type-E thermocouple	Greater of 1.0°C or 0.4% of the reading
2088G pressure transducer (0-75 psig)	± 0.2% of the span

transducer, multivariable flow transmitter, and thermocouples are based on the manufacturer specification. Typical uncertainty in TLC measurement is estimated to be ± 0.5° C. As well, uncertainty of thermal conductivity and diffusively are estimated to be ± 3 %.

The heat transfer coefficient can be presented as follows:

$h = f(Tw, Tm, Tj, Ti, t, \alpha, k)$,

Therefore, uncertainty for the heat transfer coefficient is,

$Uh = U(Tw, Tm, Tj, Ti, t, \alpha, k)$,

The variation in the parameters Tw, Tm, Tj, Ti, t, α, and k are δTw, δTm, δTj, δTi, δt, $\delta\alpha$, and δk, respectively, which cause variation in δh.

It follows that:

$$\delta h = \frac{\partial h}{\partial T_i}\partial T_i = \frac{\partial h}{\partial T_i}\partial T_i = \frac{\partial h}{\partial t}\partial t = \frac{\partial h}{\partial \bar{\alpha}}\partial \bar{\alpha} = \frac{\partial h}{\partial k}\partial k \tag{3.13}$$

The relative variation in h is a function of all other uncertainty parameters;

$$\frac{\delta h}{h} = \frac{1}{h}\frac{\partial h}{\partial T_i}\partial T_i = \frac{T_i}{h}\frac{\partial h}{\partial T_i}\frac{\partial T_i}{T_i} = \cdots = \frac{k}{h}\frac{\partial h}{\partial k}\frac{\partial k}{k} \tag{3.14}$$

So that the heat transfer coefficient uncertainty from a single test can be presented as follows;

$$Uh = \pm\sqrt{\left(\frac{T_w}{h}\frac{\partial h}{\partial T_w}\frac{\partial T_w}{T_w}\right)^2 + \left(\frac{T_m}{h}\frac{\partial h}{\partial T_m}\frac{\partial T_m}{T_m}\right)^2 + \cdots + \left(\frac{k}{h}\frac{\partial h}{\partial k}\frac{\partial k}{k_t}\right)^2} \tag{3.15}$$

It is difficult to calculate the error for the heat transfer coefficient as in Equation (3.15), where h is presented in a complex form in Equation (3.10). Therefore, the above equation is simplified to use only the term of the square root of the summation of the squares of the relative uncertainty for measuring, in order to calculate the accuracy of the heat transfer coefficient, as shown in Equation (3.16).

$$Uh = \pm\sqrt{\left(\frac{\partial T_w}{T_w}\right)^2 + \left(\frac{\partial T_m}{T_m}\right)^2 + \left(\frac{\partial T_j}{T_j}\right)^2 + \left(\frac{\partial T_i}{T_i}\right)^2 + \left(\frac{\partial t}{t}\right)^2 + \left(\frac{\partial \bar{\alpha}}{\alpha}\right)^2 + \left(\frac{\partial k}{k}\right)^2} \tag{3.16}$$

or

$$Uh = \pm\sqrt{(UT_w)^2 + (UT_m)^2 + \left(UT_j\right)^2 + (UT_i)^2 + (Ut)^2 + (U\bar{\alpha})^2 + (Uk)^2} \tag{3.17}$$

As a result, the error for each measured variable should be determined in order to calculate the accuracy for the heat transfer coefficient using Equations (3.16) or (3.17). Accordingly, the average uncertainty for the heat transfer ratio (h_f/h_o), film cooling effectiveness, Frossling number, net heat flux reduction, and blowing ratio are calculated.

The uncertainty of the heat transfer coefficient is calculated using the root mean square as in Equation (3.17), and the film cooling effectiveness uncertainty is calculated as the follows:

$$U\eta = \pm\sqrt{(UT_w)^2 + (UT_m)^2 + \left(UT_j\right)^2 + (UT_i)^2 + (Ut)^2 + (U\bar{\alpha})^2 + (Uk)^2 + (Uh)^2} \tag{3.18}$$

Moreover, the accuracy of measuring the blowing ratio can be calculated as the following:

$Br = f(P, T_m, T_j, V, A)$,

Therefore, according to the same previous theory,

$$UBr = \pm\sqrt{\left(\frac{P}{Br}\frac{\partial Br}{\partial P}\frac{\partial P}{P}\right)^2 + \left(\frac{T_m}{Br}\frac{\partial Br}{\partial T_m}\frac{\partial T_m}{T_m}\right)^2 + \left(\frac{T_j}{Br}\frac{\partial Br}{\partial T_j}\frac{\partial T_j}{T_j}\right)^2 + \left(\frac{V}{Br}\frac{\partial Br}{\partial V}\frac{\partial V}{V}\right)^2 + \left(\frac{A}{Br}\frac{\partial Br}{\partial A}\frac{\partial A}{A}\right)^2} \quad (3.19)$$

The current results are tested at atmosphere pressure; hence, the error due to pressure is neglected in Equation (3.19).

3.8 Heat transfer without film cooling

Prior to the film cooling investigation, extensive flow measurements were performed in order to guarantee the required running flow conditions. The inlet total pressure, one chord upstream of the vane leading edge, is maintained constant at 114 kPa. It corresponds to 0.23 exit free stream Mach number and 1.5E5 exit Reynolds number based on the axial chord. Inlet uniformity is measured at three different pitch-wise locations, one chord upstream from the vane. Static pressure is highly uniform and varies by less than 1 percent of the mean value. Moreover, the pressure is mapped at fourteen different locations distributed over both sides of the vane mid span. By assuming compressible flow, and using the isentropic flow relations, the corresponding Mach number at each location is computed and plotted in Figure 3.10. The figure indicates that the Mach number distribution employed in this study is subsonic on both pressure and

suction sides. The flow accelerates strongly on the suction side up to s/L = 0.4, followed by a mild adverse pressure gradient that lasts to the trailing edge. Whereas the flow on the pressure side shows continuous acceleration up to the trailing edge. The pressure expansion results in a drop in the local temperature along the vane surface, particularly on the suction side. The temperature distribution on the vane surface can be estimated using the pressure readings and the compressible flow assumption in conjunction with the computed isentropic Mach number.

The calibration vane is used for measuring the HTC without film cooling as a constant heat flux is applied via the electric heater. The vane is then subjected to the mainstream flow, which has the same mass flow rate, pressure ratio, and temperature (T_m) as the flow in the film cooling tests. When steady state is achieved, the CCD camera captures an image of the vane that displays the corresponding color contours over the TLC material. These color contours are converted to temperature contours using the code that was used during the film cooling case to obtain the surface temperature of the vane (T_w). The heat transfer coefficient can be computed by applying Equation (3.20)

$$h_o = q/(T_w - T_m) \tag{3.20}$$

The heat flux (q) is obtained from equation 3.20. Where q_h is the electric power obtained from the DC regulator inputs, and q_{loss} is the total of the estimated power loss. The losses are assumed as 10% conduction losses from the heater to the vane surface based on the

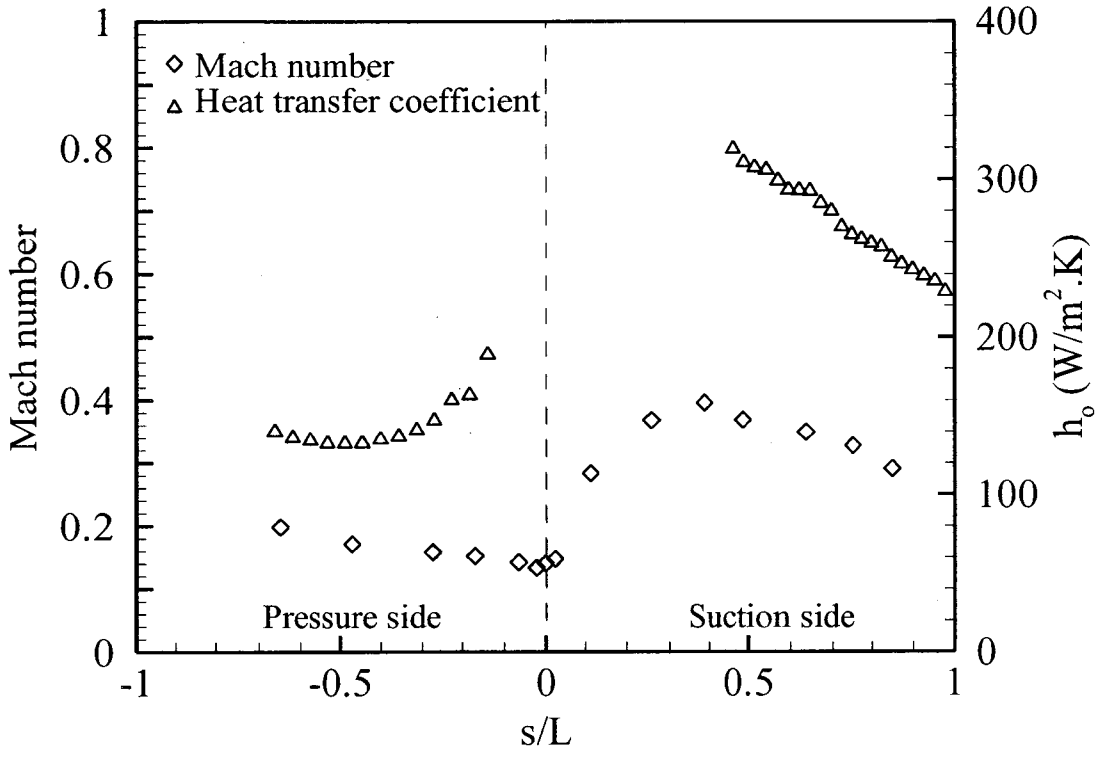

Figure 3-10 Vane Mach number and base line heat transfer coefficient distributions

thermal conductivity and constant heat flux boundary condition. The electric loss in the wiring is assumed to be 4% based on the used current, voltage and the wiring cross sectional area. In addition, the radiation loss is assumed to be (1%)

$$q = q_h - q_{loss} \tag{3.21}$$

The heat losses (q_{loss}) in terms of conduction, electric, and radiation losses are estimated to be fifteen percent of the total heat load applied by the heater (q_{elec}), hence $q=q_{elec} - q_{loss}$, or $q = 0.85\ q_{elec}$

The HTC without film cooling over both sides of the vane is also plotted in Figure (3.10). The sidewalls of the casing, which simulate the neighbouring vanes, obstruct the view of the target area. The small vane pitch and the difficulty in performing heat transfer measurements at the leading edge region add more constraints to mapping the entire vane surface. As no measurements were taken in the area upstream of the cooling holes, the suction side of the vane in this study shows a maximum heat transfer coefficient at x/C_x = 0.5, which then decays rapidly until the trailing edge. The investigated region is fully turbulent and it is characterized by the adverse pressure gradient and the thickening of the boundary layer. The pressure side shows the maximum heat transfer coefficient at x/C_x = -0.2, with rapid decay up to x/C_x = -0.3 in the transition region. The heat transfer coefficient then decreases with the surface distance as the boundary layer thickens in the fully turbulent region.

Chapter 4 - Performance of Louver Scheme over a Gas Turbine Vane

The louver scheme was proposed by Pratt and Whitney Canada to combine the benefits of the expanded exit holes and impingement over the airfoil internal surface upstream the hole exit, as shown in Figure 4.1. Immarigeon and Hassan (2006) investigated numerically its performance over a flat plate. Zhang and Hassan (2006) refined numerically the louver geometrical aspects, as shown in Figure 4.2. Continuing with numerical investigations, Zhang and Hassan (2006, 2008, and 2009) investigated numerically the louver scheme with a wide variety of conditions over both a flat plate and a symmetrical airfoil. Ghorab (2009) measured experimentally the cooling performance of the louver scheme over a flat plate. In this chapter, the performance of the louver scheme is measured experimentally at four different positions over the curved surfaces of a gas turbine vane. The temperature distribution over each side is mapped using a TLC technique with four different blowing ratios, 1, 1.35, 1.7, and 2 at 0.92 density ratio. The performance of the louver is then compared with that of different shaped holes from previous studies in order to evaluate the contribution of the louver in gas turbine cooling. Both the cooling effectiveness and the heat transfer coefficient are then combined on the form of net heat flux reduction (NHFR).

4.1 Louver scheme geometry

The geometrical aspects of the louver scheme are presented in Figure 4.2, as proposed by Zhang and Hassan (2006a). The air is delivered from the shown plenum to the bend through the throat with a base diameter (d). The coolant is then expanded in the bend where the internal surface of the airfoil is cooled by the impingement on the inner surface. The flow changes its direction loosing much of its perpendicular momentum

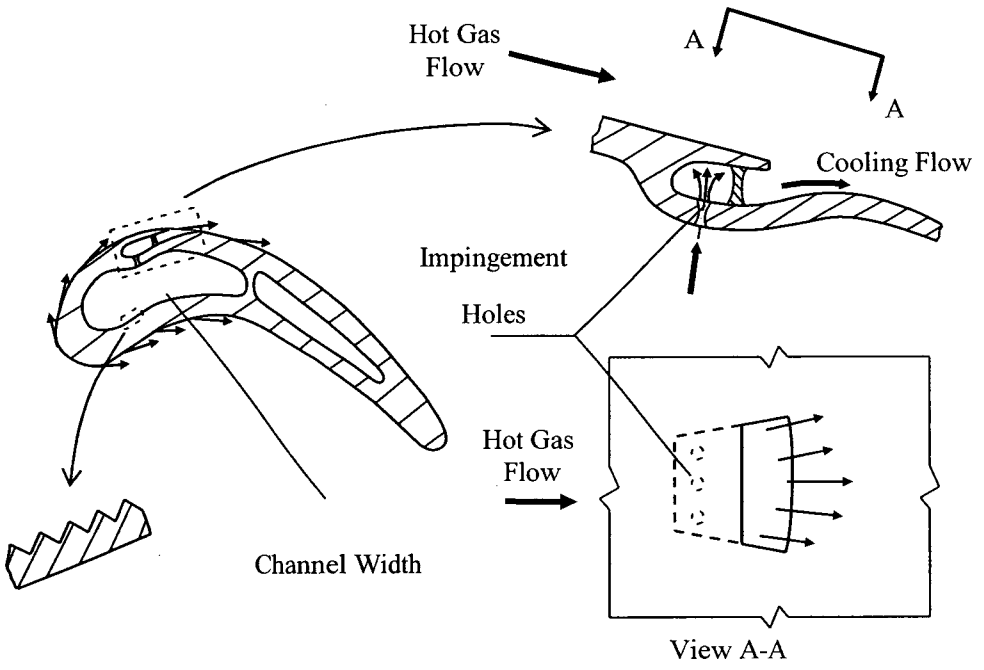

(There are several louvers in the spanwise or streamwise-flow direction)

Figure 4-1 Louver scheme on airfoil

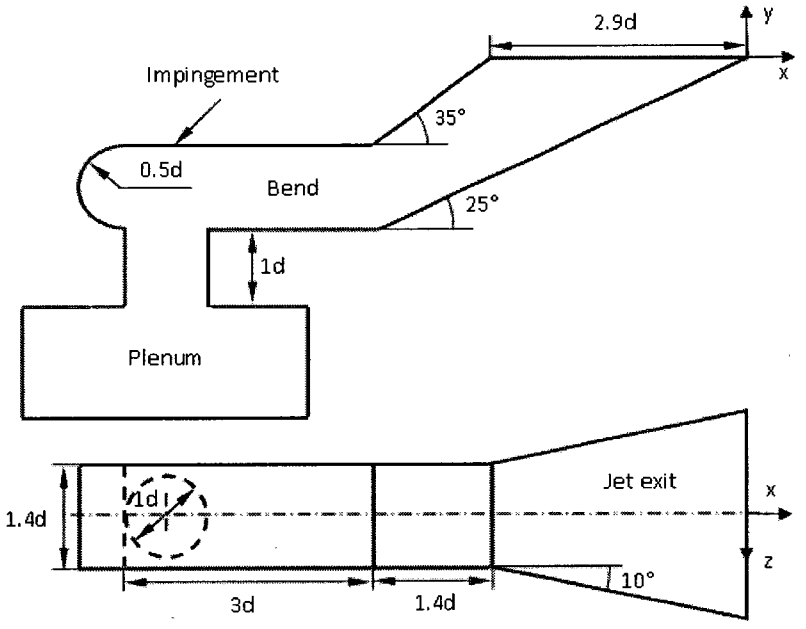

Figure 4-2 Geometrical details for louver scheme

component that existed if delivered through a standard cylindrical hole. The flow is then subjected to another deflection with expanded exit area and yields a further momentum reduction before being injected to the vane surface. The expanded exit is designed to achieve the proper shallow angle to yield the mainstream, as well as to spread the coolant laterally downstream the injection point. Measuring the cooling performance of the impingement contribution on the upstream part is beyond the scope of this study. The objective of this study is to measure the cooling performance downstream the scheme exit and to investigate the influence of the scheme location on its performance. Therefore, four rows of the louver scheme are distributed over the vane surface; two rows of diameter d_s are placed on the suction side and the other two rows of diameter d_p on the pressure side as shown in Figure 4.3. The exact hole locations, the hole spacing, and the number of holes in each row are exactly the same as the cylindrical holes discussed in Chapter Three. The rows are distributed in a stagger arrangement either on the suction side or on the pressure side.

The film cooling performance of the louver scheme is investigated on each row alone then the interaction between both rows. Therefore, a special vane was manufactured for each case; one vane for the first row only, one for the second row only, and one with both rows. Each vane has the same arrangement in both pressure and suction sides such that the pressure side holes are blocked when suction side is investigated and vice versa. Thus a total of 6 vanes are employed with four different blowing ratios (1, 1.35, 1.7, and 2); three vanes for the cylindrical hole, and three vanes with the louver scheme. The inlet total pressure, one chord upstream the vane leading edge, is maintained constant at 114 kPa. This corresponds to 0.23 exit free stream Mach

number and 1.5E5 exit Reynolds number based on the axial chord. The blowing ratio is calculated based on the flow characteristics of the mainstream at the injection point and the jet properties at the base diameter of the louver. Figure 4.4 shows the temperature contours of the louver film cooling with the different hole locations at Br = 1. The images show the difference between the film cooling effect on the pressure side and that on the suction side as well as the difference between the injections via each hole. The discrete film trace on the suction side is much clearer than that on the pressure side. The black trace of the TLC on the suction side indicates a lower recovery temperature due to a higher flow velocity.

4.2 Film cooling effectiveness on suction side

Figure 4.5 shows the local effectiveness distribution using the louver scheme at the two injection locations in addition to the double injection with four different blowing ratios compared with the cylindrical hole at the best blowing ratio (Br = 1). The exit expansion of the louver provides almost full lateral coverage downstream the hole, while the similar cylindrical hole covers almost 30% of the lateral distance downstream the first row (or maximum 50% for the second row). The wider coverage increases the protected area and provides more uniform thermal stresses over the vane surface. The bend of the louver causes a significant decrease in the coolant momentum by changing the flow direction. The momentum is then subjected to further reduction in the expanded exit, providing more reduction to the jet momentum. The sufficiently mandated momentum increases the amount of coolant adjacent to the vane surface yielding to higher effectiveness downstream the hole with more coolant amount attached to the surface for a longer distance. By increasing the coolant amount, the louver completely covers the vane

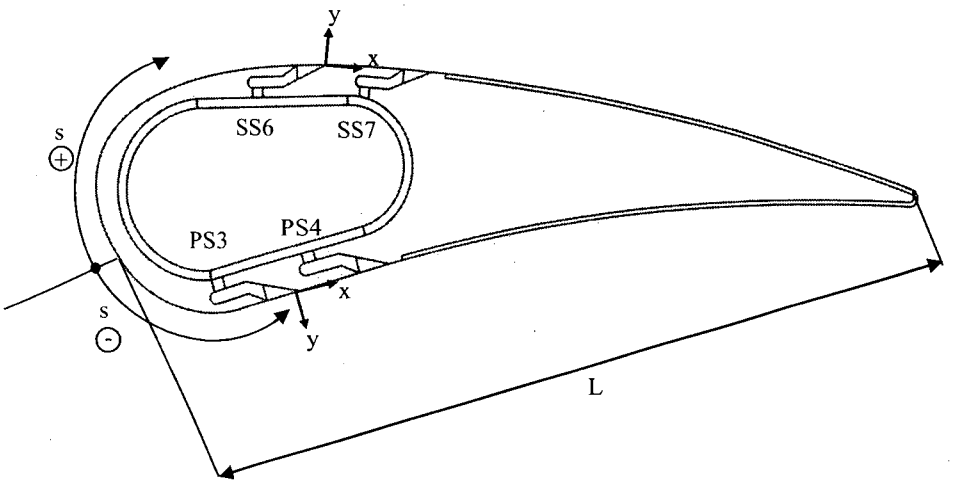

Figure 4-3 Louver scheme rows distribution on the vane

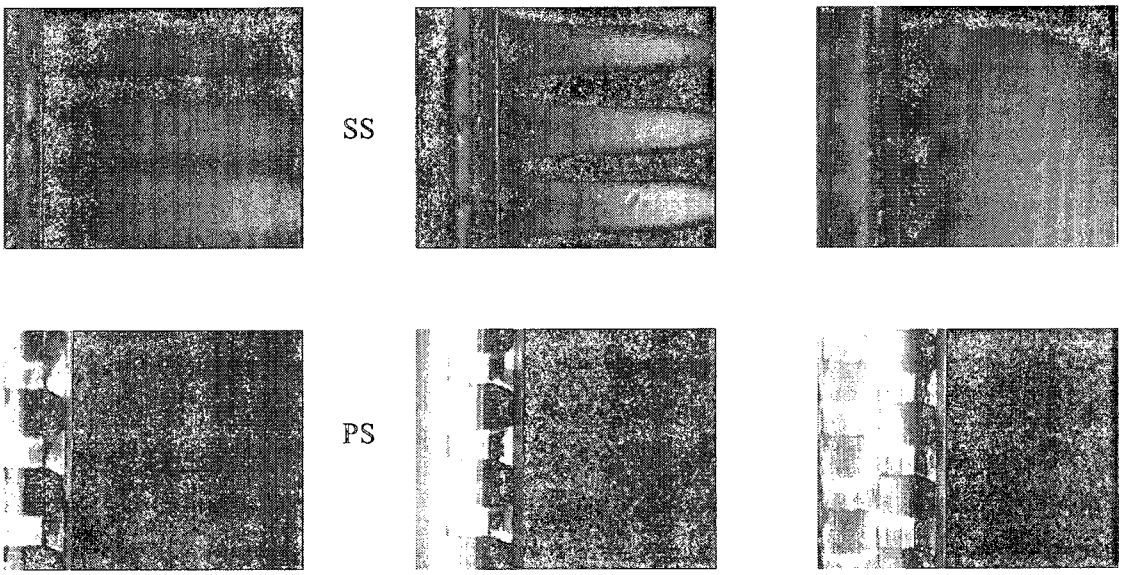

Figure 4-4 Typical film cooling image for Louver at Br = 1.

a) first row b) second row c) both rows

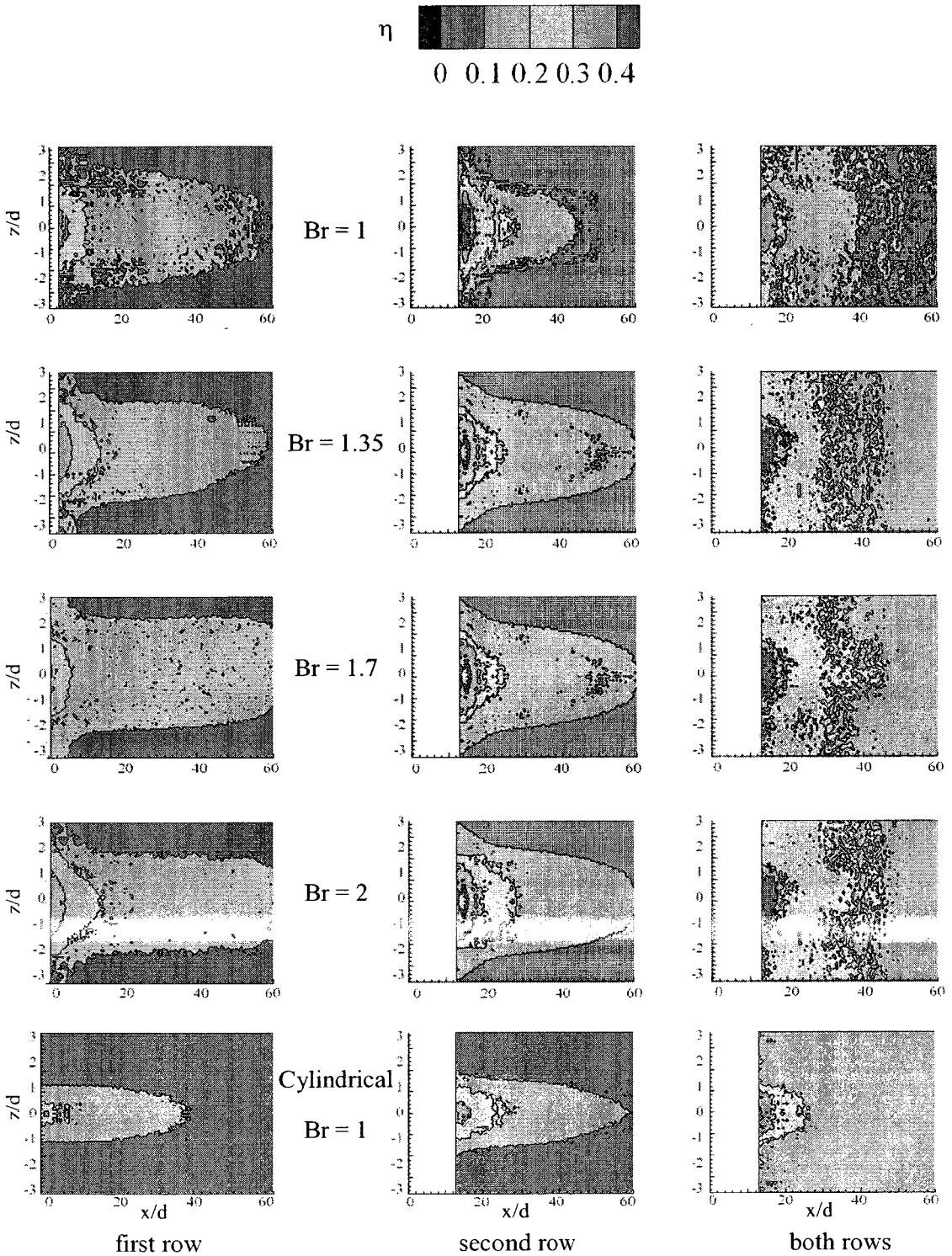

Figure 4-5 Local effectiveness distributions for suction side with louver scheme

surface with the higher effectiveness level. On the other hand, increasing the injection-blowing ratio with the cylindrical exit decreases the effectiveness level and coverage due to the severe jet lift-off. On the double injection, the jet injected from the first row causes a blockage downstream the first row and allows the coolant from the second row to be attached to the surface, causing a higher effectiveness level compared with the second row injection only. The coolants from two staggered rows are merged more efficiently together causing a higher effectiveness.

4.2.1 Average spanwise effectiveness

Figure 4.6 shows the effectiveness of the louver scheme at the moderate blowing ratio (Br = 1) compared with cylindrical and shaped holes at the same blowing ratio strength on different airfoil shapes. The cylindrical hole in the present study shows lower effectiveness compared with the cylindrical hole of Waye and Bogard (2007) due to the difference in the hole spacing. The p/d in their study was 5.6, while p/d in the present study is 7.5. Increasing the pitch to diameter ratio increases the unprotected area downstream the cooling hole, hence decreasing the lateral average spanwise effectiveness as reported by Waye and Bogard (2007). In their study, they doubled the hole spacing, from 2.8 to 5.6, and they found the effectiveness was halved at the same blowing ratio, these results are presented in Figure 4.6. The cylindrical hole of the current study has a comparable performance, about 25% less, with that of Chappell et al. (2008). The lower average effectiveness is attributed to the larger pitch to diameter ratio in the current study, compared to 6 for the other study. Both results are measured at the suction side from an injection point at 25% of C_x of both vanes. The effectiveness of shaped hole at moderate blowing ratio, Br = 0.9, from Chappell et al. (2008) is also presented in Figure

4.6. The shaped hole shows higher effectiveness compared with the cylindrical hole from the same study. The louver scheme at Br = 1 shows the highest effectiveness compared with that of the cylindrical hole of the present study for both shapes of Chappell et al. (2008), in addition to a longer coverage distance. The dissimilarity in the geometrical aspects between different airfoils and hence the flow characteristics leads also to a variation in the film effectiveness.

The previous comparison is based on the dimensionless distance downstream of the cooling hole normalized to the hole diameter. To compare with additional studies and more shapes, the performance of the cooling holes in the current study is presented versus the dimensionless axial distance normalized to the axial chord of the vane and presented in Figure 4.7. The fan shaped hole in the investigation of Gao et al. (2008) showed higher effectiveness compared with cylindrical hole with higher decay. The faster decay in that study is attributed to the boundary layer development on the gas turbine rotor which is different from that of the gas turbine stator, however this study was also conducted on a static cascade. The effectiveness of the cylindrical hole in the present study shows a good agreement with the effectiveness of the previous studies, which gives more confidence in the approach and methodology used in this study.

As shown in Figures 4.6 and 4.7, the louver scheme provides higher effectiveness compared with the current cylindrical and shaped holes. Near downstream the hole, $x/d < 10$, the louver provides the highest effectiveness, about three times that of cylindrical hole of similar hole spacing. As shown from the effectiveness local distribution in Figure 4.5, the jet of low momentum is attached to the vane surface and maximizes the surface protection. This indicates the ability of the modified jet to expand laterally early

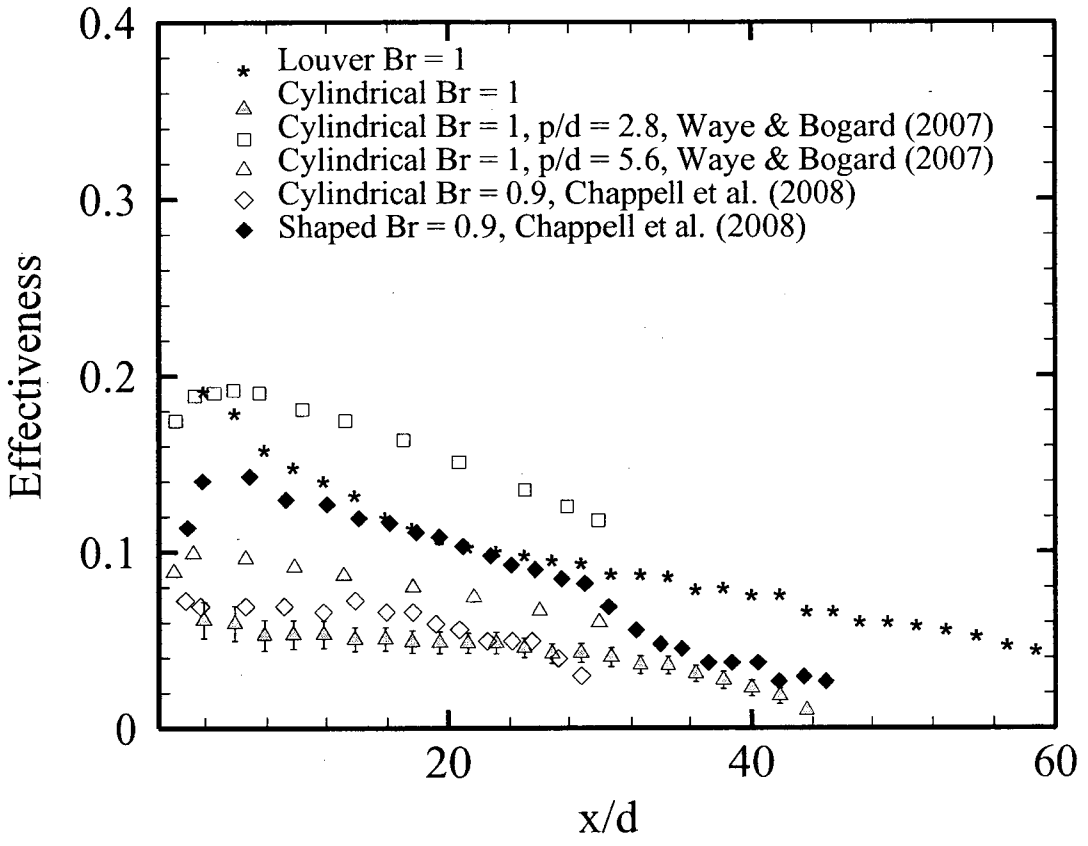

Figure 4-6 Average-spanwise effectiveness for louver, 1st injection, with different hole shapes on the suction side (normalized to hole diameter)

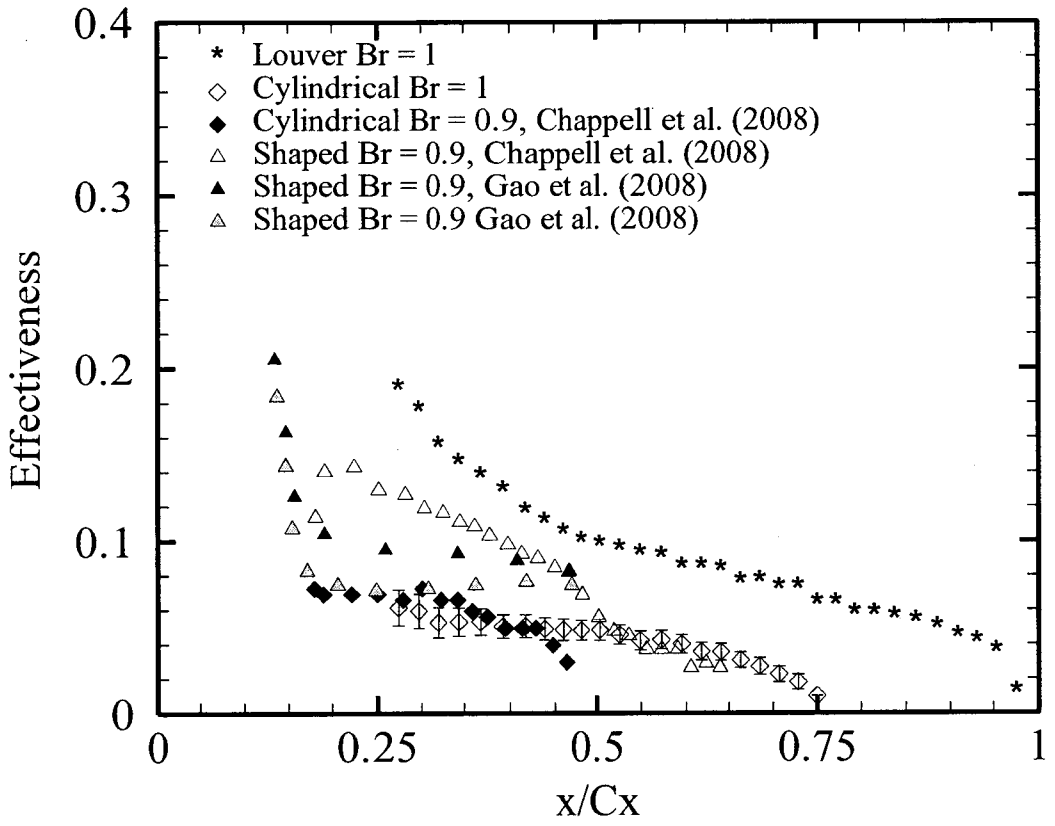

Figure 4-7 Average-spanwise effectiveness for louver, 1st injection, with different hole shapes on the suction side (normalized to the axial chord)

downstream without a high amount of mixing with the mainstream. When compared with the cylindrical holes with narrower spacing, the louver scheme provides equivalent effectiveness, giving a high advantage to the louver in terms of machining time and mechanical strength of the vane surface. Also, the louver provides higher effectiveness than the shaped hole by about 30% near the downstream region. Farther downstream up to x/d <30, the attached jet to the surface provides wider span protection as seen in Figure 4.5, which is reflected as a steady lateral average spanwise effectiveness, shown in Figure 4.6. In this region, the louver has comparable performance with the other geometries.

Far downstream x/d > 30, the louver provides a slight decrease in the spanwise protection distance, as shown in Figure 4.5. Therefore, the lateral-average effectiveness shows a slight decrease which is another advantage of the louver compared with other shapes which lost their effectiveness due to mixing with the mainstream. The louver has a superior effectiveness such that it provides more cooling far downstream, compared to the cylindrical holes near downstream or shaped holes moderately downstream of the injection point. This is because the well-designed lateral expansion exit allows more jet spreading in the spanwise direction in addition to decreasing the jet momentum. The coolant then forms a barrier flow that protects the surface far downstream. This shows an additional advantage of the louver scheme as it allows the second row to be positioned farther downstream than the first row, hence decreasing the number of machined rows on the airfoil surface.

4.2.2 Influence of injection location and blowing ratio

Moving the position of injection further downstream improves the film cooling performance for both the louver scheme and the cylindrical exit as shown in Figure 4.8.

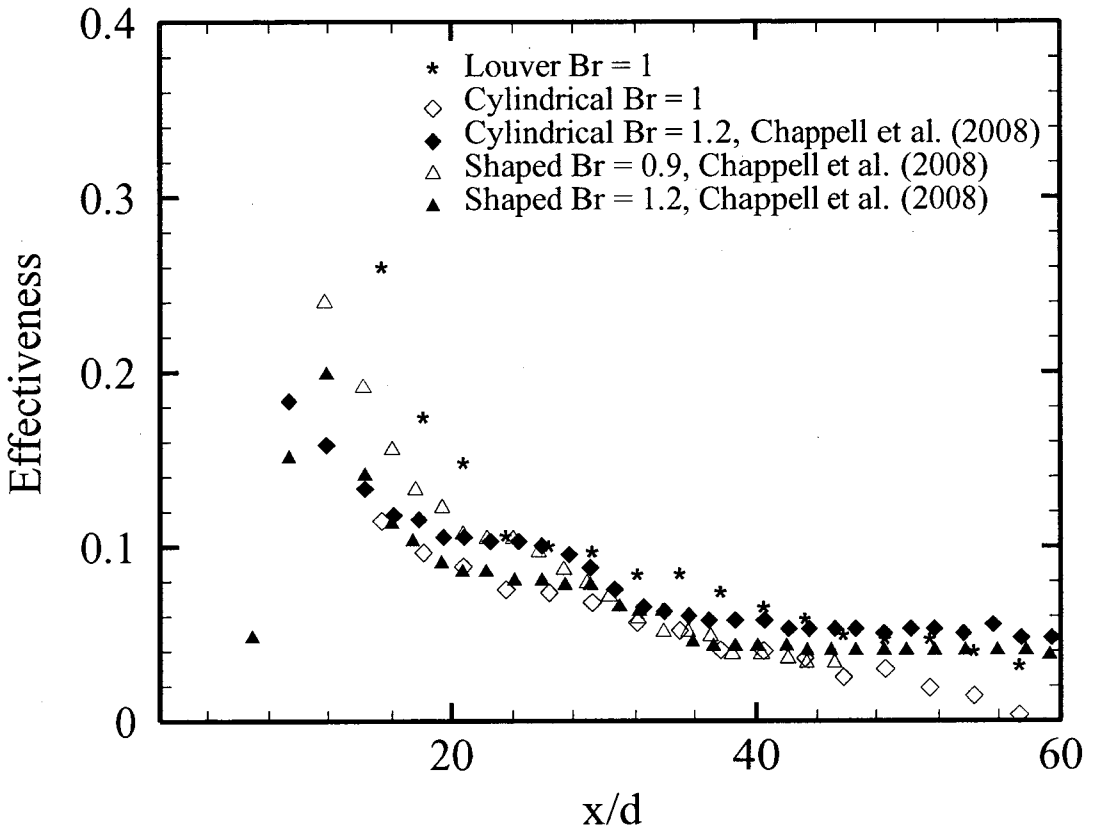

Figure 4-8 Average-spanwise cooling effectiveness for the 2nd row on the suction side

The improvement in the effectiveness is caused by the adverse pressure gradient created by the flow deceleration and the more flat surface of the vane at the second injection location. The louver scheme shows higher effectiveness compared with that of the shaped holes of Chappell et al. (2008), as well as the cylindrical exit. The shaped hole provides lower effectiveness with increased blowing ratio; however the coolant amount at the higher blowing ratio is enough to cover a longer distance downstream. On the second row of injection, the shaped hole provided lower effectiveness compared with the cylindrical hole. In the current study, the louver provides double effectiveness near downstream of the hole compared with that of the cylindrical hole on the second injection location. While the louver provides effectiveness equal to three times the cylindrical effectiveness in the first injection case. This may be attributed to the shallower injection angle at the second location which decreased the cylindrical jet lift-off, yielding more efficient injection with higher effectiveness.

The interaction between both rows is investigated based on the same coolant amount. The mass of the coolant flowing through the first row is added to that of the second flow and then applied through the plenum to both rows together. The static pressure in the plenum at the case of both rows is higher than that of the first row by 20%. This difference may cause discrepancy on the local blowing ratio at each row yielding to a higher coolant amount to flow through the second row. However, this difference is not considered as the objective of the study is to investigate the effect of the interaction between both jets based on the same coolant amount applied on the real case geometry. The results of this investigation are presented in Figure 4.9 and compared with the findings of similarstudies. The performance of cylindrical holes in the study of Drost

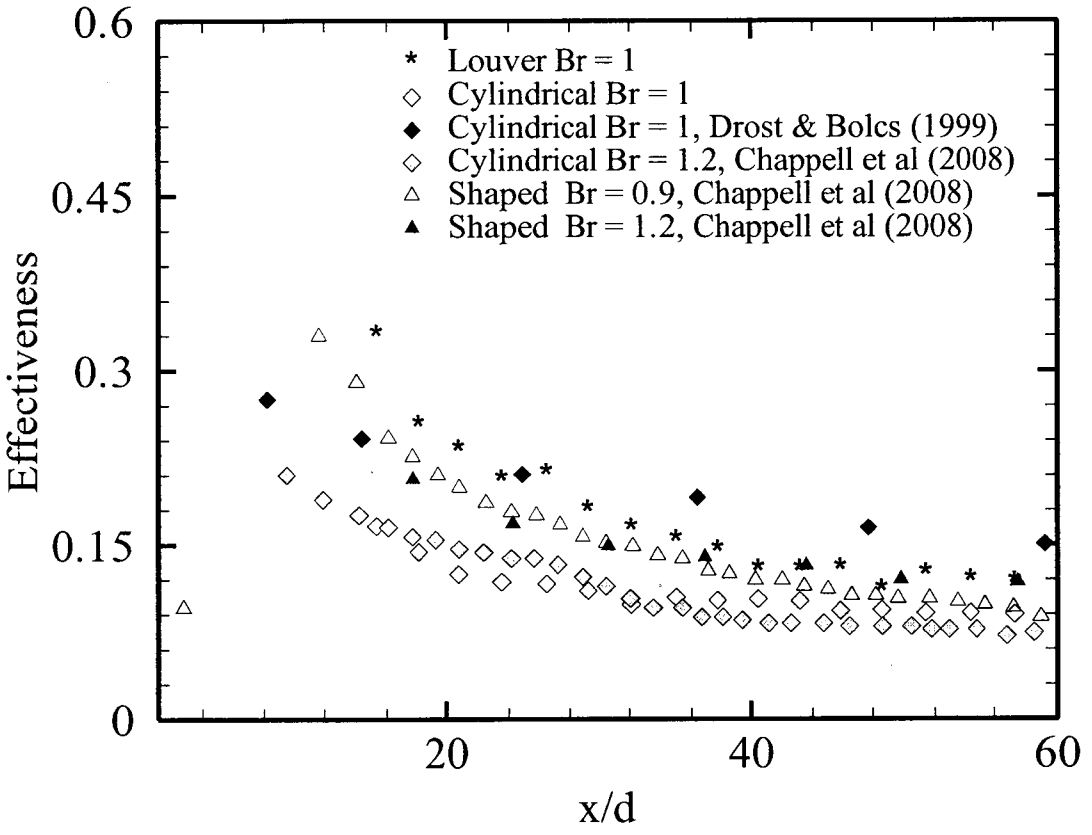

Figure 4-9 Louver double injection effectiveness compared with similar studies on the suction side

and Bolcs (1999) shows a 25% increase in the effectiveness over the cylindrical effectiveness of the current study. This increase is attributed to the smaller pitch to diameter ratio, p/d = 3.75, compared with that of the current study, p/d = 7.5.

The louver provides higher protection compared with either the shaped or the cylindrical hole of Chappell et al. (2008). The first injection location gives a longer cooling trace downstream of the hole, which allows the remaining coolant to merge with the second injection, causing significant increase in the effectiveness. Therefore, the louver with double injection shows a noticeably better effectiveness than that estimated using the superposition principle with the individual effectiveness of each row. The combined injection shows better performance compared with the superposition resultant, which matches the findings of Zhang and Moon (2007). The superposition effectiveness is calculated based on the superposition model as presented by Jiang and Han (1996).

$$\eta = \eta_1 + \eta_2 (1-\eta_1) \qquad (4.1)$$

The principle of superposition is applied to the louver scheme on the suction side. The effectiveness of the first row is added to that of the second row at the points downstream of the second row. The summation is plotted in Figure 4.10 and compared with the real effectiveness of the double injection. Figure 4.11 presents the effect of blowing ratio at different injection locations. At the first row of holes shown in Figure 4.11a, there is a slight increase in the effectiveness by increasing the blowing ratio near downstream of the hole. At the mid region, all blowing ratios provide similar effectiveness which indicates full attached coolant for different blowing ratios. Far downstream at the higher blowing ratios, 1.7 and 2, the coolant amount is much more

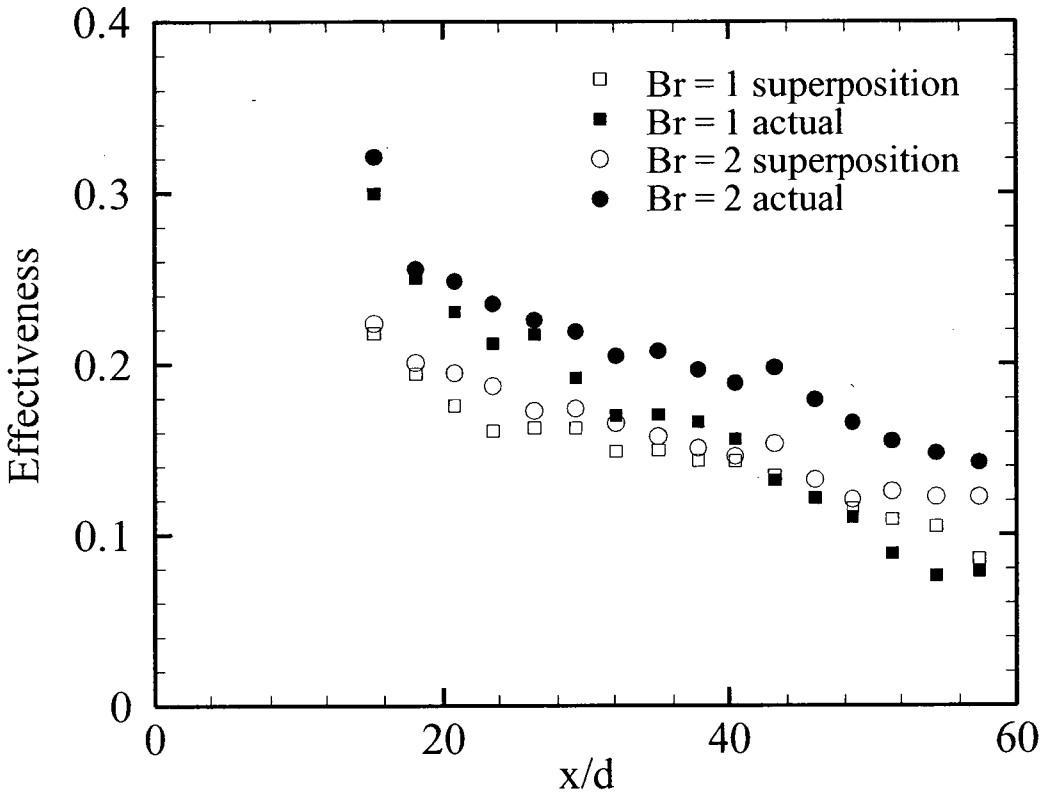

Figure 4-10 Effectiveness using superposition principle with the louver scheme

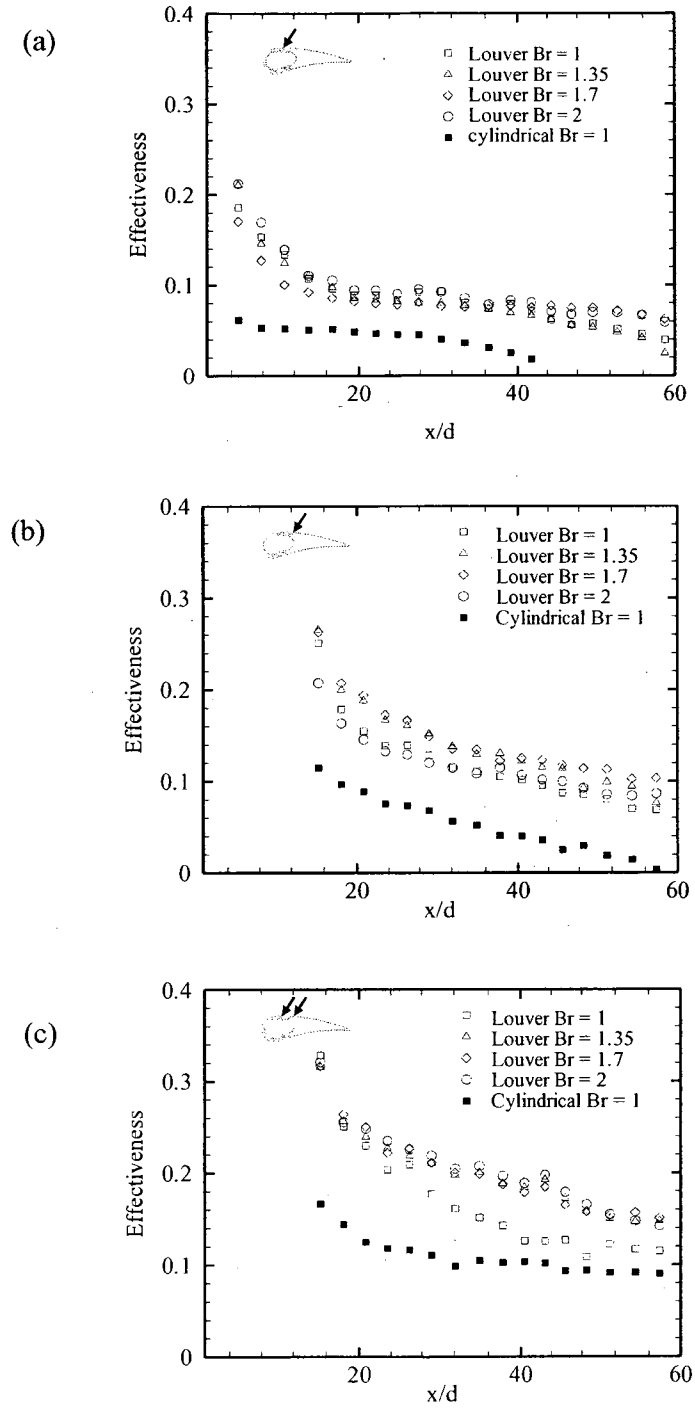

a)1st row b) 2nd row c) both rows

Figure 4-11 Effect of blowing ratios at different locations on the suction side

than that of moderate blowing ratios yielding a higher effectiveness. At the second injection location shown in Figure 4.11b, the increase in the blowing ratio yields more coolant amount to be delivered to the jet causing higher effectiveness. At the highest blowing ratio, Br = 2, there is a slight decrease in the effectiveness which indicates the starting of the jet lift-off. Consequently, at double injection, the effectiveness increases with the increase of the blowing ratio with a slight increase for Br = 1 as the coolant amount of the first row is not enough to provide further coolant far downstream, as shown in Figure 4.11c. Generally, the cooling effectiveness of the louver scheme, on contrary with the standard cylindrical exit or other shapes, increases with the increase of the blowing ratio due to the significant reduction of the jet momentum. As the blowing rate increases, more coolant is delivered to the jet causing higher effectiveness far downstream, which is another advantage of the louver scheme compared with the common schemes.

4.3 Film cooling effectiveness on pressure side

As on the suction side, the performance of the scheme is tested at two different locations and compared with the standard cylindrical hole that has the same base diameter. Figure 4.12 shows the local effectiveness distribution using the louver scheme at the two injection locations in addition to the double injection with four different blowing ratios compared with the cylindrical hole at the best blowing ratio (Br = 1). The louver scheme provides full lateral coverage downstream of the hole, while the similar cylindrical hole covers almost 50% of the lateral distance downstream of the cooling hole. The bend of the louver causes a significant decrease in the coolant momentum by changing the flow direction before the exit. The momentum is then subjected to further

reduction in the expanded exit, causing a reduction in the jet momentum. The jet momentum is then significantly decreased yielding more coolant to be adjacent to the vane surface. The effectiveness increases downstream of the hole with more coolant staying attached to the surface for a longer distance. By increasing the blowing ratio, the louver completely protects the vane surface with a higher effectiveness level. On the other hand, increasing the blowing ratio with the cylindrical exit decreases the effectiveness level and the coverage due to the severe jet lift-off. For the double injection, the coolants from two staggered rows are merged more efficiently together causing a higher effectiveness.

The cooling effectiveness of the louver scheme at the first row on the pressure side is shown in Figure 4.13 for Br = 1 compared with the effectiveness of the cylindrical hole at similar blowing ratio from previous studies. The effectiveness of the cylindrical hole of the current study shows a good agreement with that of Drost and Bolcs (1999) with relatively lower values near downstream of the hole exit. The holes in their study had a compound angle of 30° which caused a better coverage near downstream of the hole yielding an increase in the lateral average effectiveness. The results of Schwarz and Goldstein (1989) on a concave surface is also presented in Figure 4.13 at two density ratios, DR = 0.95 and 2. The higher density ratio, which is more comparable to actual engine conditions, shows a higher effectiveness, especially near downstream of the hole. The effectiveness of the cylindrical hole in the present study shows relatively lower values compared with that for the lower density ratio, which is close to that used by Schwarz and Goldstein (1989). This difference is attributed mainly to the nature of the low over the pressure side that has a concave profile; however there is a convex surface

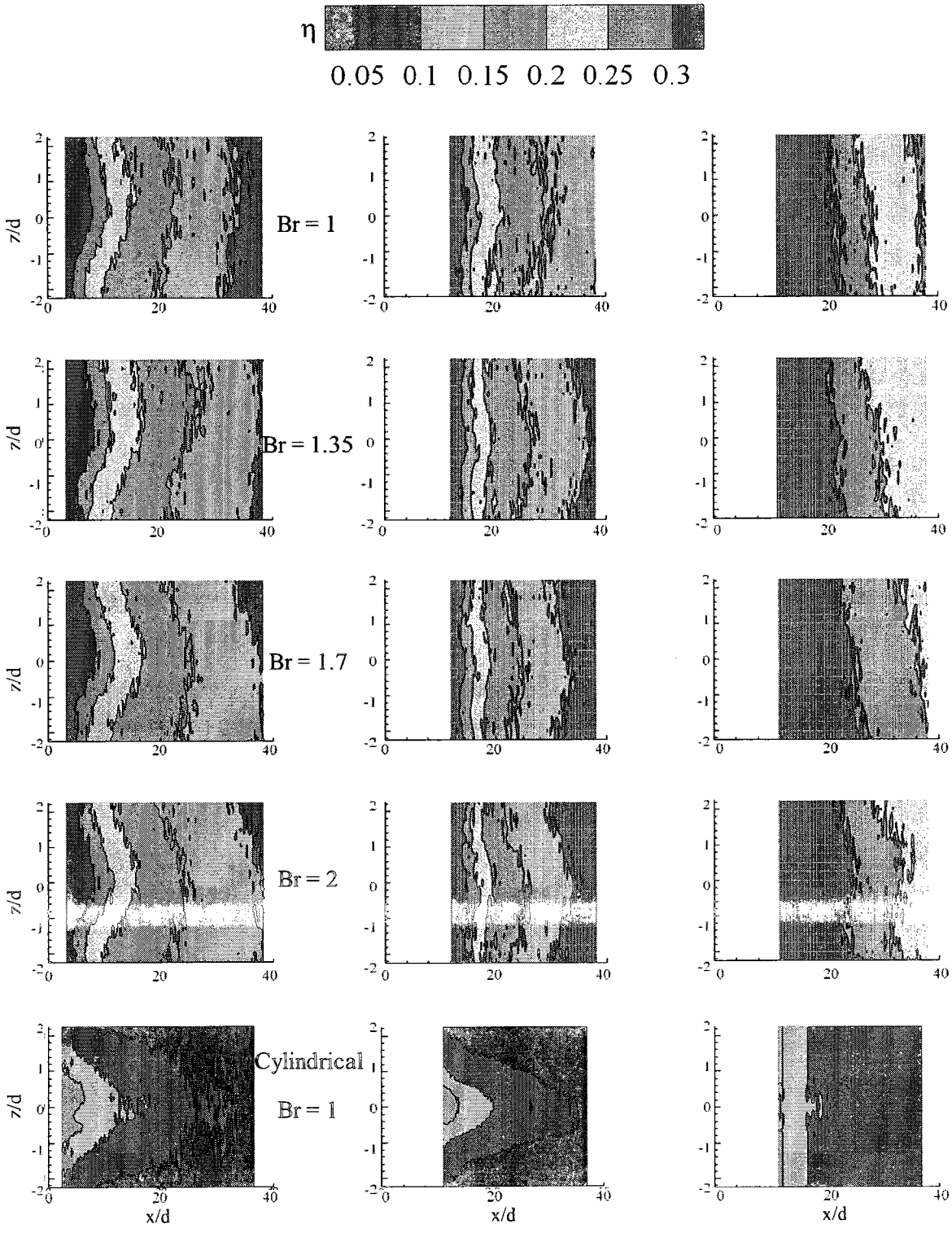

Figure 4-12 Local effectiveness distribution for pressure side with louver scheme

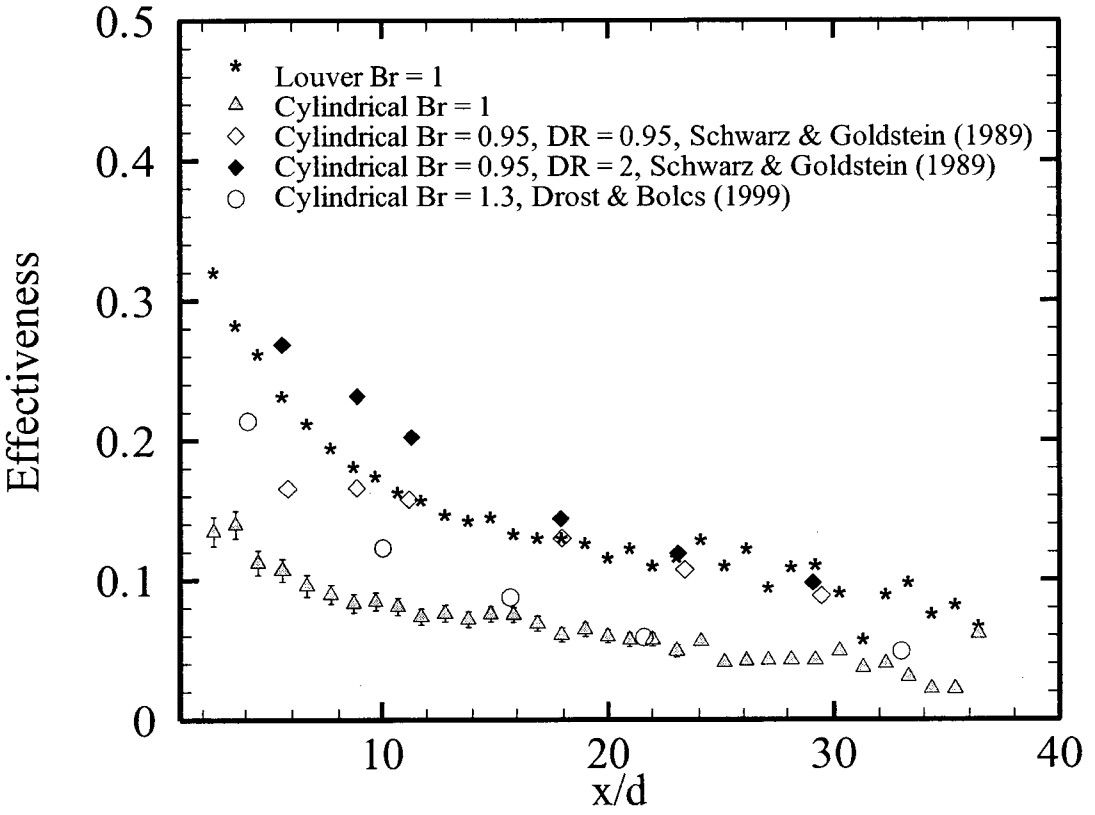

Figure 4-13 Average-spanwise cooling effectiveness for the louver 1st row on the pressure side

upstream that mainly affects the flow nature. Another reason for the higher values in their study is the pitch to diameter ratio of 3 compared with 4.5 for the present study. As expected from the suction side results, the louver shows higher effectiveness compared with that of the cylindrical hole. The louver provides reasonable effectiveness far downstream of the hole which is equal to the cylindrical effectiveness early mid downstream.

4.3.1 Single injection

Figure 4.14 presents the effectiveness of the louver scheme at different blowing ratio on both pressure and suction side. The blowing ratio has a slight influence on the louver effectiveness with a tendency to increase the effectiveness with increased blowing ratio on both pressure and suction side. This figure provides a full view for both the louver scheme and the standard cylindrical holes at different injection location. The pressure side, in general, provides higher effectiveness near downstream of the hole with steeper decay compared with the suction side as shown for the first row in Figure 4.14a. Increasing the effectiveness near downstream of the hole is attributed to the tangential component of the jet momentum ($I \cos^2\alpha$). This component causes the coolant to be attached to the concave surface of the pressure side and move the coolant away from the convex surface of the suction side. By developing the flow farther downstream of the hole, two mechanisms affect the flow on the pressure side causing the rapid decay, the flow instability over concave surface and the cross-stream pressure gradient. The concave instability enhances the mixing between the mainstream and the coolant, in addition to the high pressure of the cross stream that tends to move the coolant away from the concave surface, as shown by Schwarz et al. (1991).

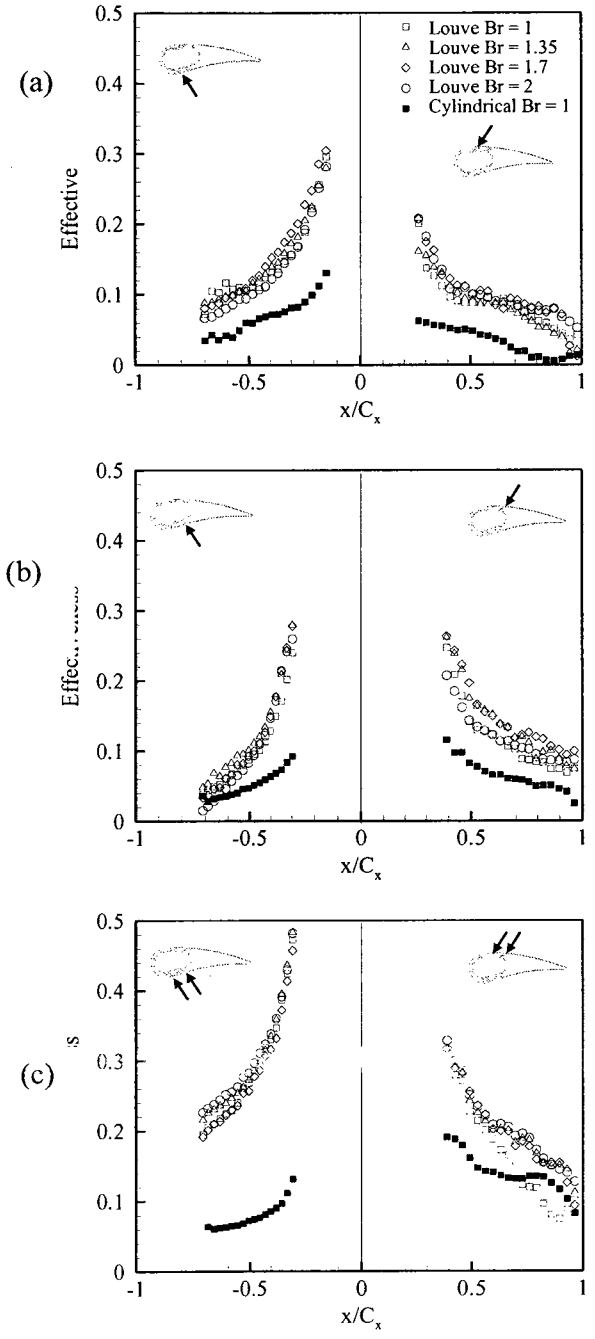

a) first row b) second row c) both rows

Figure 4-14 Vane complete coverage using louver scheme

Due to the higher local main velocity at the second row compared with the first row, the second row needs a higher coolant flow rate to achieve the desired blowing ratios. This flow increase causes the static pressure in the plenum at the second row to be higher than that of the first row by 15%. This difference has been accounted for in the calculation of the blowing ratio to assure the exact blowing ratio in each case. The injection from the second row of louver scheme on the pressure side shows relatively the same effectiveness near downstream as that of the first row with steeper decay farther downstream, as shown in Figure 4.14b. This is contrary to what occurs on the suction side, where the second row provides a higher effectiveness than the first row as shown in previous section. This finding matches the findings of both Jiang and Han (1996), and Ames (1998), for the cylindrical hole and Gao et al. (2008) for the shaped hole. This rapid decrease is attributed to the fact that both injections on the suction side are in the region of the adverse pressure gradient, while the injection on the pressure side is in the favourable pressure region. In addition the turbulence level on the pressure side is higher than that of the suction side due to the flow instabilities on the concave surfaces. The high local values of the turbulence along with the favourable pressure gradient on the pressure surface caused a rapid decrease in the effectiveness, as shown by Ames (1998). The decrease on the second row on the pressure side may be attributed to the higher local Re number at the second row than that at the first row by 35%. The increase in Re number yields a more turbulent boundary layer which increases the mixing possibility between both streams. This mix could occur when a highly fluctuated interface between both streams diffuse through each other, causing a rapid dissipation of the jet, hence an effectiveness reduction.

The cylindrical hole on the pressure side shows slightly lower effectiveness at the second row with less steep decay compared with the louver scheme. The turbulent boundary layer has low influence on the cylindrical jet compared with the louver scheme. This is because the jet on the louver is dispersed laterally losing its momentum, while the cylindrical jet is more concentrated and penetrating through the boundary layer. This indicates that the larger interface surface between the main flow and the dispersed jet causes less efficient cooling far downstream. However, the significant effectiveness increase near downstream accounts for this drawback, in addition to the more uniform thermal stresses accompanying the spread jet. Contrary to the cylindrical exit, the louver effectiveness increases as the blowing ratio increases, up to Br = 2. This indicates that the coolant amount is enough with the controlled momentum to keep an effective barrier between the mainstream and the surface.

4.3.2 Double injection

The interaction between both rows is investigated based on the same coolant amount, as done on the suction side. The mass of the coolant flowing through the first row is added to that of the second flow and applied through the plenum to both rows together. The plenum in the case of both rows is subjected to a higher static pressure than that of the first row by approximately 25%. This difference may cause a discrepancy on the local blowing ratio at each row yielding a higher coolant amount to flow through the second row. The louver scheme in the double injection on the pressure side shows superior effectiveness compared either with the second row only on the pressure side or with the double injection on the suction side, as shown in Figure 4.14c. As mentioned in part I of this paper, the boundary layer is thickened due to the injection of the first row.

The boundary layer upstream from the second row is then thicker than its normal thickness without first row injection, and it is also enriched with the coolant. The coolant from the second row is injected in this appropriate environment yielding a proper coverage and the aforementioned superior effectiveness. In addition, the pitch/diameter ratio on the pressure side is almost half that of the suction side which improves merging between the adjacent holes.

Another reason that may cause this superior effectiveness is the concave instability that promotes the blockage by the first row injection, as mentioned by Schwartz et al. (1991). This blockage is then supported by the second row injection creating a more efficient barrier that prevents the mainstream from piercing the coolant layer as it does on the suction side, as show in Figure 4.4. The double injection using the cylindrical hole does not provide the same proper enhancement as the louver scheme. The nature of the concentrated circular jet allows the main stream to break through the injected coolant from the first row. A direct interaction between the second row injection and the mainstream is then invoked causing the dilution of the coolant. Moreover, the direct interaction between both streams enhances the strength of the kidney vortices that is created due to the injection process, yielding a dilution of the coolant on the mainstream. The drawback of the diffused exit that causes the steep decay on the pressure side single injection enhances the efficiency of the double injection yielding a superior effectiveness.

Figure 4.15 presents the effectiveness of the louver scheme at the mid span of the three injection cases. The mid span effectiveness of the first and the second rows show similar values to the lateral average values, which is expected from the effectiveness local

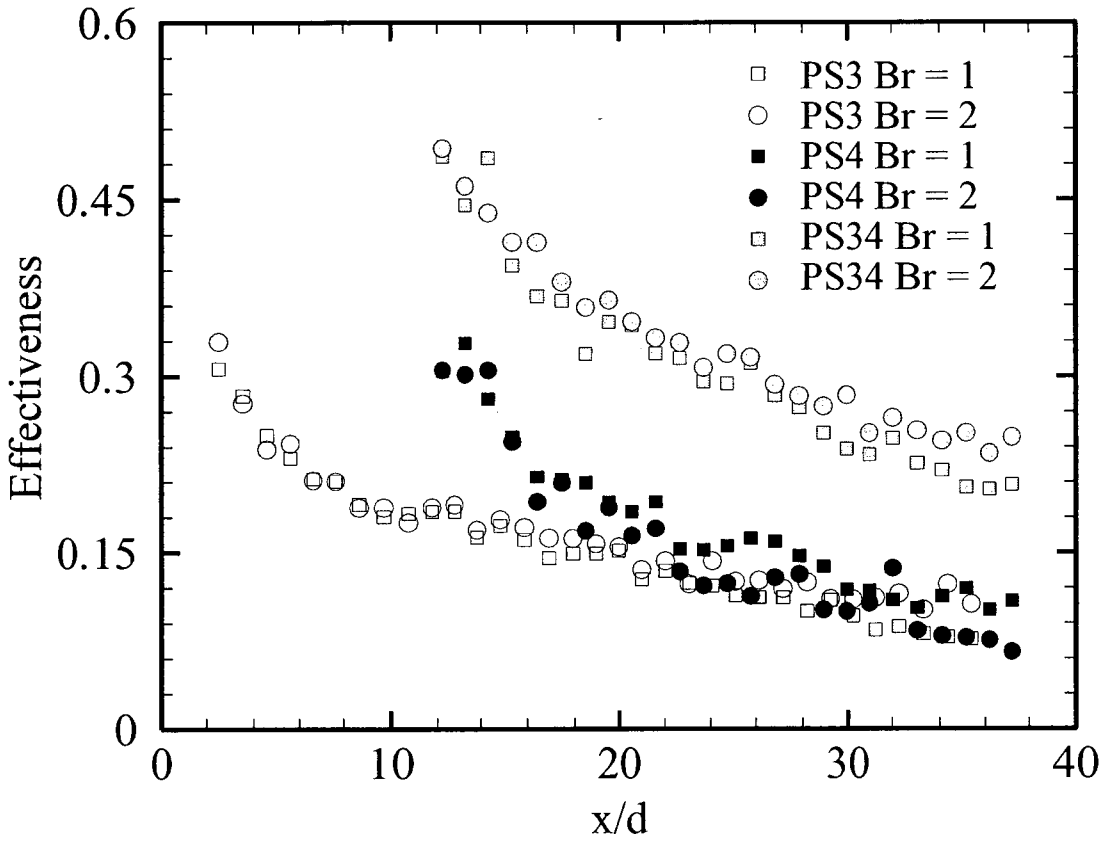

Figure 4-15 Mid span cooling effectiveness for the three louver injection cases.

distribution as shown in Figure 4.12. The mid span of the double injection case is considered as the mid span of the second row, and its effectiveness shows a significant enhancement compared with the second row injection only. This indicates an increase in the effectiveness compared with the superposition principle as found on the suction side. The elevated increase of the double injection mid span effectiveness compared with the second row only, more than the direct superposition with the first row only, supports the justification for the superior increase of the double injection.

Figure 4.16 presents the spanwise effectiveness of the louver scheme for the three injection cases at Br = 1 compared with the similar injection cases in the cylindrical exit at the same blowing ratio. The louver shows more lateral spreading which is better in terms of thermal stresses as it keeps a uniform thermal load over the vane surface. The two row injection shows a noticeable increase in the mid span effectiveness because the remaining coolant comes from the first row, especially in the cylindrical case.

4.4 Suction side heat transfer coefficient

The local HTC on the vane suction side is obtained by solving Equation (3.10) and the contours are plotted in Figure 4.17. The HTC of the louver scheme at different hole locations and four blowing ratios is presented and compared with the cylindrical hole HTC at Br = 1. The louver scheme affected area is wider than that of the cylindrical hole. However, the cylindrical hole HTC values are higher and extend over a longer distance downstream of the hole. The louver redistributes the thermal load over the surface, resulting in uniform thermal stresses. Increasing the blowing ratio increases the amount of the coolant, hence disturbing the jet and causing further increase in the HTC.

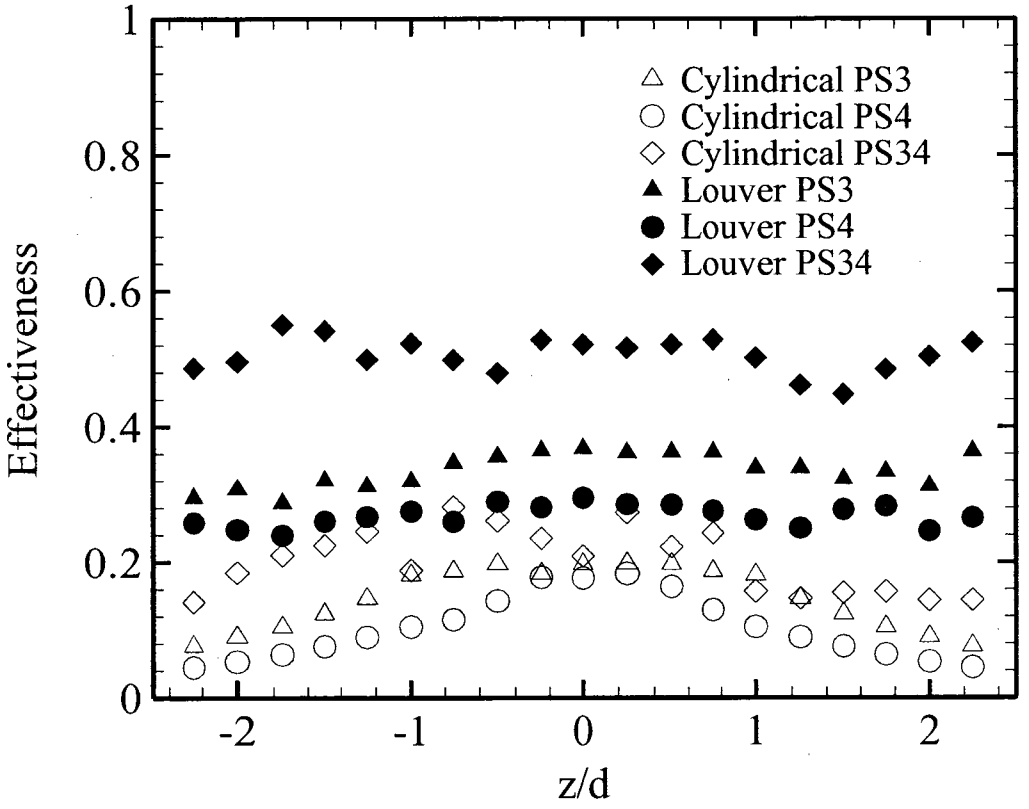

Figure 4-16 Spanwise cooling effectiveness for different injection profiles with louver and cylindrical hole, Br = 1

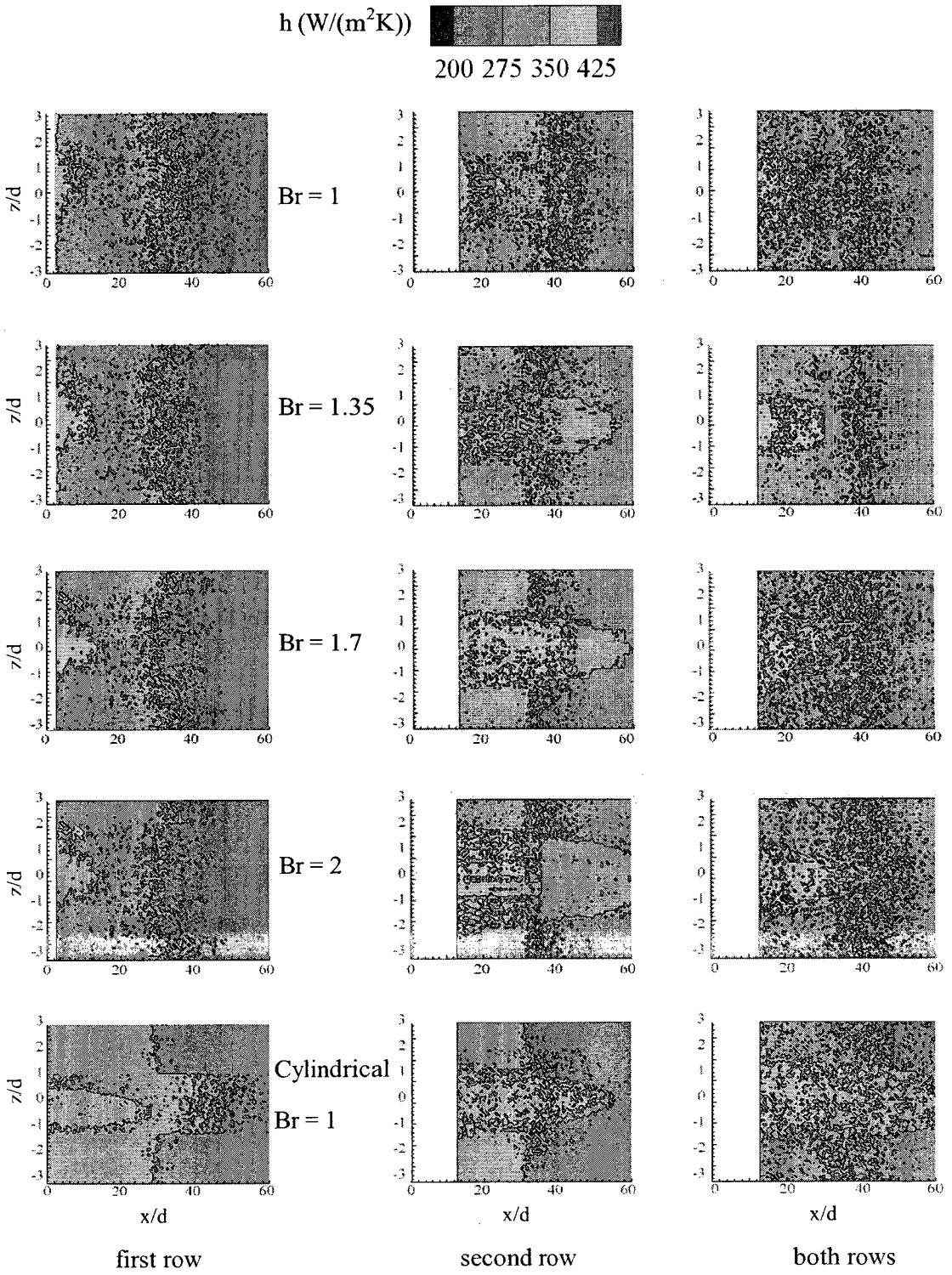

Figure 4-17 Local heat transfer coefficient distribution for suction side with louver scheme

The local HTC with film cooling over the vane surface is divided by the corresponding HTC without film cooling and presented in the lateral-averaged normalized form. The line that passes by the trailing edge of the louver scheme on the first row is selected to be the reference coordination point, see Figure 4.3. Figure 4.18 compares the HTC of the louver at the first injection location with that of the cylindrical hole at moderate and high blowing ratios. In the present study, the cylindrical hole HTC at Br = 1 shows good agreement with that of Drost and Bolcs (1999). The cylindrical exit local HTC values are slightly higher than those of the louver at Br = 1. Far downstream, x/d > 50, the louver jet loses its effect on the main flow, while the cylindrical jet still has enough momentum to disturb the flow and cause a higher heat transfer enhancement. At higher blowing ratios, the cylindrical hole provides higher momentum jet such that it increases the HTC, particularly far downstream, as shown by Drost and Bolcs (1999). The louver scheme causes an increase in the HTC as the blowing ratio is increased; however the jet momentum is still lower than that of the cylindrical jet. Therefore, the HTC increases near the hole exit on the downstream side, with a tendency to decrease further downstream.

The effect of varying blowing ratio on the HTC is presented in Figure 4.19 in terms of the average-spanwise normalized values and the centerline values at moderate and high blowing ratios, Br = 1 and Br = 2, respectively. Figure 4.19a shows the effect of the blowing ratio on the first row. The lateral average HTC slightly increases with increasing blowing ratio. The centerline shows the same HTC values near downstream due to the steep velocity gradient within the boundary layer and the slightly increasing HTC with increasing blowing ratio. Moving the injection location downstream, towards

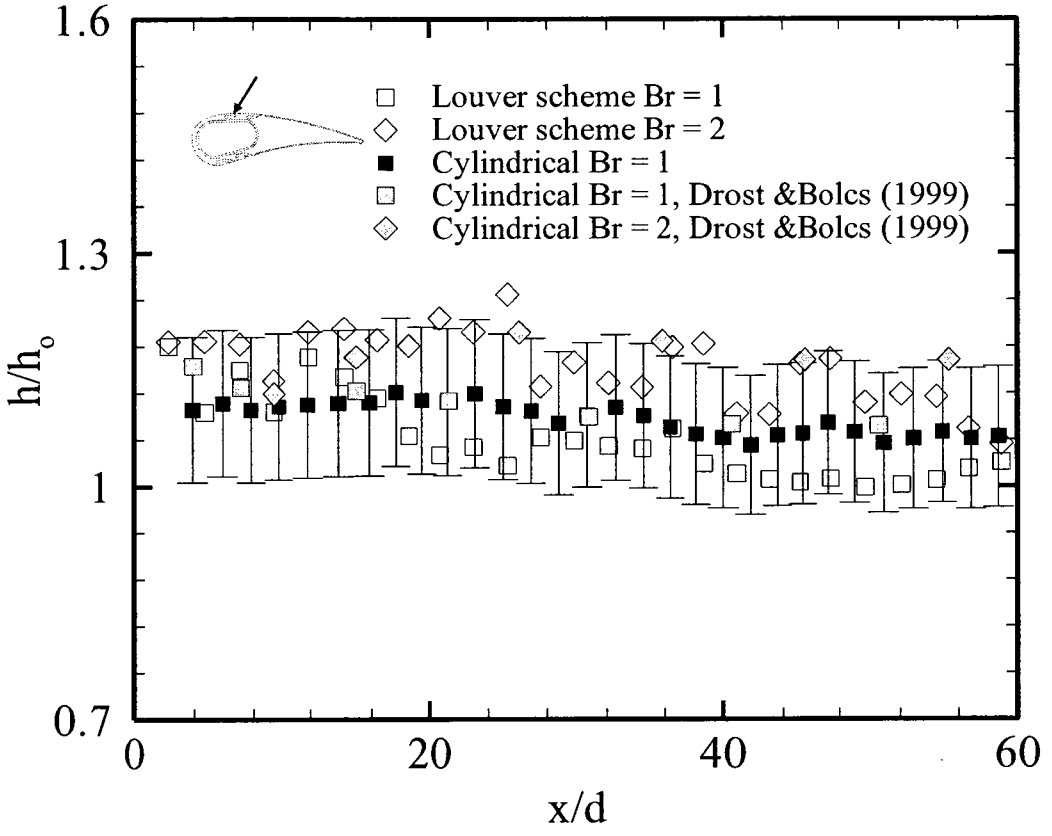

Figure 4-18 Average-spanwise normalized heat transfer coefficient 1st row, suction side

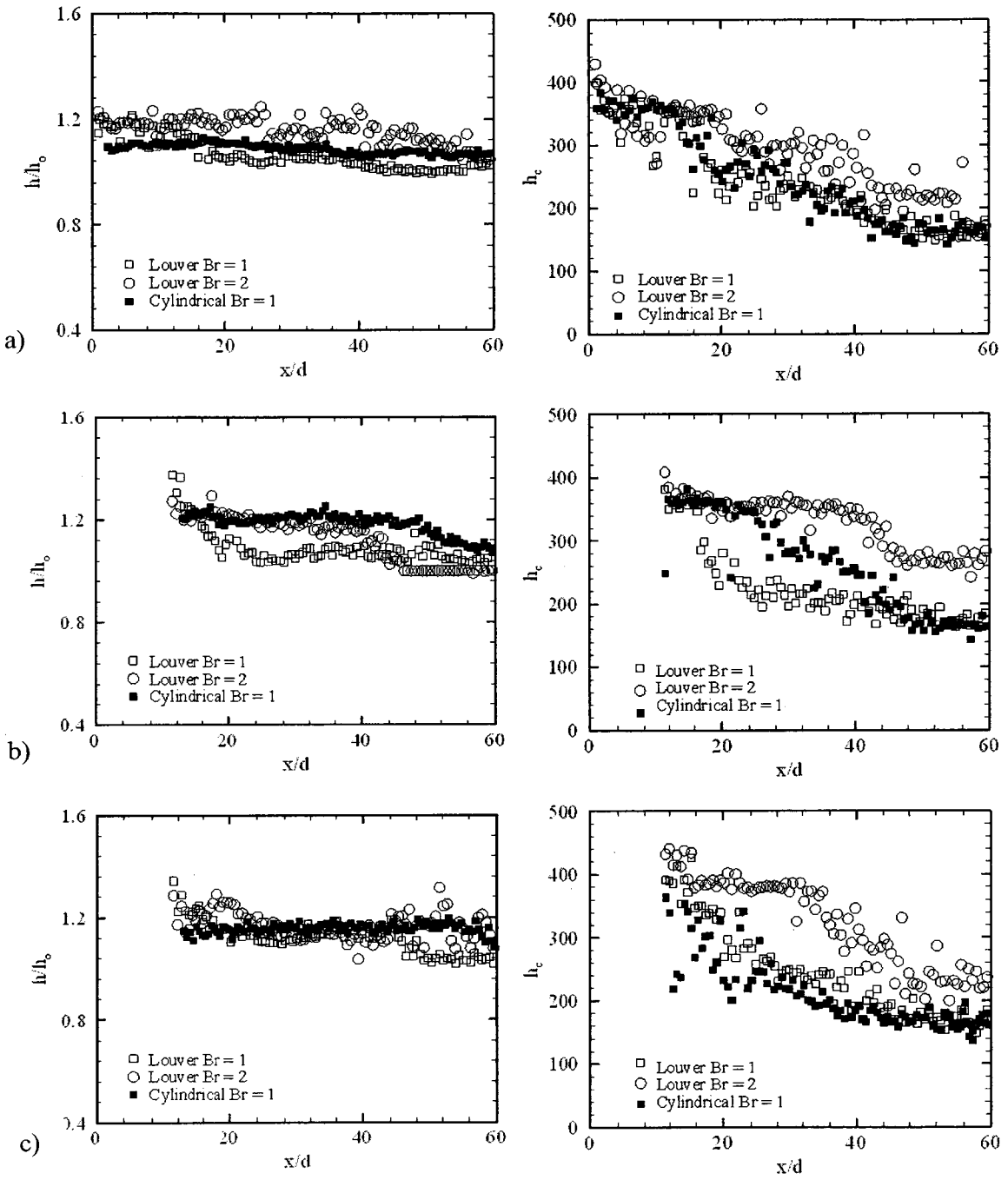

a) first row b) second row c) both rows

Figure 4-19 Average-spanwise normalized and centerline heat transfer coefficient for the louver on the suction side

the second row, the HTC shows higher values just downstream of the hole exit, as shown in Figure 4.19b, due to the change in the boundary layer thickness. The boundary layer at the second location is more developed and the velocity gradient is less steep, so the jet disturbs the mainstream within the boundary layer causing a higher HTC. Increasing the blowing ratio increases the amount of coolant delivered, yielding a higher disturbance level which extends over a longer distance downstream. The cylindrical exit, at Br = 1, shows similar values to the louver at the highest blowing ratio, Br = 2. In addition, far downstream, the cylindrical hole at Br = 1 HTC is higher than that of the louver scheme even at Br = 2. This may be attributed to the expanded exit of the louver that distributes the coolant laterally causing rapid dilution of the coolant with the mainstream.

The centerline HTC continuously decreases with the distance downstream of the first hole. The HTC values are higher than those obtained without film cooling, but the trend in HTC variation with the downstream distance is similar to that of the HTC without film cooling. Just downstream of the second hole, the centerline HTC is higher than h_o. It then decreases suddenly but remains higher than h_o. The difference in HTC variation between both rows is due to the difference in boundary layer development. On the first location, the boundary layer allows the jet flow to enter the mainstream flow and cause a gradual decrease in HTC. On the second location, the boundary layer encourages the flow to locally disturb the mainstream flow before joining it. At Br = 1, the cylindrical exit provides slightly higher HTC than the louver just downstream of the hole, but the trends in HTC variation are similar mid and far downstream. At Br = 2, the louver HTC is slightly higher than that of the cylindrical hole due to the equivalent momentum. In addition, the louver shows higher values mid and far downstream due to the increase in

the coolant amount. At the second row location, the relative behaviour between cylindrical, at Br = 1, and louver, at Br = 1 and 2, shows a similar but more pronounced trend than that of the first row. This is attributed to the fact that the jet flow is relatively stronger than the mainstream within the boundary layer.

Figure 4.19c presents the effect of blowing ratio on the HTC using the louver scheme double injection. The distance between the two rows is too small to contain the TLC sheet; therefore there is no data available upstream of the second row of holes. The louver scheme generally results in a lower HTC than the cylindrical hole. At Br = 1, the louver double injection shows a mild decay of the HTC as opposed to the steep decay obtained with injection from the second row only. During the double injection, the coolant coming from the first row, in a stagger arrangement, increases the heat transfer coefficient in between the holes of the second row but maintains a similar HTC on the centerline trace. The laterally averaged HTC increases downstream of the second row, then remains constant mid and far downstream as the effect of the first row is dissipated. By increasing Br to 2, an increase in the average value is recorded for double injection compared with the second row only. At Br = 2, the double injection provides higher lateral-averaged HTC far downstream than that obtained with injection from the second row only. The coolant from the first row has a longer effect at the higher blowing ratio, which extends up to the trailing edge of the vane, causing the higher averaged HTC. Interestingly, the double injection centerline HTC at Br = 2 is lower than that of the second row injection mid and far downstream. This may be attributed to the effect of the coolant from the first row as it spreads laterally and merges with the coolant from the second row, causing an increase in the heat transfer coefficient mid-span the holes, at the

interfacial line, with a decrease in the centerline value. At Br = 1, the cylindrical hole, shows a similar behaviour, with an earlier decrease in the HTC just downstream of the second row of holes for the double injection. The jet flow from the first row causes a blockage to the main stream; hence the coolant injected from the second row is laterally dispersed yielding the aforementioned decrease in the centerline HTC.

4.5 Pressure side heat transfer coefficient

As on the suction side, the performance of the louver scheme is tested at two different locations and compared with that of the standard cylindrical hole of the same base diameter. The results are presented in both local distribution and lateral-averaged normalized values. The local HTC on the vane pressure side is plotted in Figure 4.20 for the louver scheme at different hole locations and for four blowing ratios and compared to that of the cylindrical hole at Br = 1. As on the suction side, the louver scheme results in an affected area that is wider than that of the cylindrical hole. However, the effect of the louver extends over a further distance downstream of the hole. More disturbances are recorded downstream of the first row than the second row. By increasing the blowing ratio, the amount of the coolant increases, hence disturbing the jet flow and causing further increase in the HTC.

The local heat transfer coefficient at each pixel on the vane surface is divided by the corresponding baseline heat transfer coefficient to obtain a normalized form. Figure 4.21 presents the normalized heat transfer coefficient of the first row on the pressure side for both geometries of the exit hole, louver scheme and standard cylindrical, at Br = 1. The heat transfer coefficient obtained with the cylindrical hole shows good agreement with that of Drost and Bolcs (1999). It also shows a good agreement with that of Dittmar

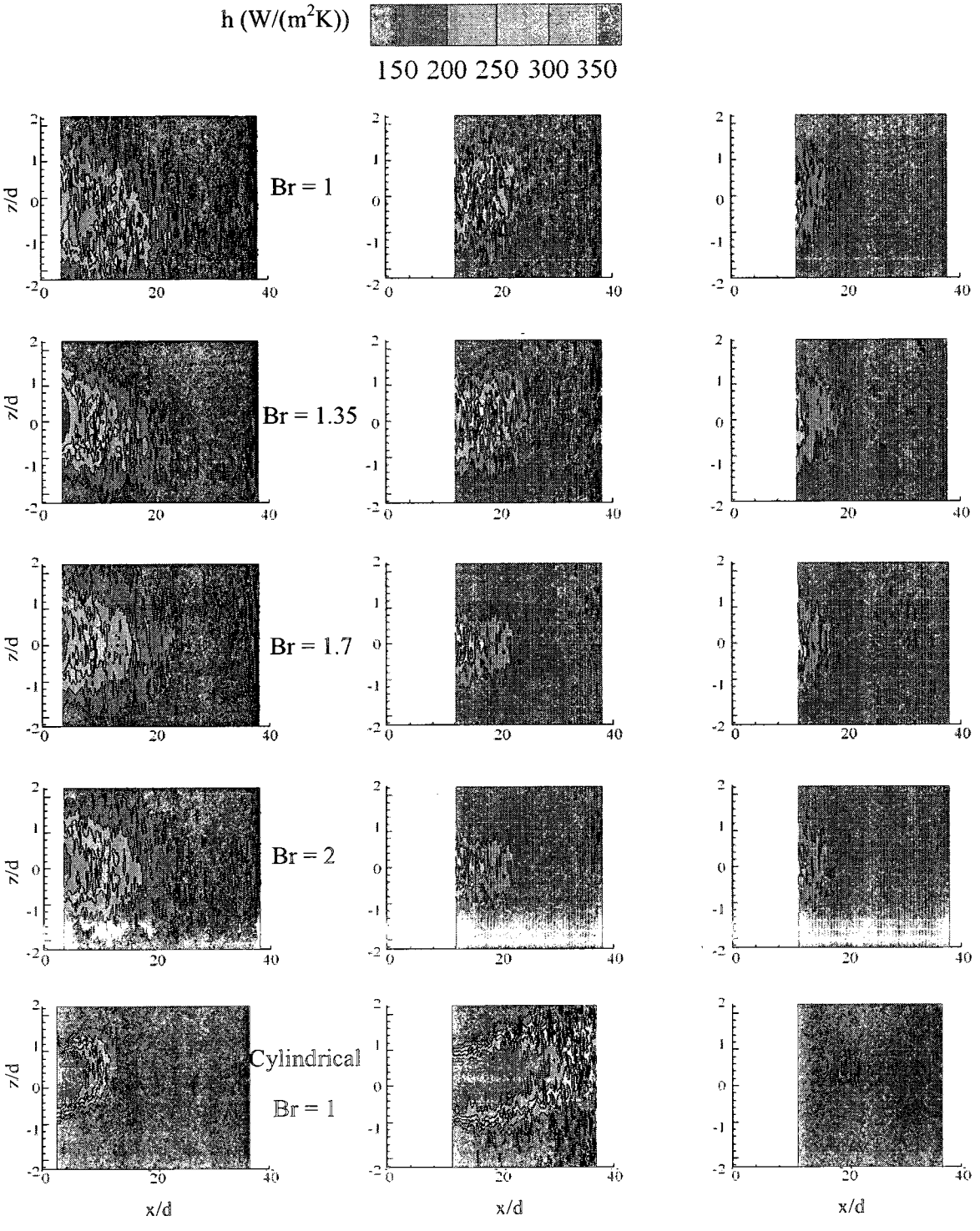

Figure 4-20 Local heat transfer coefficient distribution for pressure side with louver scheme

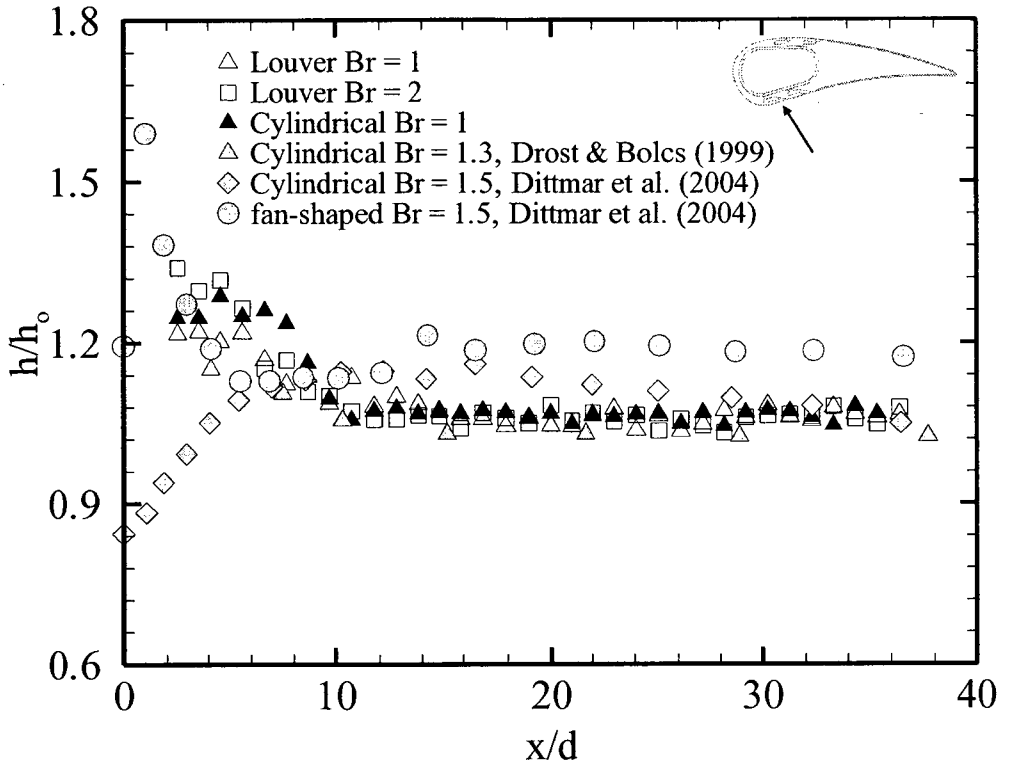

Figure 4-21 Average-spanwise normalized heat transfer 1st row, pressure side

et al. (2003) mid and far downstream. Near downstream, the heat transfer coefficient increases asymptotically to unity, however the HTC of the shaped hole investigated in the same study decreases asymptotically to one. The louver scheme HTC is slightly lower than that of the cylindrical hole of the present study near downstream of the hole and is similar to it mid and far downstream. By increasing the blowing ratio from Br = 2 to Br =1, the HTC increases near downstream of the louver and increases slightly mid and far downstream.

Figure 4.22 presents the normalized HTC on the pressure side obtained with the second row injection using the louver scheme at different blowing ratio and compares it to that of the cylindrical hole at Br = 1. The relatively high Reynolds number on the second injection location on the pressure side provides a more turbulent boundary layer upstream from the hole location. This causes the coolant to strongly mix in the laminar boundary layer, hence causing a significant increase in the HTC. As the blowing ratio increases, the jet momentum increases with more disturbances at the interaction region accompanied by stronger vortices causing an increase in the HTC. For all blowing ratios, the mixing between the two streams increases as the surface distance increases and the HTC decreases asymptotically to unity. The louver scheme results in lower HTC at all blowing ratios than the cylindrical holes at Br =1. The expanded exit allows the jet to spread laterally. Furthermore, the laid-back angle increases the hydraulic diameter hence decreasing the jet momentum. This decrease in the jet momentum permits the flow to penetrate the boundary layer more smoothly and causes the pre-mentioned reduction in the HTC compared with the cylindrical hole. The cylindrical jet has higher momentum

causing a significant disturbance to the main stream yielding higher HTC. The coolant encounters a slight jet lift-off with rapid reattachment 10 x/d after the injection point.

Figure 4.23 presents the normalized lateral-averaged HTC for the louver scheme double injection at four different blowing ratios compared with the cylindrical exit at Br = 1. The double injection on the pressure side results in a lower HTC compared with the second row only. It might be attributed to the boundary layer thickness on the pressure side being larger than that of the suction side. The jet of the first row enters smoothly the boundary layer, increasing its thickness. The boundary layer is then developed and thickened upstream of the second row. The coolant of the second row is then injected into a thicker boundary layer compared with the second row single injection. The coolant is then introduced to the thicker boundary layer without the significant disturbances to the mainstream causing a rapid decay of the HTC. The jet lift-off that occurred in the second row injection has low strength and reattaches earlier at5 x/d downstream of the injection point.

4.6 Momentum ratio and net heat flux reduction (NHFR)

The performance of the louver scheme can be summarized in terms of average lateral effectiveness at different momentum flux ratios. The momentum flux ratio (I) can be defined as $I = [(\rho v^2)_j/(\rho v^2)_m$, and it represents the ratio between the coolant mass flow rate to that of the mainstream. Figure 4.24 compares the louver performance on suction side and pressure side in terms of averaged effectiveness versus the momentum ratio (I) at different x/d locations for the first row of injection. Near downstream, the louver provides higher effectiveness on the pressure side at low and moderate momentum ratios. The tangential component of the jet momentum keeps the coolant attached to the concave

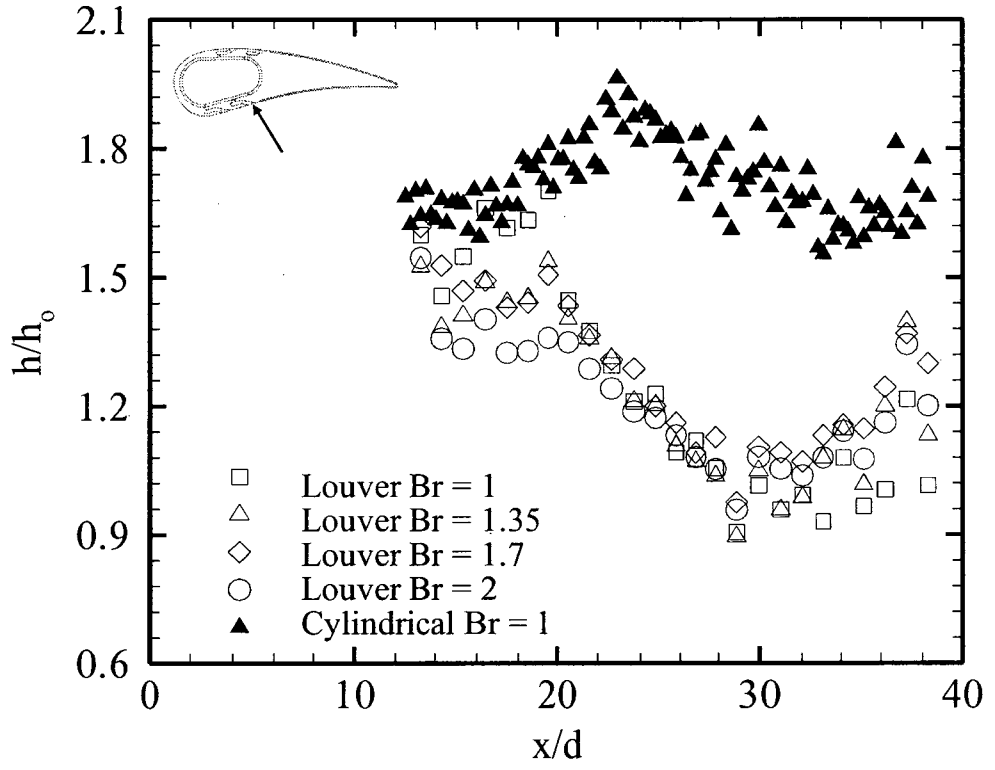

Figure 4-22 Average-spanwise normalized heat transfer coefficient for the 2nd row, pressure side

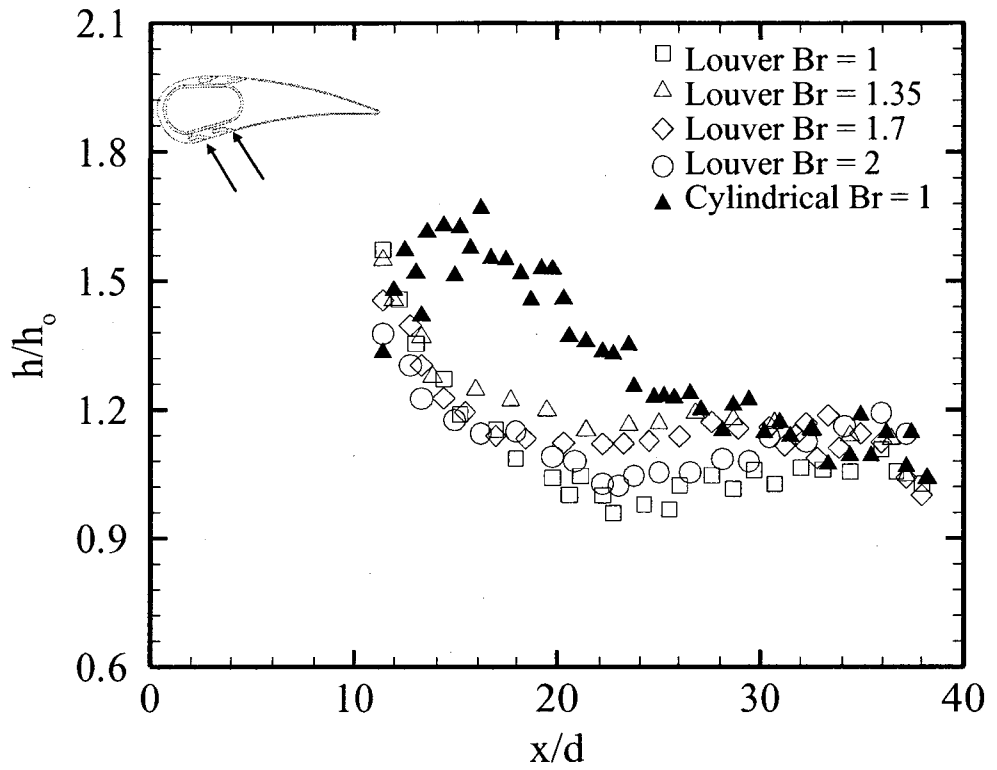

Figure 4-23 Average-spanwise normalized heat transfer coefficient for double injection, pressure side

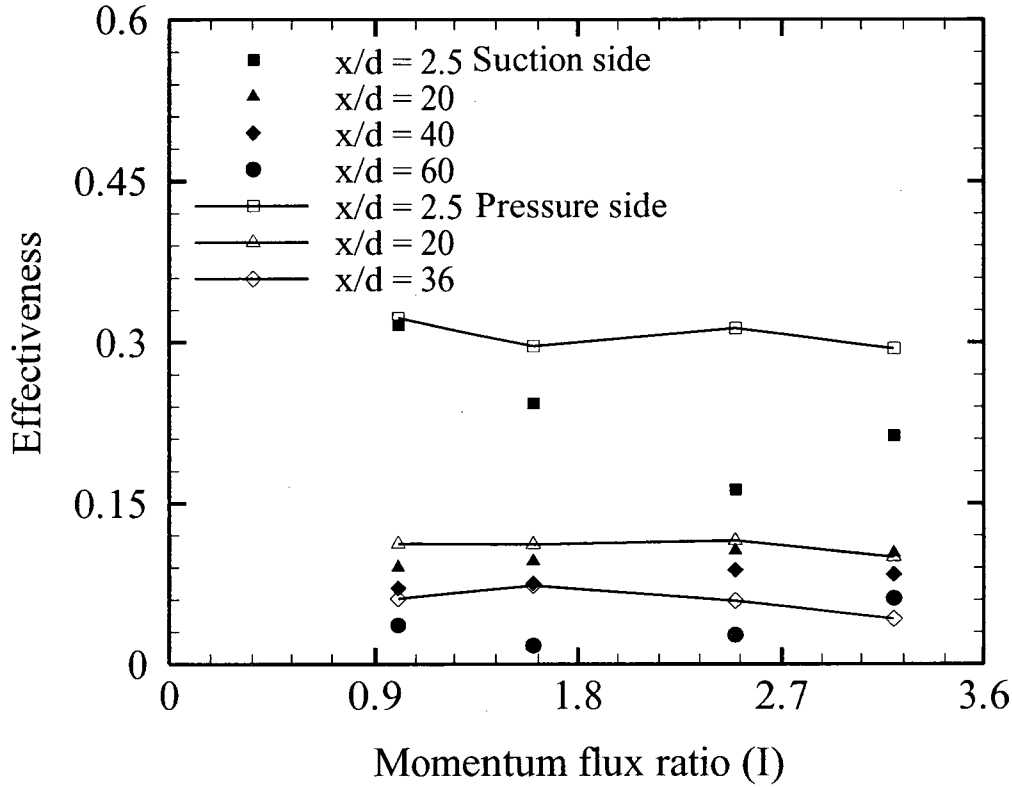

Figure 4-24 Lateral-averaged effectiveness at different position on the vane surface

surface of the pressure side. The suction side performance shows a slight decrease as the radius of curvature of the jet trajectory is increased, hence increasing the momentum ratio and pushing the coolant away from the convex surface. By increasing the distance downstream, a steep decay in the louver performance over the pressure side is observed while the suction side preserved the benefits of the louver, specifically at higher momentum ratios. Far downstream, the suction keeps low effectiveness up to x/d = 60, while the pressure side cannot keep this protection more than x/d = 40. This observation was also reported by Gao et al. (2008) for different hole shapes and it illustrates why the pressure side needs more rows of cooling holes than the suction side.

The Net Heat Flux Reduction (NHFR) is used to combine both parameters into one evaluation parameter to conclude the benefit of using the louver scheme. NHFR can be defined as the ratio between the total heat transferred to the vane surface with film cooling (q_f) and the total heat transferred to the vane surface without film cooling (q_o). NHFR can be calculated according to Equation (4.2),

$$NHFR = \frac{q_f}{q_o} = \left(\frac{h_f}{h_o} \left(1 - \frac{\eta}{\phi} \right) \right) \tag{4.2}$$

where ϕ is the overall cooling effectiveness and ranges from 0.5 to 0.7 for a typical airfoil cooling system. The value of ϕ is the inverse of θ which is f(T_m, T_j, and T_w), therefore its value depends on the location on the vane surface, and it can be calculated from Equation (4.3).

$$\theta = \frac{T_m - T_j}{T_m - T_w} \tag{4.3}$$

The current study is performed using the transient technique and the temperature of the wall changes during the test duration, therefore the value of ϕ is selected to be 0.6. In the steady state experiments the surface temperature is spatially changed but it is steady with time.

Figure 4.25 presents the averaged spanwise NHFR for both rows on the suction side and the pressure side using the louver scheme. Two blowing ratios using the louver scheme are employed in this figure, moderate (Br = 1) and high (Br = 2), and compared with the cylindrical exit at the best blowing ratio, Br = 1. Despite the higher heat transfer rate of the louver scheme near downstream of the injection point, as shown in part I of this paper, the higher effectiveness at this region yields to lower NHFR. By increasing the distance in the downstream direction, the heat transfer rate decreased, accompanied by a decrease in effectiveness, and therefore an increase in the NHFR is observed. At the trailing edge of the suction side a heat reduction of about 72% is obtained at the higher blowing ratio. Compared with the cylindrical hole of the present study, the louver scheme provides superior heat load reduction on the pressure side as well as better heat load reduction on the suction side.

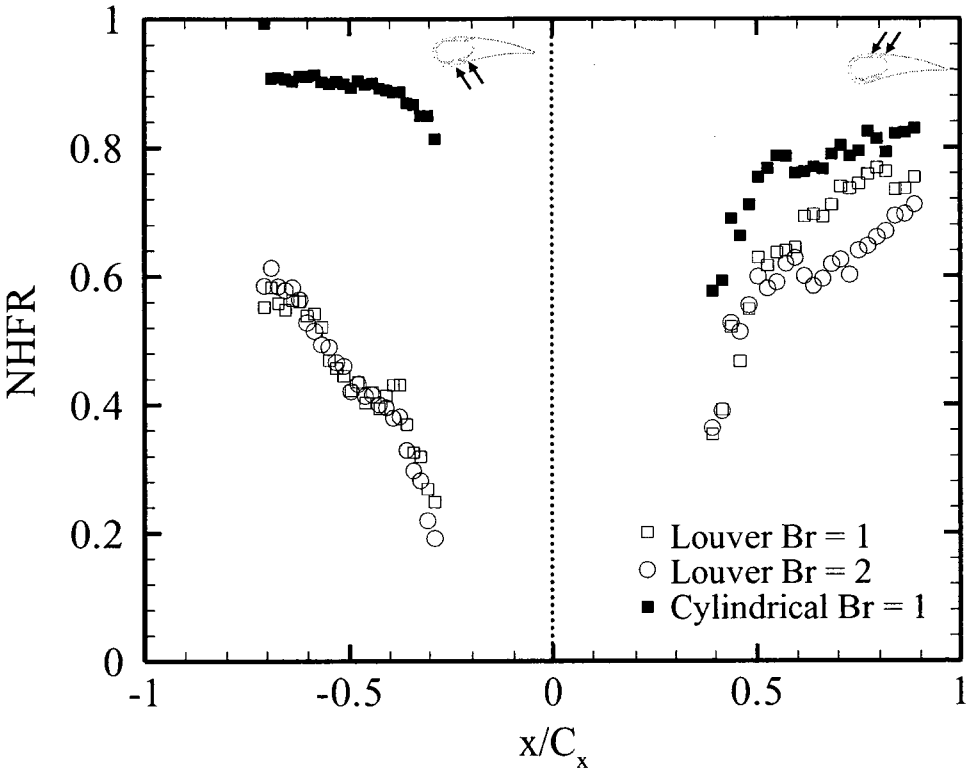

Figure 4-25 NHFR for double injection using louver scheme

4.7 Summary

The performance of the louver scheme has been measured at four different locations on both sides of a gas turbine vane. Two different positions are located on the convex surface of the suction side in addition to two others on the concave surface of the pressure side. Four blowing ratios are employed in this study at 0.92 density ratio. The detailed local effectiveness distributions as well as the lateral-averaged effectiveness have been presented in addition to the corresponding changes in the heat transfer coefficient. The louver scheme provides higher lateral-averaged effectiveness and slightly lower HTC compared with the cylindrical hole that has the same base diameter and is supplied with the same amount of coolant. The local distribution of the HTC shows that the louver scheme spreads the coolant laterally downstream the shaped exit causing a uniform distribution of the HTC over the protected surface. However, the distribution of the HTC is concentrated downstream the exit of the cylindrical hole causing higher thermal stresses on the protected surface. The bend in the louver scheme upstream from the exit in addition to the well designed exit shape cause a significant reduction to the jet momentum. This sufficiently mandated jet decreases the mixing degree between both the mainstream and the coolant. The effectiveness increases slightly with the increase of the blowing ratio due to the fully attached coolant at both moderate and high blowing ratios.

The second row injection on the suction side shows better performance and a higher HTC compared with that of the first row location because of the adverse pressure gradient created by the flow deceleration and the more flat surface of the vane at the second injection location. The second row on the pressure side shows similar effectiveness with lower HTC as that on the first row with steeper effectiveness decay

due to the flow instabilities on the concave surface. The combined injection on both sides of the vane shows a higher effectiveness compared with the effectiveness resulting from the superposition principle, with a superior development in the case of the pressure side. The combined injection redistributes the HTC downstream of the second row by merging the coolant from the first row with that of the second row. The changes in heat transfer coefficient using the louver scheme are combined with the effectiveness development, showing a lower net heat flux reduction compared with the cylindrical case. The louver provides a promising performance compared with either the cylindrical hole and different hole shapes found in literature. The presented performance recommends the louver scheme to improve the cooling capacity on the next generation of gas turbines with more investigations required for its performance with different compound angles.

Chapter 5 – Investigation of Smooth Expansion Exit on the Leading Edge

There are some constrains in investigating the cooling performance over the leading edge region. The high curvature of the surface, small wall thickness, and the viewing angle through a limited space are the main obstacles in this region. It is a challenge to attain precise cooling performance data in a heat transfer experiment due to the thermal conduction through the small wall thickness of the leading edge. The correction of the conduction error cannot eliminate the existing error especially at the highly curved surface with complex hole geometry. However, obtaining the heat transfer coefficient in addition to the effectiveness helps to understand the overall cooling performance at the most critical region on the airfoil. A smooth expansion is proposed at the exit of the standard cylindrical hole to redistribute the coolant jet uniformly on the stagnant region while decreasing the heat transfer by reducing the mixing between both streams.

5.1 Smooth expansion geometry

Figure 5.1 shows the proposed smooth expansion at the leading edge region at two inclination angles, 0° and 30° with the main stream. Two levels of expansion were investigated, 2d and 4d, in addition to the standard cylindrical exit. Only one row, with 10 holes, has been employed on the stagnation line to examine the performance of the aforementioned geometries. A different vane is used for each different hole arrangement thus a total of 6 vanes are employed with four different blowing ratios (1, 1.35, 1.7, and 2). The spanwise spacing of the holes is 4.5d in all cases; all geometrical details of

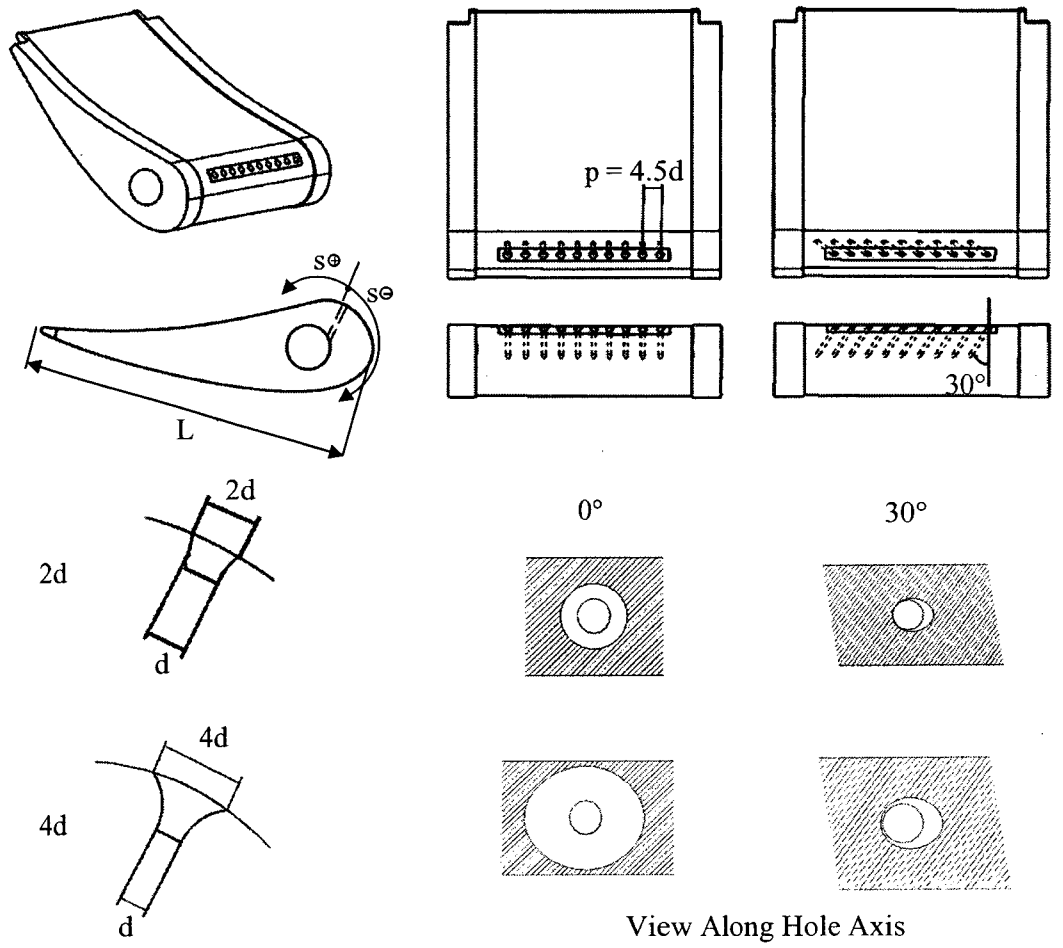

Figure 5-1 Geometrical aspects of the smooth expansion exit

cooling holes are tabulated in Table 5.1. The inlet total pressure, one chord upstream the vane leading edge, is maintained constant at 114 kPa. This corresponds to 0.23 exit free stream Mach number and 1.5E5 exit Reynolds number based on the axial chord. The blowing ratio is calculated based on the flow characteristics of the mainstream at the injection point and the jet properties at the base diameter of the cooling hole. The coolant amount delivered to the cylindrical hole for a given blowing ratio was measured and delivered to the proposed exit to compare between both geometries based on the same coolant amount. The camera is positioned such that it views the leading edge from the pressure side. Therefore, the measurements are recorded for a distance equal to 12 x/d on the pressure side, while the measurements are available only for 8 x/d on the suction side due to the highly curved surface.

5.2 Cooling effectiveness measurement

Figure 5.2 shows the effectiveness local distribution downstream the different expansion levels and the cylindrical hole at the four investigated blowing ratios. The suction side has lower effectiveness level compared with the pressure side. However applying the expansion geometry significantly enhances the effectiveness downstream the hole towards the suction side. Increasing the blowing ratio slightly improves the effectiveness downstream the cylindrical hole. Using the smooth expansion, the effectiveness downstream the hole increases with the blowing ratio. The shown contours clarify the main purpose of the proposed geometry. Firstly, increases the effectiveness downstream the cooling holes by increasing the blowing ratio. Moreover, the coolant distributes uniformly downstream the cooling hole and enhances the effectiveness towards the suction side as well as the pressure side.

Table 5.1 Cooling hole arrangement

Angle to the stagnation line	0
Orientation angle (compound)	90° radial
Hole angle (deg.)	0°, 30°
No. of holes	10
Spacing (p/d)	4.5
Expansion levels	2d, 4d

Figure 5.3 presents the average-lateral effectiveness downstream the leading edge on the pressure side for the standard cylindrical hole with two inclination angles at Br = 1. According to the best of the author's knowledge, the previous work on the leading edge investigated the cooling performance of the showerhead arrangement. The current work focused on the cooling performance of a row of cooling hole located at the stagnation line; therefore few results from the literature have been presented. The experimental results from Gao and Han (2009) are shown in the figure and show a good agreement with the present results. The numerical prediction from Islami et al. (2010) is also presented in Figure 5.3 for an injection hole located on the pressure side of the gas turbine blade. Their result shows a qualitatively similar trend with the present study as their investigation was performed on an airfoil which had a similar surface curvature. However, there is a quantitative decrease in the effectiveness of the present study after x/d = 4. The injection in the present study is located exactly on the stagnation line, while the injection location in their study was located later downstream. The injection in the stagnation region counters high free stream interaction that yields a rapid dilution of the coolant on the mainstream. The effectiveness of the cylindrical hole in the present study shows good agreement with the effectiveness of the previous studies, which gives more confidence in the approach and methodology used in this study.

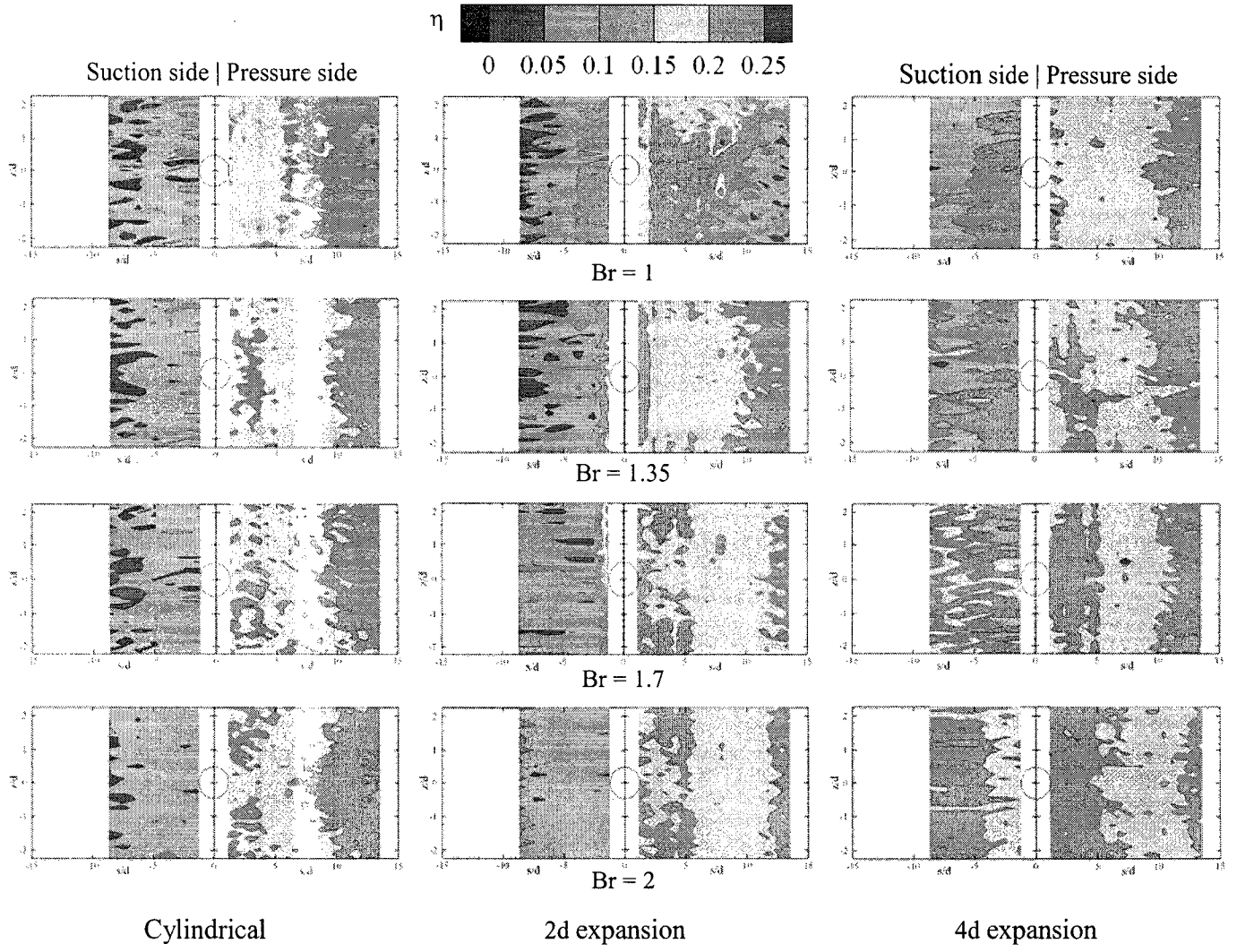

Figure 5-2 Effectiveness local distribution for 30° inclination

5.2.1 Effect of the expansion level

Figure 5.4 presents the local distribution of the effectiveness over the pressure side for the two levels of expansion, 2d expansion, and 4d expansion at Br = 1. The standard cylindrical exit is also presented in the figure with two hole inclination angles for each expansion level. For the first inclination angle, 30^{o} with the surface, the standard cylindrical hole shows the lower effectiveness value just downstream of the hole, $x/d < 4$. The momentum of the jet in addition to the highly curved surface at the stagnation region allows the jet to lift-off. However the inclined angle of the hole divided the jet momentum into two components; the major component, *Icos30*, leads to the jet lift-off and confronts the mainstream causing the high interaction between both flows. The minor component, *Isin30,* is yielded to the mainstream and reattached again to the vane surface causing the maximum effectiveness at the reattachment point. By applying the first expansion level, the jet starts to expand before interfacing with the mainstream hence the jet momentum decreases allowing the coolant to stay close to the surface and increasing the effectiveness. Further increase in the expansion level causes a further decrease in the jet momentum and a corresponding increase in the effectiveness.

Farther downstream, $x/d > 4$, the coolant dilutes in the mainstream causing a reduction in the effectiveness. The second expansion level provides the highest effectiveness due to the reduction of the jet momentum that yields a continuous barrier flow hence more efficient cooling. The first expansion level provides the lowest effectiveness compared with both the second expansion level and the standard cylindrical exit. The further decrease of the first expansion level effectiveness being lower than that of the standard cylindrical can be attributed to the short expansion length that does not

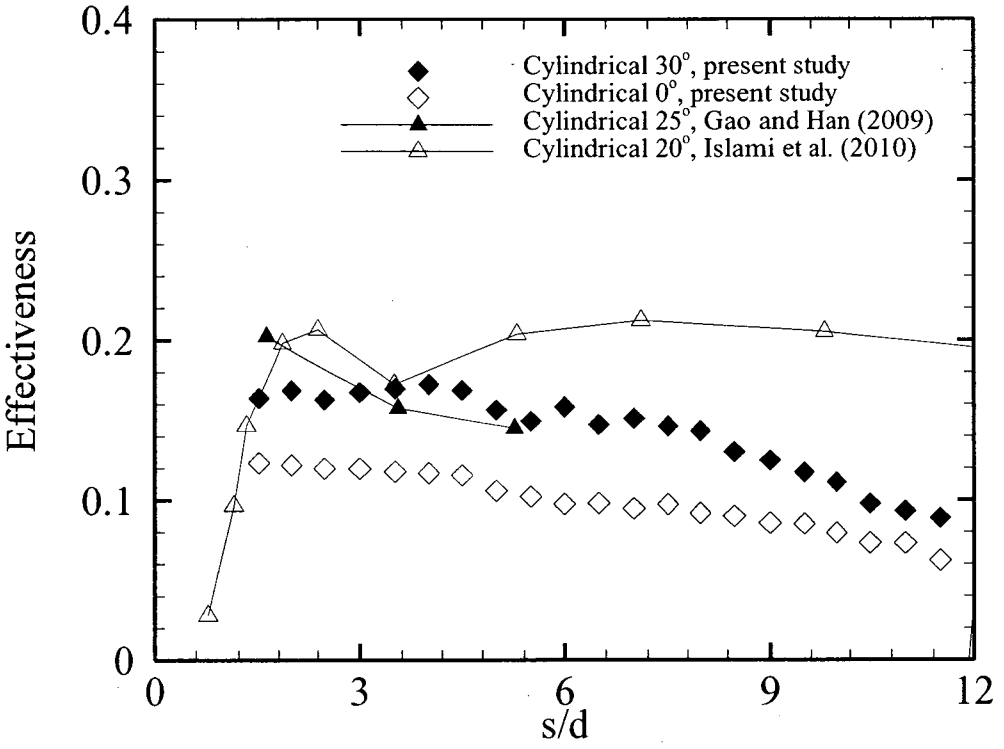

Figure 5-3 Cooling effectiveness on the leading edge, Br = 1

allow the coolant flow to be fully developed. The jet is then strongly interacting with the mainstream causing additional vortices that increase the mixing degree between the jet and the mainstream. As the mixing degree increases, the coolant quickly dilutes in the mainstream losing its cooling capacity.

For the second inclination angle, 0^{o}, the momentum of the jet is completely confronting the mainstream without any component yielding with the main flow. This strong interaction causes a complete mixing between both the jet and the main flow, leading to a significant effectiveness reduction compared with the 30^{o} inclination angle. Moreover, the complete confronting between the coolant and the mainstream spreads the coolant away from the surface and may cause main flow ingestion. The standard cylindrical hole provides the highest jet momentum so it faces the largest mixing degree with the mainstream and the lowest effectiveness. The first expansion level, 2d, shows a similar performance to the standard cylindrical hole that is attributed to the short expansion length. The momentum in this case decreases however the flow is not developed yet, so it strongly mixes with the mainstream. By increasing the expansion level to the highest level, 4d, the jet momentum significantly decreased yielding less confrontation between both flows. The coolant is then attached to the surface causing the highest effectiveness for the 0^{o} inclination angle. The direct confrontation still has an effect on the coolant causing a mixing between both flows and leading to lower effectiveness compared with the 30^{o} inclination angle.

5.2.2 Effect of the blowing ratio

Figure 5.5 presents the effect of the blowing ratio with each expansion level, at 30^{o} inclination angle, on the effectiveness towards both pressure and suction directions

downstream the cooling holes. The suction side shows significantly lower effectiveness compared with the pressure side for the standard cylindrical hole, as shown in Figure 5.5a. The surface downstream the stagnation line towards the suction side has a highly curved surface compared with the pressure side. The ejected coolant from the film hole follows the streamlines in both directions, however it is easily attached to the pressure surface rather than the suction surface. Therefore the point of reattachment on the suction side is shifted later downstream the injection point, at x/d = 6, compared with x/d = -2 on the pressure side. The effectiveness shows the peak values at Br = 1.35, and decreases by increasing the blowing ratio due to the further increase of the jet momentum.

The two expansion levels provide an increase in the effectiveness by increasing the blowing ratio on both the pressure and suction side. This indicates the momentum reduction of the jet by increasing the exit hole area. Figure 5.5b shows the effectiveness downstream the first expansion level, 2d. The effectiveness shows a significant increase by increasing the blowing ratio to Br = 1.35 due to the increase of the coolant amount. The undeveloped expanded jet most likely forms a vortex which transports a small amount of the coolant to reattach to the surface at x/d = 6. By further increase of the

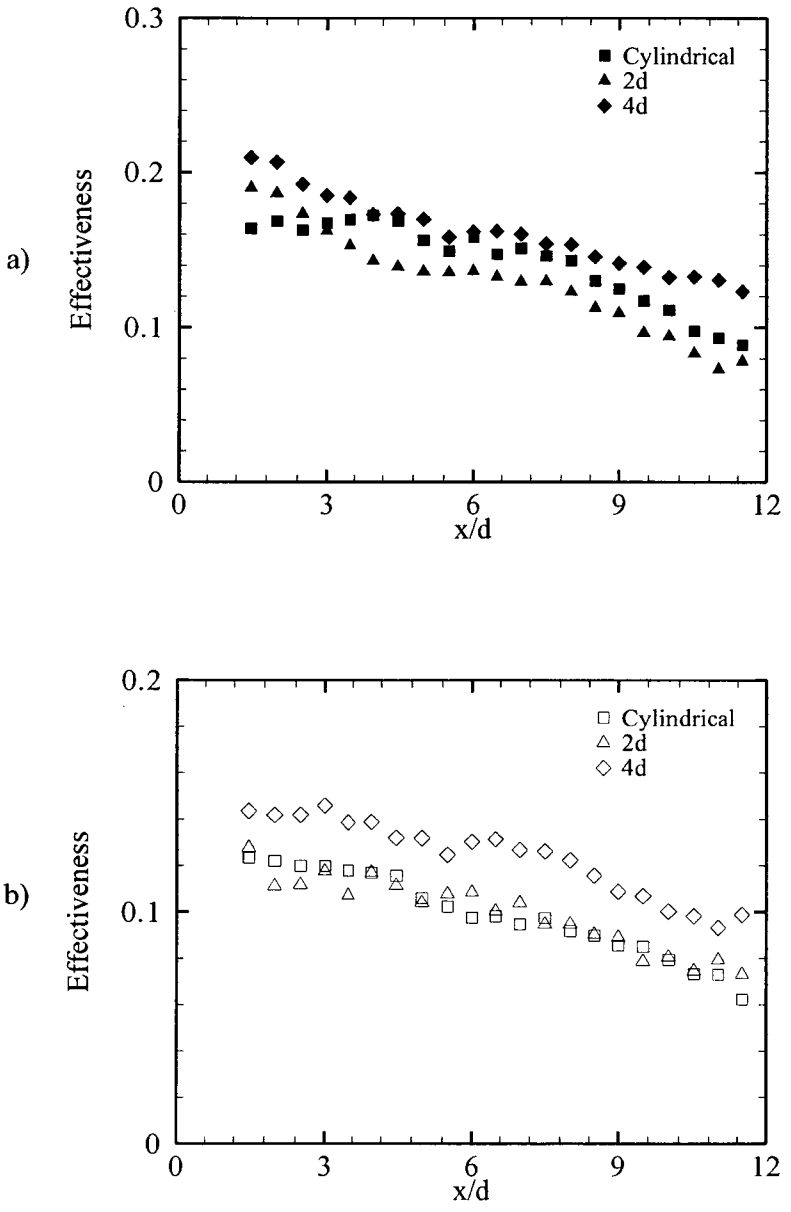

Figure 5-4 Effect of expansion level on effectiveness, Br = 1 a)30° inclination angle b) 0° inclination angle

blowing ratio, the coolant amount increases providing more cooling capacity farther downstream. The benefit of the smooth expansion appears on the suction side. The jet spreads well out of the hole causing the ejected coolant to flow attached to the vane surface. The peak point which appears at x/d = 6 on the standard cylindrical hole has now disappeared and the maximum effectiveness occurs just downstream the hole and it increases with the blowing ratio increase. The disadvantage of the smooth expansion appears at the lower blowing ratio as there is no cooling effect traced at Br = 1. The jet momentum is significantly decreased due to the magnification of the exit area that causes a quick dissipation of the coolant into the mainstream.

Figure 5.5c shows the effectiveness downstream the second level of expansion, 4d. The effectiveness has a high level at the moderate blowing ratio, Br = 1, compared with the other exit shapes, as seen in Figure 5.4. Increasing the blowing ratio causes a slight increase in the effectiveness that indicates the full attachment of the coolant at all blowing ratios. In addition, the jet is expected to be fully developed through the expansion region, therefore there is no findings supporting the formation of vortices as seen with the first level of expansion. Increasing the expansion level shows higher effectiveness on the suction side compared with the first level of expansion. The further increase on the exit area provides more reduction on the jet momentum causing the full attachment of the coolant flow to the vane surface. However, as in the first expansion level, this causes a quick dissipation of the coolant in the mainstream. The TLC material cannot trace a temperature change on the protected area at Br = 1, as found on the first expansion level.

Figure 5.6 presents the effect of the blowing ratio with each expansion level, at 0^{o} inclination angle, on the effectiveness towards both pressure and suction directions downstream the cooling holes. This inclination angle causes a strong interaction between the jet and the mainstream because of the complete confrontation between both flows, therefore a significant decrease in the effectiveness is expected. Figure 5.6a shows an effectiveness reduction with the increase of the blowing ratio over the pressure side. While on the suction side, there is no influence of the blowing ratio on the effectiveness near downstream with reduction mid and far downstream with the blowing ratio increases. At the highest blowing ratio, Br = 2, there is no coolant trace on the TLC sheet that indicates a high jet lift-off with no attachment to the vane surface. Therefore, no effectiveness could be measured and no results are presented.

For the first expansion level, 2d, the effectiveness shows a tendency to decrease by increasing the blowing ratio to 1.35, as shown in Figure 5.6b. A further effectiveness reduction has been measured at Br = 1.7. By increasing the blowing ratio to two, the jet lift off pushed the coolant away from the surface such that the TLC material cannot sense any temperature change. Therefore, there is no data available to be presented for that blowing ratio. By increasing the expansion level, a noticeable increase in the effectiveness is recorded compared with the first level, as shown in Figure 5.6c. The effectiveness decreases by increasing the blowing ratio as seen for the second expansion level. However, at the highest blowing ratio, the jet momentum reduction allows the coolant to yield with the mainstream and reattach to the vane surface, enabling the TLC material to trace the coolant. At both expansion levels, the coolant is totally dissipated on the suction side and no coolant could be traced downstream the cooling hole.

a)

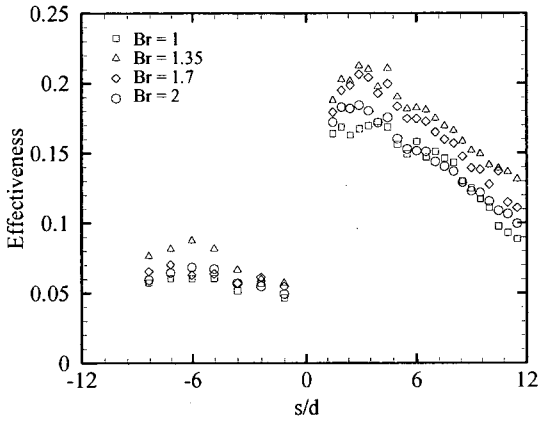

b)

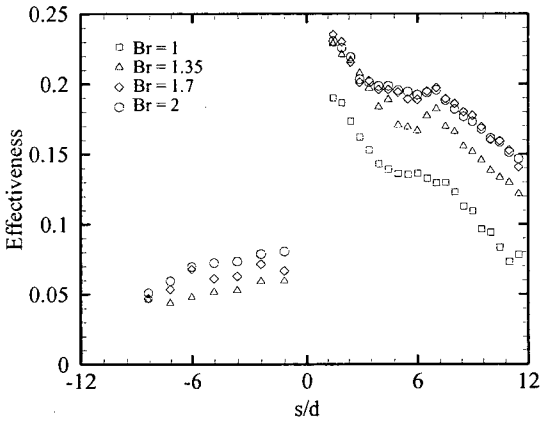

c)

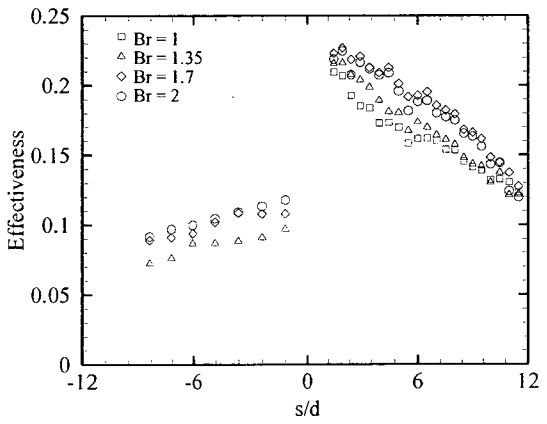

Figure 5-5 Effect of blowing ratio with 30° inclination angle a) cylindrical b) 2d c) 4d

5.3 Heat Transfer coefficient measurement

Equation 3.9 is solved using the least square regression method to obtain both the effectiveness and the heat transfer coefficient. Figure 5.7 presents the local distribution of the heat transfer coefficient downstream the two expansion levels in addition to the cylindrical hole. The enhancement in the heat transfer coefficient towards both the pressure side and suction side is presented at four different blowing ratios. The suction side shows higher heat transfer coefficient compared with the pressure side. However the proposed expansion geometry causes a reduction on the heat transfer coefficient downstream the hole on both sides, particularly on the suction side. Increasing the blowing ratio insignificantly affects the heat transfer coefficient.

The film cooling heat transfer coefficient is normalized by dividing it over the heat transfer coefficient without film cooling. Figure 5.8 shows the normalized lateral-averaged heat transfer coefficient over the pressure side for the three expansion levels: standard cylindrical, 2d, and 4d at Br = 1. Each expansion level is presented at two hole inclination angles, 0° and 30°, and the normalized heat transfer coefficient of the York and Leylek (2002) is presented as well. The hole in their study was standard cylindrical inclined 20° with respect to the vane surface. The heat transfer coefficient was lower than that of the present study as the inclination angle in their study was shallower than that of the present study. As the inclination angle is shallower, the major momentum component of the jet is in the direction of the mainstream. Hence, the interaction between the jet and the main flow is then reduced causing the reduction of the heat transfer coefficient. By changing the geometry exit to the 2d expansion level, there are some vortices that are formed due to the short expansion length hence a slight increase in the heat transfer

a)

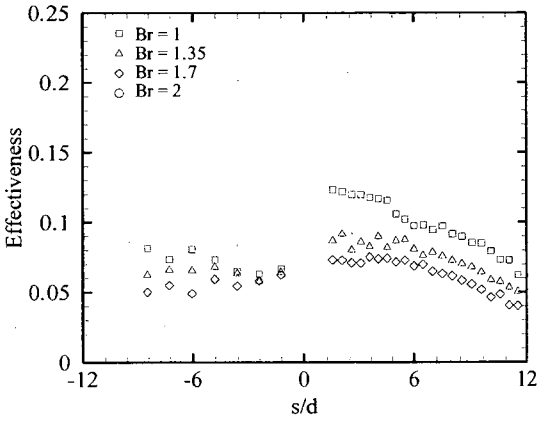

b)

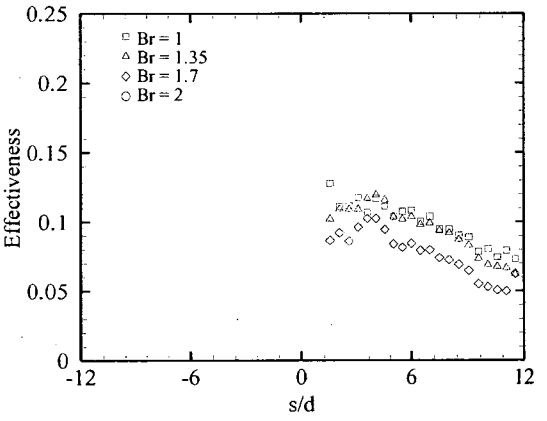

c)

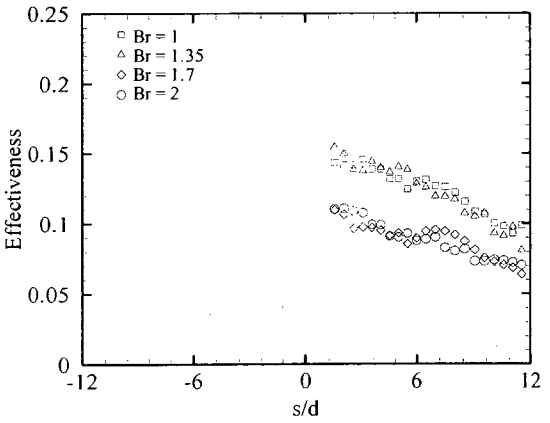

Figure 5-6 Effect of blowing ratio with 0^{o} inclination angle a) cylindrical b) 2d c) 4d

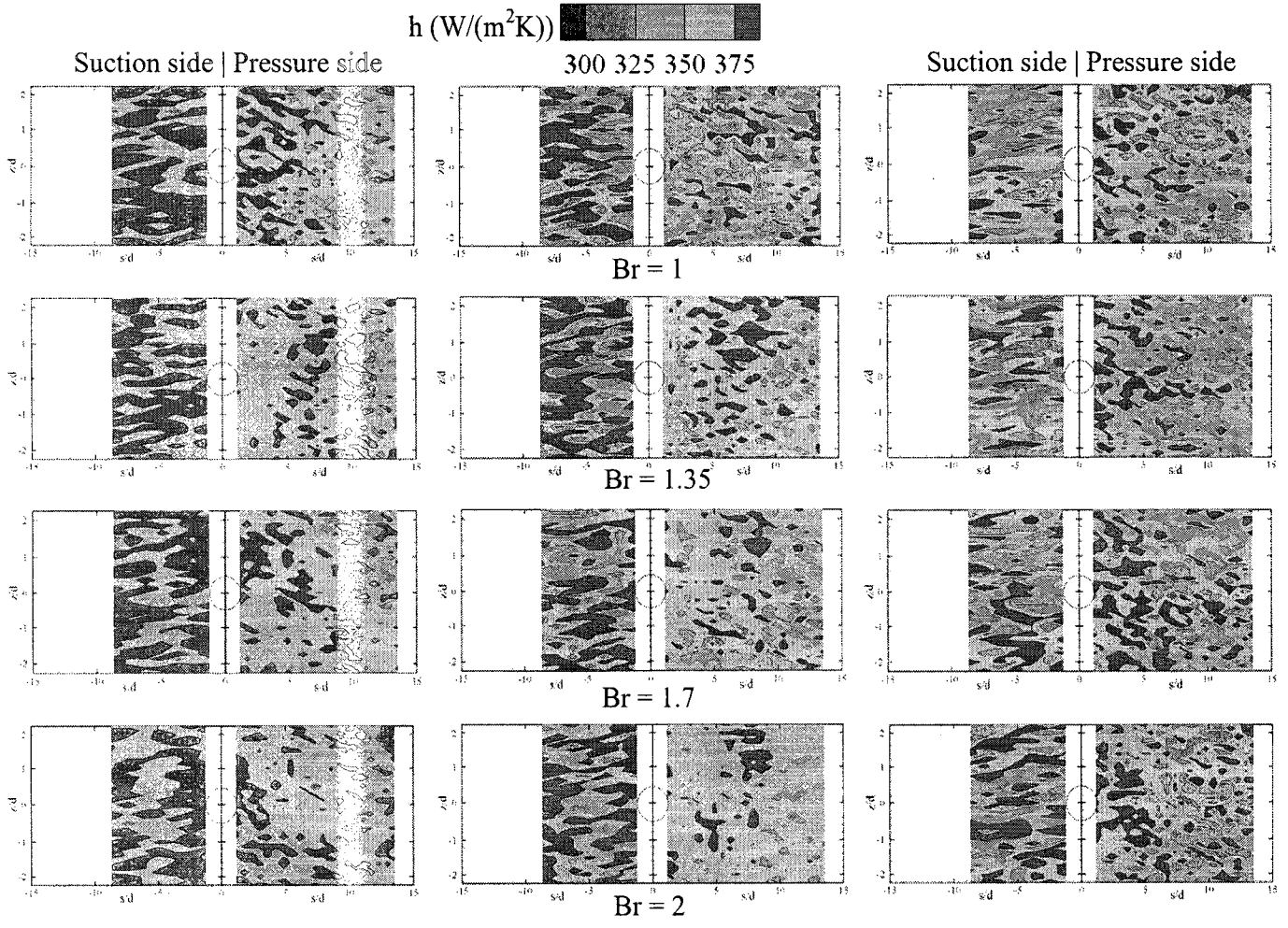

Figure 5-7 Heat transfer coefficient local distribution for 30° inclination

coefficient is observed. At the highest expansion level, 4d, the coolant is expanded in the longer smooth portion of the hole and yields to the main flow causing a noticeable reduction in the heat transfer coefficient. As the inclination angle changes from 30^{o} to 0^{o}, the coolant jet is completely on the opposite direction of the mainstream. No component of the jet momentum is yielded to the mainstream, hence the disturbance caused by the flow interaction increases causing higher heat transfer coefficient. The expansion level changes have insignificant effect on the heat transfer coefficient due to the complete confrontation between both streams in all cases.

Figure 5.9 presents the effect of the blowing ratio on the heat transfer coefficient at 30^{o} inclination angle towards the pressure and suction directions downstream the cooling hole. In all cases, the suction side shows lower heat transfer coefficient than the pressure side. The high curvature downstream the cooling hole towards the suction side keeps the coolant away from the vane surface. The unattached coolant causes the disturbances to occur away from the vane surface, causing the lower heat transfer coefficient, and lower effectiveness as seen before. The cylindrical exit shows insignificant change in the heat transfer coefficient with the blowing ratio in both the pressure and suction sides, as shown in Figure 5.9a. By implementing the first expansion level as shown in Figure 5.9b, the disturbances occurred by the coolant increased due to the undeveloped flow through the short expansion length, causing an increase in the heat transfer coefficient on the pressure side. The flow deviating towards the suction side tends to decrease and a reduction in the heat transfer coefficient is observed. Increasing the blowing ratio causes a slight increase in the heat transfer coefficient downstream the first expansion level on both sides of the vane. The highest expansion level provides the

lower heat transfer coefficient because of the further decrease of the jet momentum, as shown in Figure 5.9c. A reduction in the heat transfer coefficient is also observed at the suction side for the highest expansion level compared with the other expansion levels.

Figure 5.10 presents the effect of the blowing ratio on the heat transfer coefficient at a 0^{o} inclination angle towards the pressure and suction directions downstream the cooling hole. The overall view of the figure shows the slight effect of the blowing ratio on the HTC. However, the 0^{o} inclination angle shows higher heat transfer coefficient values compared with the 30^{o} inclination angle at all expansion levels. The complete confrontation between the coolant and the mainstream induces a high disturbance level that overcomes the expansion of the coolant jet and the subsequent decrease in momentum. For both expansion levels the coolant flow towards the suction side is completely diluted through the mainstream. Therefore, no temperature changes can be traced on the TLC material and no enough data is available on the suction side to be processed.

5.4 Net heat flux reduction (NHFR)

The previous sections presents the effectiveness increase using the smooth expansion exit with the standard cylindrical hole. In addition the heat transfer coefficient has been changed by implementing the different expansion level and the inclination angles as well. The increase in the heat transfer coefficient with the film cooling holes provides more thermal stresses on the airfoil surface by increasing the heat load that is transported to the surface. Figure 5.11 presents the averaged spanwise NHFR for different expansion levels at the 30^{o} inclination angle. The heat reduction downstream the

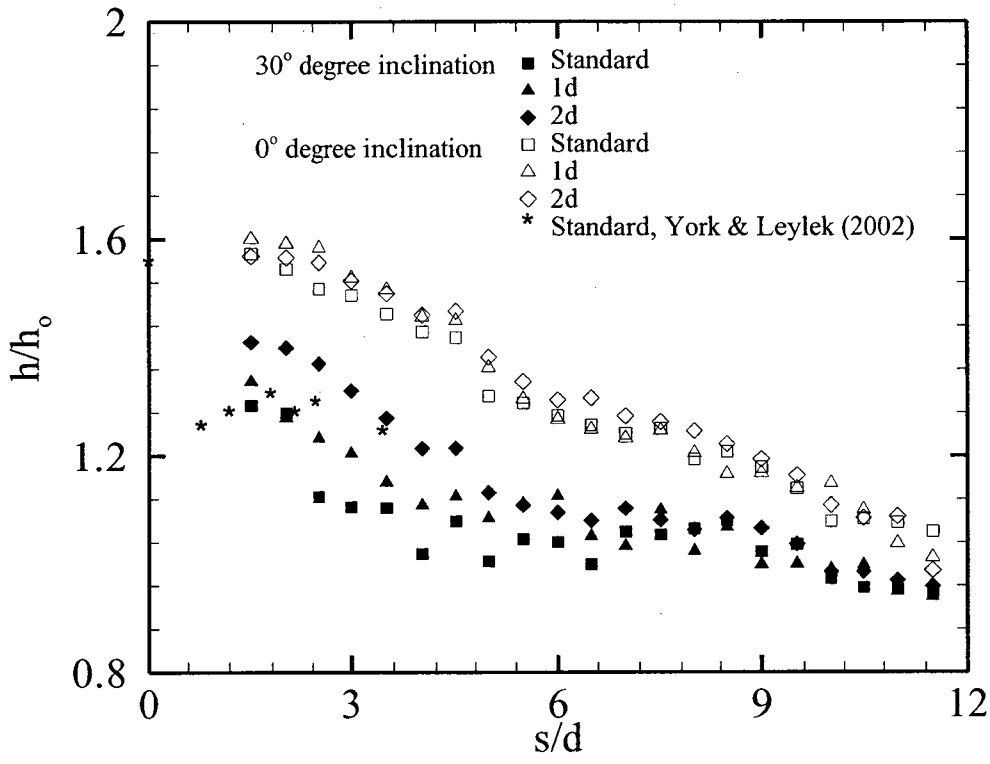

Figure 5-8 Effect of expansion level on heat transfer coefficient, Br = 1

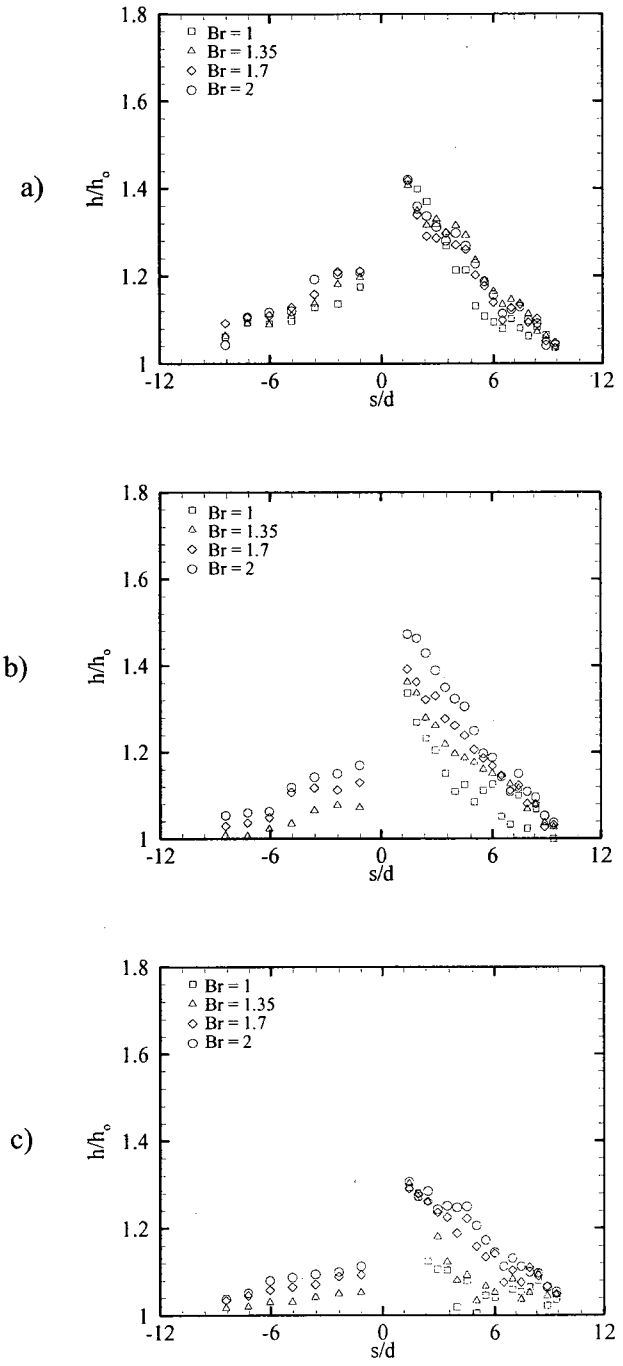

Figure 5-9 Effect of blowing ratio with 30° inclination angle a) cylindrical b) 2d c) 4d

cooling hole towards both the suction side and the pressure side is plotted at different blowing ratios. The blowing ratio shows insignificant influence on the heat load reduction, while the geometry of the hole provides the significant change on the cooling performance. Figure 5.11a shows the heat load reduction downstream the cooling hole towards both the pressure and suction side for the standard cylindrical hole. The cylindrical hole provides moderate effectiveness downstream the cooling hole towards the pressure side. However, the heat transfer coefficient shows a high impact on the heat load reduction in that critical region and overcomes the gained effectiveness, keeping the heat load the same as no cooling is applied. Farther downstream, the effectiveness decreases but the heat transfer coefficient decreases with higher rate causing a reduction in the heat load, around 20% of the load without film cooling. The standard cylindrical hole shows the worst performance just downstream the hole towards the suction side. The effectiveness is low with high heat transfer coefficient that causes an increase in the heat load over that without film cooling. The heat load returns to a normal level later downstream due to the reduction in the heat transfer coefficient.

Figure 5.11b shows the heat load reduction with the first expansion level and reveals the benefit of using the smooth expansion on that critical region of the vane. A heat load reduction of about 10% is gained downstream the hole towards the pressure side with further reduction later downstream. The lowest blowing ratio, Br = 1, shows the lowest heat load reduction, while other blowing ratios provide more than 30% reduction. Another benefit of the smooth expansion is keeping the heat load on the suction side similar to that without film cooling. Figure 5.11c shows a significant reduction in the heat load using the highest expansion level. Moreover, the heat load is characterized by steady

performance over the investigated area while decreasing the difference in heat load between the pressure side and the suction side. The steady heat load, in addition to the similar values downstream the cooling hole in both sides, yields uniform thermal stresses in that critical region of the vane and increases the endurance of the protected material.

Figure 5.12 presents the averaged spanwise NHFR for different expansion levels at the 0° inclination angle. The direct confrontation between the coolant and the mainstream provides higher heat transfer coefficient compared with that of the 30° inclination angle. Moreover, the direct contact causes a dissipation of the coolant into the mainstream yielding lower effectiveness. The NHFR accordingly shows the worst heat load achieved in the present study. The standard cylindrical hole shows a significant increase in the heat load, about 40% as shown in Figure 12a, just downstream of the cooling hole. This over load decreases farther downstream, returning to the load seen in the case without film cooling. Implementing the first expansion level with 0° inclination angle causes a reduction of approximately 10% in the heat load farther downstream the cooling hole. However, early downstream the direct confrontation and the resultant turbulence keep the over load as high as the standard cylindrical hole, as shown in Figure 5.12b. There is no data presented for Br = 2 as the coolant has a high momentum, causing a severe jet lift-off, keeping the coolant away from the surface, hence no measurements are sensed by the TLC material. Applying the second expansion level provides a severe reduction in the jet momentum yielding the coolant at the highest blowing ratio to be attached to the surface. The TLC material can trace the coolant and the measurement can be recorded. The heat load, which is greater than that without film cooling, is still present but slightly lower than in the case of the first expansion level. A lower heat reduction is

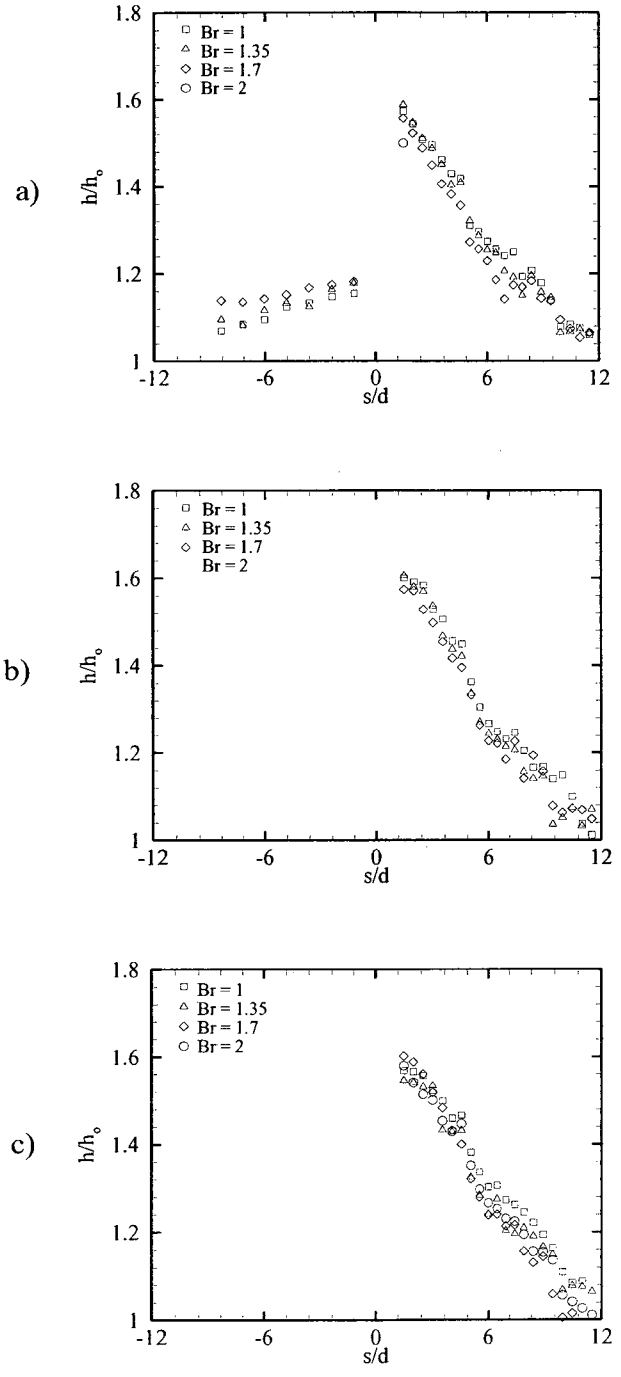

Figure 5-10 Effect of blowing ratio with 0° inclination angle a) cylindrical b) 2d c) 4d

also gained later downstream as shown in Figure 5.12c. The 0^{o} inclination angle shows poor cooling performance even with the smooth expansion and is not recommended to be implemented on the leading edge region.

5.5 Summary

The cooling performance of the smooth expansion exit has been evaluated at the leading edge of a gas turbine stator. Two expansion levels, 2d and 4d, have been investigated at two inclination angles, 0^{o} and 30^{o}, in addition to the standard cylindrical hole. The lateral-average cooling effectiveness and normalized heat transfer coefficient have been determined using the transient TLC technique at four different blowing ratios, 1, 1.35, 1.7, and 2. The smooth expansion exit shows higher effectiveness compared with the standard cylindrical exit when supplied with the same coolant amount. The highly curved surface of the leading edge, accompanied by the high blowing ratio, result in a severe jet lift-off with lower effectiveness. The magnification of the exit area in the proposed exit causes a significant decrease in the jet momentum and subsequent effectiveness increase with the blowing ratio increase. The suction side shows lower effectiveness compared with the pressure side in all cases because of the highly curved surface which keeps the jet away from the vane surface. However, the highest expansion level shows relatively higher effectiveness increase on the suction side compared with that gained on the pressure side. The proposed expansion exit provides lower heat transfer coefficient compared with the standard cylindrical exit with insignificant change with the blowing ratio.

The smoother inclination angle, 30^{o}, provides a component of the jet momentum that yields to the main flow and decreases the interaction between both streams. The

steep inclination angle, 0^{o}, hardly faces the mainstream, yielding a significant decrease in the effectiveness accompanied with a slight increase in the heat transfer coefficient. The jet momentum in that case completely confronts the mainstream, causing high disturbance hence higher heat transfer coefficient. There is no data presented for some cases especially on the suction side because there is no color traced by the TLC range used. This indicates no effectiveness gained however the heat transfer coefficient changes cannot be predicted.

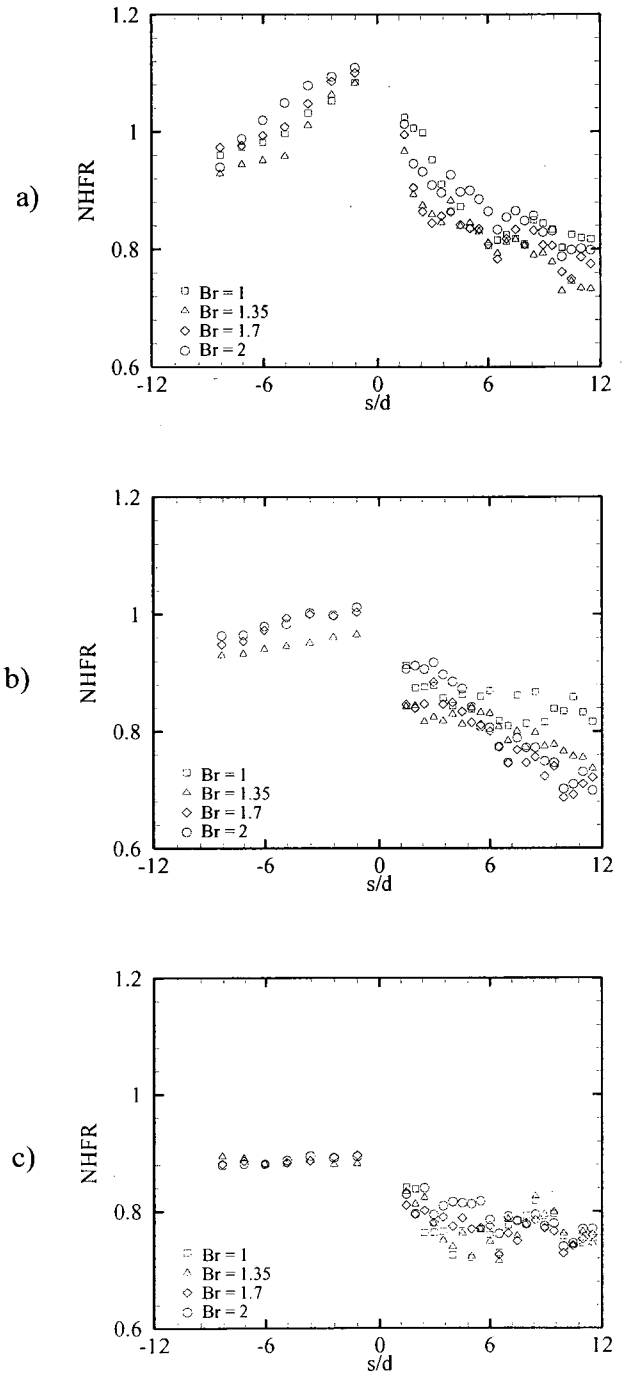

Figure 5-11 Heat load reduction with 30° inclination angle a) cylindrical b) 2d c) 4d

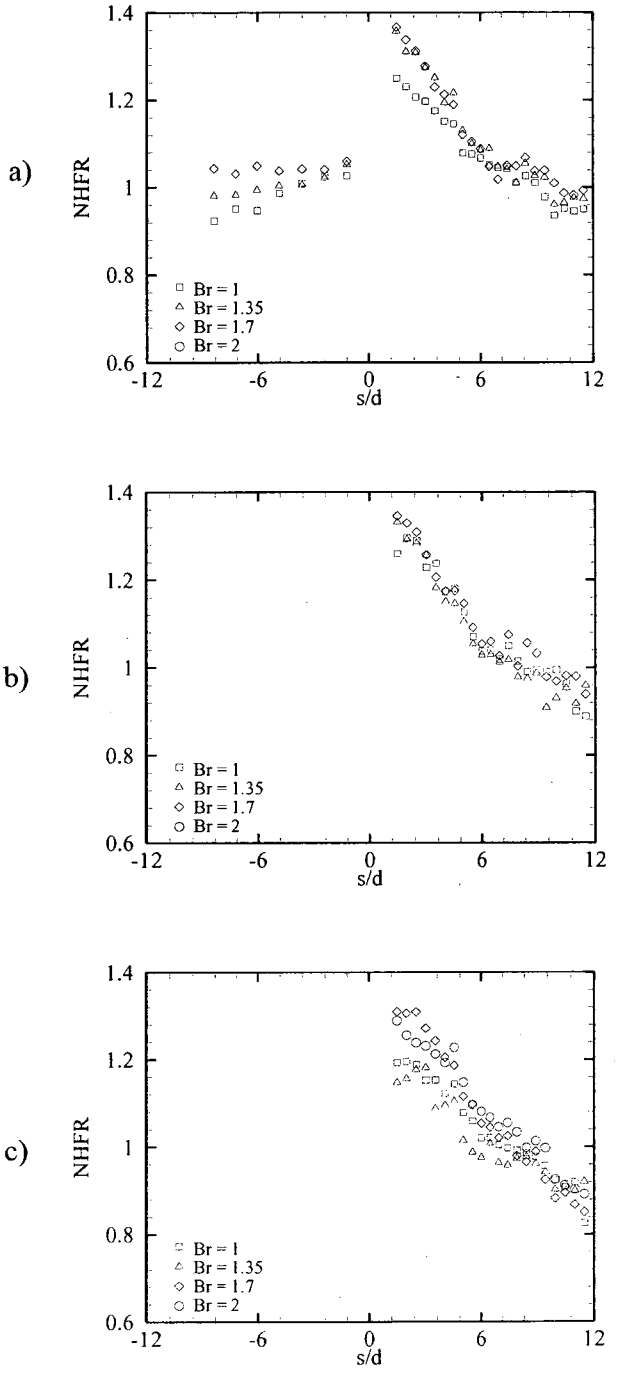

Figure 5-12 Heat load reduction with 0^{o} inclination angle a) cylindrical b) 2d c) 4d

Chapter 6 - Conclusion and Future Directions

6.1 Conclusion

The objective of this study is to measure the film cooling performance of advanced cooling schemes over the actual curved surface of a gas turbine vane. A two dimensional cascade has been designed and constructed in a subsonic wind tunnel in order to investigate the heat transfer over the curved surfaces of gas turbine airfoils. An in-situ calibration technique has been developed to map the surface temperature without disturbing the aerodynamic flow around the vane. Investigating the flow over the curved surface needs some cautions due to the change of the streamline behaviour, hence a subsequent change in the flow properties.

The film cooling performance of two shaped holes was then investigated at different positions on the gas turbine stator, either on the concave or the convex surfaces in addition to the highly curved surface on the leading edge. The louver performance, in previous studies, has been investigated numerically at a variety of conditions over a flat plate and over a symmetrical airfoil. Those investigations presented the improvement in the effectiveness and the changes in the heat transfer coefficient. The current work presents the corresponding changes of the heat transfer coefficient, which gives an overview to the total heat load over the vane surface. Not only was the performance of the individual row was studied, but also the interaction between two staggered rows was investigated as well. Therefore, this is the first study that provides the film cooling performance of the louver scheme, including the heat transfer coefficient, over the actual curved surface of a gas turbine vane. Moreover, this study includes the performance of

the louver at different positions over the entire surface of the vane and the performance of a double row interaction.

The louver scheme in the current study provides a significant reduction in the heat load. The gained reduction is affected by the position of the hole on the surface of the vane. The suction side with the convex surface provoke a flow acceleration accompanied by a favourable pressure gradient. The coolant jet is then kept attached to the surface with longer trace and higher lateral averaged effectiveness. In contrary, the pressure side with the concave surface has flow insatiability accompanied by an adverse pressure gradient. The coolant partially detached from the surface yielding a shorter trace and lower averaged effectiveness. The corresponding heat transfer coefficient increases but still lower than that of the similar circular hole which results in a higher heat load reduction. The performance of the film holes changes with the position of the hole, which is supported by the current findings, with detailed measurements in terms of cooling effectiveness and heat transfer coefficient. Moreover, the cooling performance is measured in the case of double injection on both surfaces. The stagger arrangement provides a flow blockage, particularly at the pressure side. The coolant injected from the first row is strongly support the coolant from the second row causing a higher effectiveness with lower heat transfer coefficient.

The leading edge is characterized by a high rate of heat transfer and high jet lift-off with low possibility to reattach due to the highly curved surface, particularly towards the suction side. The smooth expansion proposed a decrease in the jet momentum and redistributes the coolant uniformly towards both the suction side and the pressure side. The smooth expansion provides higher cooling performance compared with the standard

cylindrical hole. The highly curved nature of the leading edge disperses the coolant away from the surface, while the smooth expansion impedes this dispersion due to the further reduction in the jet momentum. The proposed expansion redistributes the coolant over the leading edge region causing significant heat load reduction not only downstream the cooling hole towards the pressure side but also towards the suction side. The complete confrontation of the jet with the mainstream leads to significant dissipation of the coolant with high reduction on the effectiveness, particularly towards the suction side.

Both shaped holes investigated in the current study provide a higher net heat flux reduction compared with the similar cylindrical holes and other shaped holes in the literature, which helps to enhance the cooling performance in the next generation of gas turbines. The current study provides the heat transfer designer with the data required to analyse the performance of the shaped holes on the actual vane surface. Moreover, this data can be used in the validation process of the CFD code in order to perform further investigations of the shaped holes under more realistic conditions.

6.2 Recommendations

Through this study, caution has been taken when dealing with the heat conduction through the vane material as it increases the uncertainty in the result. The heat conduction is considered as a high source of uncertainty in film cooling investigations. This type of uncertainty is eliminated on the flat plate investigation as there is a possibility of using thick plates. Using thick material on the airfoil investigations is limited by the available cross section area of the test section, which is limited by the approaching flow velocity to the airfoil and the capability of the airflow source. In the present work, the experimental time has been reduced until the used methodology could trace reliable results. Moreover,

the plenum design has changed to minimize the conduction effect to approximately 20% of its initial value, however more efforts should be provided to completely eliminate this effect.

The present study presents the change in the heat transfer coefficient, which is a resultant of the flow interaction between the coolant jet and the mainstream. These measurements provide an indication of the total heat load affect the vane surface. However, the nature of the flow interaction between the mainstream and the jet is still not obvious. This interaction causes the change in the heat transfer coefficient and more information about the physics of that interaction shed enough light to improve the geometrical aspects of the shaped hole. The Particle Image Velocimetry technique is recommended to perform a flow visualization measurement on the vane surface to clarify the interaction nature at these critical regions.

The shaped holes investigated in the current study show an improvement in the cooling performance of a gas turbine vane; however more cooling capacity is still required. The performance of the investigated hole shapes can be developed by further modifications to the positioning (e.g. compound angle on the pressure side and suction side, and shallower angle on the leading edge). Choosing different positions for the film cooling hole could provide more cooling capacity due to the curvature effect of the surface. In addition, more investigations are needed to prove the performance of the investigated shapes at more realistic conditions, higher Reynolds number and Mach number, and higher turbulent intensity. Investigating the film cooling performance depends on the experimental measurements and the numerical investigations due to the complexity of the flow interaction. More analytical efforts are still required to model the

flow interaction or assign empirical formulas in order to predict the cooling performance of the shaped hole. The simple case of a circular hole over a flat plate could be the start of such research.

Publications from this work

Journal

Elnady, T., Hassan I., Kadem L., Lucas T., "Experimental Investigation of Louver Cooling Scheme on Gas Turbine Stator; Part I: Heat Transfer Coefficient" ASME Journal of Heat Transfer, paper submitted on 23 Jun 2010.

Elnady, T., Hassan I., Kadem L., Lucas T., "Experimental Investigation of Louver Cooling Scheme on Gas Turbine Stator; Part I: Cooling Effectiveness" ASME Journal of Heat Transfer, paper submitted on 23 Jun 2010.

Under preparation:

Elnady, T., Hassan I., Kadem L., Lucas T., "Experimental Investigation of Smooth Expansion Film Cooling Holes for Leading Edge; Part I: Cooling Effectiveness" will be submitted to AIAA Journal of Power and Probulsion.

Elnady, T., Hassan I., Kadem L., Lucas T., "Experimental Investigation of Smooth Expansion Film Cooling Holes for Leading Edge; Part II: Heat Transfer Coefficient" will be submitted to AIAA Journal Power and Probulsion.

Conference

Elnady, T., Hassan I., Kadem L., "Experimental Investigation of Film Cooling Effectiveness for a New Shaped Hole at The Leading Edge", Proceedings of ASME IMECE, Vancouver, BC, Canada, Nov. 12-18, 2010.

Elnady, T., Hassan I., Kadem L., Lucas T., "Experimental Investigation of Louver Cooling Scheme on Gas Turbine Vane Pressure Side", Proceedings of IHTC-14, Washington D.C., USA, Aug. 8-13, 2010.

Elnady, T., Saleh, W., Hassan I., Kadem L., "Film cooling performance of shaped hole over vane with flow visualization", Proceeding of 14th AMME, Cairo, Egypt, May 25-27,2010

Hassan I, Kim, S. I., Zhang, C. X-Z, Ghorab, M., **Elnady, T.,** Saleh, W., Kadem, L., Lucas, T., "Investigation of Novel Cooling Schemes for the Next Generation of Gas Turbine", Proceedings of ICEAE 2009, Bangalore, India, May 18-22, 2009.

Under Preparation

Elnady, T., Hassan I., Kadem L., Lucas T., "Experimental Investigation of Louver Cooling Scheme on Gas Turbine Vane Suction Side", to be submitted to ASME Turbo Expo 2011, Vancouver, BC, Canada, June 6-10, 2010.

Elnady, T., Hassan I., Kadem L., "Experimental Investigation of Film Cooling Performance for a New Shaped Hole at The Leading Edge", to be submitted to ASME Turbo Expo 2011, Vancouver, BC, Canada, June 6-10, 2010.

References

[1] Aga, V., Rose, M., and Abhari, R.S., 2008, "Experimental Flow Structure Investigation of Compound Angled Film Cooling," ASME Journal of Turbomachinery, **130**(3), p. 031005.

[2] Ai, D., Ding, P., and Chen, P., 2001, "The Selection Criterion of Injection Temperature Pair for Transient Liquid Crystal Thermography on Film Cooling," International Journal of Heat and Mass Transfer, **44**(7), pp. 1389-1399.

[3] Al-Hamadi, A.K., Jubran, B.A., and Theodoridis, G., 1998, "Turbulence Intensity Effects on Film Cooling and Heat Transfer from Compound Angle Holes with Particular Application to Gas Turbine Blades," Energy Conversion and Management, **39**(14), pp. 1449-1457.

[4] Ames, F.E., 1998, "Aspects of Vane Film Cooling with High Turbulence: Part II-Adiabatic Effectiveness," ASME Journal of Turbomachinery, **120**(4), pp. 777-784.

[5] Bell, C.M., Ligrani, P.M., Hull, W.A., and Norton, C.M., 1999, "Film Cooling Subject to Bulk Flow Pulsations: Effects of Blowing Ratio, Freestream Velocity, and Pulsation frequency," International Journal of Heat and Mass Transfer, **42**(23), pp. 4333-4344.

[6] Bell, C.M., Hamakawa, H., and Ligrani, P.M., 2000, "Film Cooling from Shaped Holes," ASME Journal of Heat Transfer, **122**(2), pp. 224-232.

[7] Bons, J. P., MacArthur, C. D., and Rivir, R. B., 1996, "The Effect of High Free-Stream Turbulence on Film Cooling Effectiveness," ASME Journal of Turbomachinery, **118**(4), pp. 814-825.

[8] Chappell, J., Ligrani, P., Sreekanth, S., and Lucas, T., 2008, "Suction Side Gill Region Film Cooling: Effects of Hole Shape and Orientation on Adiabatic Effectiveness and Heat Transfer Coefficient," ASME Paper No. GT-2008-50798.

[9] Cho, H. H., Rhee, D.H, and Kim, B.G., 2001, "Enhancement of Film Cooling Performance Using a Shaped Film Cooling Hole with Compound Angle Injection," JSME International Journal, Series B, **44**(1), pp. 99-110.

[10] Colban W., Gratton A., Thole K.A., and Haendler M., 2006, "Heat Transfer and Film Cooling Measurements on a Stator Vane with Fan Shaped Cooling Holes," ASME Journal of Turbomachinery, **128**(1), pp. 53-61.

[11] Coulthard, S.M., Volino, R.J., and Flack, K.A., 2006, "Effect of Unheated Starting Lengths on Film Cooling Experiments," ASME Journal of Turbomachinery, **128**(3), pp. 579-588.

[12] Daniels, L.C., and Schultz, D.L., 1983, "Heat Transfer Rate to Blade profiles – Theory and Measurement in Transient Facilities," VKI Lecture Series.

[13] Dittmar, J., Schulz, A., and Wittig, S., 2003, "Assessment of Various Film Cooling Configurations Including Shaped and Compound Angle Holes Based on Large Scale Experiments," ASME Journal of Turbomachinery, **125**(1), pp. 57-64.

[14] Dittmar, J., Schulz, A., and Wittig, S., 2004 "Adiabatic Effectiveness and Heat Transfer Coefficient of Shaped Film Cooling Holes on a Scaled Guide Vane Pressure Side Model," International Journal of Rotating Machinery, **10**(5), pp. 345-354.

[15] Drost, U., and Bolcs, A., 1997, "Utilization of the Transient Liquid Crystal Technique for Film Cooling Effectiveness and Heat Transfer Investigations on a Flat Plate and a Turbine Airfoil," ASME Paper No. 97-GT-26.

[16] Drost, U., and Bolcs, A., 1999, "Investigation of Detailed Film Cooling Effectiveness and Heat Transfer Distributions on a Gas Turbine Airfoil," ASME Journal of Turbomachinery, **121**(2), pp. 233-242.

[17] Ekkad, S.V., Zapata, D., and Han, J.C., 1997, "Film Effectiveness Over a Flat Surface with Air and CO_2 Injection Through Compound Angle Holes Using a Transient Liquid Crystal Image Method," ASME Journal of Turbomachinery, **119**(3), pp. 587-593.

[18] Ekkad, S.V., Ou, S., and Rivir, R.B., 2004, "A Transient Infrared Thermography Method for Simultaneous Film Cooling Effectiveness and Heat Transfer Coefficient Measurements from a Single Test," ASME Journal of Turbomachinery, **126**(4), pp. 597-603.

[19] Ethridge, M.I., Cutbirth, J.M., and Bogard, D.G., 2001, "Scaling of Performance for Varying Density Ratio Coolants on an Airfoil with Strong Curvature and Pressure Gradient Effect," ASME Journal of Turbomachinery, **123**(2), pp. 231-237.

[20] Ghorab, G. M., 2009, "Experimental Investigation of Advanced Film Cooling Schemes for a Gas Turbine Blade," PhD thesis, Concordia University, Montreal.

[21] Gao, Z., Narzary, D.P., and Han, J.C., 2008 "Film Cooling on a Gas Turbine Blade Pressure Side or Suction Side with Axial Shaped Holes," International Journal of Heat and Mass Transfer, **51**(9-10), pp. 2139-2152.

[22] Gao, Z., Narzary, D.P., and Han, J.C., 2009 "Film Cooling on a Gas Turbine Blade Pressure Side or Suction Side with Compund Angle Shaped Holes," ASME Journal of Turbomachinery, **131** (1), p. 011019.

[23] Gao, Z., and Han, J.C., 2009, "Influence of Film-Hole Shape and Angle on Showerhead Film Cooling Using PSP Technique," ASME Journal of Heat Transfer, **131**(6), p.061701

[24] Gritsch, M., Schulz, A., and Witting, S., 1998, "Adiabatic Wall Effectiveness Measurements of Film Cooling Holes with Expanded Exit," ASME Journal of Turbomachinery, **120**(3), pp. 549-556.

[25] Gritsch, M., Schulz, A., and Witting, S., 2000, "Film-Cooling Holes with Expanded Exits: Near-Hole Heat Transfer Coefficients," International Journal of Heat and Fluid Flow, 21(2), pp. 146-155.

[26] Gritsch, M., Schulz, A., and Witting, S., 2003, "Effect of Internal Coolant Crossflow on the Effectiveness of Shaped Film Cooling Holes," ASME Journal of Turbomachinery, **125**(3), pp. 547-554.

[27] Gritsch, M., Colban, W, Schär, H., and Döbbeling, K., 2005, "Effect of Hole Geometry on the Thermal Performance of Fan-Shaped Film Cooling Holes," ASME Journal of Turbomachinery, **127**(4), pp. 718-725.

[28] Guangchao, L., Huiren, Z., and Huiming, F., 2008, "Influences of Hole Shape on Film Cooling Characteristics with CO_2 Injection," Chinese Journal of Aeronautics, **21**(5), pp. 393-401.

[29] Hale, C.A., Plesniak, M.W., and Ramadhyani, S., 2000, "Film Cooling Effectiveness for Short Film Cooling Holes Fed by a Narrow Plenum," ASME Journal of Turbomachinery, **122**(3), pp. 553-557.

[30] Han, J.C., Dutta, S., and Ekkad, S.V., 2000 "Gas Turbine Heat Transfer and Cooling Technology," Published by Taylor & Francis, New York, NY.

[31] Han, J.C., Park, J.S., and Lie, C.K., 1984, "Heat Transfer and Pressure Drop in Blade Cooling Channels with Turbulence Promoters," Texas A&M University (prepared for NASA CR-3837).

[32] Hoffs, A., Drost, U., and Bolcs, A., 1997, "Investigation of Effectiveness and Heat Transfer on a Showerhead-Cooled Cylinder," ASME Paper No. 97-GT-69.

[33] Huiren, Z., Duchun, X., Tao, G., and Songling, L., 2004, "Effects of Film Cooling Hole Shape on Heat Transfer," Heat Transfer – Asian Research, **33**(2), pp. 73-80.

[34] Immarigeon, A., and Hassan, I., 2006, "An Advanced Impingement/Film Cooling Scheme for Gas Turbines – Numerical Study," International Journal of Numerical Methods for Heat & Fluid Flow, **16**(4), pp. 470-493.

[35] Islami, S.B., Tabrizi, A., Jubran, B., and Esmaeilzadeh, E., 2010, "Influence of Trenched Shaped Holes on Turbine Blade Leading Edge Film Cooling," Heat Transfer Engineering, **31**(10), pp. 889-906.

[36] Jiang, H.W., and Han, J.C., 1996, "Effect of Film Hole Row Location on Film Effectiveness on a Gas Turbine Blade," ASME Journal of Heat Transfer, **118**(2), pp. 327-333.

[37] Jubran, B.A., and Maiteh, B.Y., 1999, "Film Cooling and Heat Transfer from a Combination of Two Rows of Simple and/or Compound Angle Holes in Inline and/or Staggered Configuration," Heat and Mass Transfer, **34**(6), pp. 495-502.

[38] Jung, I.S., and Lee, J.S., 2000, "Effects of Orientation Angles on Film Cooling Over a Flat Plate: Boundary Layer Temperature Distributions and Adiabatic Film Cooling Effectiveness" ASME Journal of Turbomachinery, **122**(1), pp 153-160.

[39] Karni, J., and Goldstein, R.J., 1990, "Surface Injection Effect on Mass Transfer From a Cylinder in Crossflow: A Simulation of Film Cooling in the Leading Edge Region of a Turbine Blade," ASME Journal of Turbomachinery, **112**(3), pp. 418-427.

[40] Kline, S. J., and McClintock, F. A., 1953, "Describing Uncertainties in Single-Sample Experiments," ASME Mechanical Engineering, **75**, pp. 3-8.

[41] Lebedev, V.P., Lemanov, V.V., Misyura, S.Y., and Terekhov, V.I., 1995, "Effects of Flow Turbulence on Film Cooling Efficiency," International Journal of Heat and Mass Transfer, **38**(11), pp. 2117-2125.

[42] Lu, Y., Allison, D., and Ekkad, S.V., 2007, "Turbine Blade Showerhead Film Cooling: Influence of Hole Angle and Shaping," International Journal of Heat and Fluid Flow, 28(5), pp. 922-931

[43] Lu, Y., Dhungel, A., Ekkad, S.V., and Bunker, R.S., 2009, "Effect of Trench Width snd Depth on Film Cooling from Cylindrical Holes Embedded in Trenches," ASME Journal of Turbomachinery, **131**(1), p. 011003.

[44] Lu, Y., Dhungel, A., Ekkad, S.V., and Bunker, R.S., 2009, "Film Cooling Measurements for Cratered Cylindrical Inclined Holes," ASME Journal of Turbomachinery, **131**(1), p. 011005.

[45] Lutum, E., von Wolfersdorf, J., Semmler, K., Naik, S., and Weigand, B., 2001, "Film Cooling on a Convex Surface: Influence of External Pressure Gradient and Mach Number on Film Cooling Performance," Heat and Mass Transfer, **38**(1-2), pp. 7-16.

[46] Mayhew, J. E., Baughn, J. W., and Byerley, A. R., 2003, "The Effect of Freestream Turbulence on Film Cooling Adiabatic Effectiveness," International Journal of Heat and Fluid Flow, **24**(5), pp. 669-679.

[47] Mehendale, A.B., and Han, J.C., 1992, "Influence of High Mainstream Turbulence on Leading Edge Film Cooling Heat Transfer: Effect of Film Hole Spacing," International Journal of Heat and Mass Transfer, **35**(10), pp. 2593-2604.

[48] Mhetras, S., Han, J.C., and Rudolph, R., 2007, "Effect of Flow Parameter Variations on Full Coverage Film-Cooling Effectiveness for a Gas Turbine Blade," ASME Paper No. GT2007-27071

[49] Moffat, R. J., 1988, "Describing the Uncertainties in Experimental Results"; Experimental Thermal and Fluid Science, **1**(1), pp. 3-17.

[50] Nirmalan, N.V., Hylton, L.D., 1990, "Experimental Study of Turbine Vane Heat Transfer with Leading Edge and Downstream Film Cooling", ASME Journal of Turbomachinery, **112**(3), pp. 477-487.

[51] Okita, Y., and Nishiura, M., 2007, "Film Effectiveness Performance of an Arrowhead-Shaped Film-Cooling Hole Geometry," ASME Journal of Turbomachinery, **129**(2), pp.331-339.

[52] Ou, S., and Han, J.C., 1992, "Influence of Mainstream Turbulence on Leading Edge Film Cooling Heat Transfer Through Two Rows of Inclined Film Slots," ASME Journal of Turbomachinery, 114(4), pp. 724-733.

[53] Reiss, H., Bolcs, A., and Drost, U., 1998, "The Transient Liquid Crystal Technique Employed for Sub- and Transonic Heat Transfer and Film Cooling Measurements in a Linear Cascade," 14th bi-annual symposium on Measurement Techniques in Transonic and Supersonic Flow in Cascades and Turbomachines, University of Limerick.

[54] Reiss, H., and Bolcs, A., 2000, "Experimental Study of Showerhead Cooling on a Cylinder Comparing Several Configurations Using Cylindrical and Shaped Holes," ASME Journal of Turbomachinery, **122**(1), pp. 161-169.

[55] Russin, R.A., Alfred, D., and Wright, L.M., 2009, "Measurement of Detailed Heat Transfer Coefficient and Film Cooling Effectiveness Distributions Using PSP and TSP," ASME Paper No. GT2009-59975

[56] Salcudean, M., Gartshore, I., Zhang, K., and Barnea, Y., 1994, "Leading Edge Film Cooling of a Turbine Blade Model Through Single and Double Row Injection: Effects of Coolant Density," ASME Paper No. 97-GT-2.

[57] Schwarz, S.G., and Goldstein, R.J., 1989, "Two-Dimensional Behavior of Film Cooling Jets on Concave Surfaces," ASME Journal of Turbomachinery, **111**(2), pp. 124-130.

[58] Schwarz, S.G., Goldstein, R.J., and Eckert, E.R.G., 1991, "Influence of Curvature on Film Cooling Performance," ASME Journal of Turbomachinery, **113**(3), pp. 472-478.

[59] Sen, B., Schmidt, D. L., and Bogard, D. G., 1996, "Film Cooling With Compound Angle Holes: Heat Transfer," ASME Journal of Turbomachinery, **118**(4), pp. 800-806.

[60] Teng, S., Han, J., and Poinsatte, P.E., 2001, "Effect of Film Hole Shape on Turbine-Blade Heat-Transfer Coefficient Distribution," AIAA Journal of Thermophysics and Heat Transfer, **15**(3), pp. 249-256.

[61] Vedula, R.J., Metzger, D.E., 1991, "A Method for the Simultaneous Determination of Local Effectiveness and Heat Transfer Distributions in Three-Temperature Convection Situations," ASME Paper No. 91-GT-345.

[62] Waye, S.K., Bogard, D.G., 2007, "High-resolution Film Cooling Effectiveness Comparison of Axial and Compound Angle Holes on the Suction Side of a Turbine Vane," ASME Journal of Turbomachinery, **129**(2), pp. 202-211.

[63] Weigand, B., Falcoz, C., and Ott, P., 2006, "Experimental Investigations on Showerhead Cooling on a Blunt Body," International Journal of Heat and Mass Transfer, 49(7-8), pp. 1287-1298.

[64] York, W.D. and Leylek, J.H., 2002, "Leading-Edge Film-Cooling Physics – Part I: Adiabatic Effectiveness," ASME Paper No. 2002-GT-30166.

[65] York, W.D. and Leylek, J.H., 2002, "Leading-Edge Film-Cooling Physics – Part II: Heat Transfer Coefficient," ASME Paper No. 2002-GT-30167.

[66] York, W.D. and Leylek, J.H., 2003, "Leading-Edge Film-Cooling Physics – Part III: Diffused Hole Effectiveness," ASME Journal of Turbomachinery, **125**(2), pp. 252-259.

[67] Yu, Y., Yen, C.H., Shih, T.I., Chyu, M.K., and Gogineni, S., 2002, "Film Cooling Effectiveness and Heat Transfer Coefficient Distributions Around Diffusion Shaped Holes," ASME Journal of Heat Transfer, **124**(5), pp. 820-827.

[68] Yuen, C.H.N., and Martinez-Botas, R.F., 2003, "Film Cooling Characteristics of a Single Round Hole at Various Streamwise Angles in a Cross Flow: Part I: Effectiveness," International Journal of Heat and Mass Transfer, **46**(2), pp. 221-235.

[69] Yuen, C.H.N., and Martinez-Botas, R.F., 2003, "Film Cooling Characteristics of a Single Round Hole at Various Streamwise Angles in a Cross Flow: Part II: Heat Transfer Coefficients," International Journal of Heat and Mass Transfer, **46**(2), pp. 237-249.

[70] Yuen, C.H.N., and Martinez-Botas, R.F., "Film Cooling Characteristics of Rows of Round Holes at Various Streamwise Angles in a Cross flow: Part I: Effectiveness," International Journal of Heat and Mass Transfer, **48**(23-24), pp. 4995-5016.

[71] Yuen, C.H.N., and Martinez-Botas, R.F., 2005, "Film Cooling Characteristics of Rows of Round Holes at Various Streamwise Angles in a Cross flow: Part II: Heat Transfer Coefficients," International Journal of Heat and Mass Transfer, **48**(23-24), pp. 5017-5035.

[72] Zhang, X. Z., and Hassan, I., 2006, "Numerical Investigation of Heat Transfer on Film Cooling with Shaped Holes," International Journal of Numerical Methods for Heat & Fluid Flow, **16**(8), pp. 848-869.

[73] Zhang, X.Z., Hassan, I., and Lucas, T., 2006, "Louver Cooling Scheme for Gas Turbines: Multiple Rows," AIAA Journal of Thermophysics and Heat Transfer, **20**(4), pp. 764-771.

[74] Zhang, X.Z. and Hassan, I., 2006, "Film Cooling Effectiveness of an Advanced-Louvre Cooling Scheme for Gas Turbines," AIAA Journal of Thermophysics and Heat Transfer, **20**(4), pp. 754-763.

[75] Zhang, X. Z., Kim, S. I., and Hassan. I., 2008, "Detached-Eddy Simulation of a Louver-Cooling Scheme for Turbine Blades", AIAA Journal of Propulsion and Power, **24**(5), pp.1133-1140.

[76] Zhang, X.Z., and Hassan, I., 2009, "Computational Study of the Effects of Shock Waves on Film Cooling Effectiveness," ASME Journal of Engineering for Gas Turbines and Power, **131**(3), p. 031901.

[77] Zhang, L., and Moon, H.K., 2006, "Turbine Blade Film Cooling Study - The Effects of Showerhead Geometry," ASME Paper No. GT2006-90367.

[78] Zhang, L., and Moon, H., 2007, "Turbine Blade Film Cooling Study: The Effects of Film Hole Location on the Pressure Side," ASME Paper No. GT2007-27546.